

PROGRESS IN THE RECOVERY OF GASEOUS OLEFINS. THE COMBINED ROLE OF MEMBRANES, FACILITATED TRANSPORT AND IONIC LIQUIDS

Progresos en la recuperación de olefinas gaseosas.
El papel combinado de membranas,
transporte facilitado y líquidos iónicos

Marcos Fallanza Torices

Santander, July 2013

SUPERVISORS:

Prof. Dr. Inmaculada Ortiz Uribe
Dr. Daniel Gorri Cirella



UC

UNIVERSIDAD
DE CANTABRIA

Memoria de Tesis Doctoral presentada para optar al título de Doctor por la Universidad de Cantabria en el Programa de Doctorado en Ingeniería Química y de Procesos

Departamento de Ingeniería Química y Química Inorgánica
UNIVERSIDAD DE CANTABRIA



Departamento de Ingeniería Química y
Química Inorgánica

UNIVERSIDAD DE CANTABRIA

**Progress in the recovery of gaseous olefins.
The combined role of membranes, facilitated
transport and ionic liquids**

(Progresos en la recuperación de olefinas gaseosas.
El papel combinado de membranas,
transporte facilitado y líquidos iónicos)

Memoria de Tesis Doctoral presentada para optar al título de:
Doctor por la Universidad de Cantabria. Doctorado en Ingeniería
Química y de Procesos.

Supervisors:

Prof. Dr. Inmaculada Ortiz Uribe

Dr. Daniel Gorri Cirella

Marcos Fallanza Torices

Santander, July 2013

Programa Oficial de Doctorado en Ingeniería Química y de Procesos (BOE núm. 36, de 10 de febrero de 2010. RUCT: 5311209) con Mención hacia la Excelencia (BOE núm. 253, de 20 de Octubre de 2011. Referencia: MEE2011-0031)

The research described in this thesis was carried out at the Advanced Separation Processes Research Group in the Chemical Engineering and Inorganic Chemistry Department at University of Cantabria. The research is financially supported by the Spanish Ministry of Economy and Competitiveness (MINECO) through the project CTQ2008-00690/PPQ. Marcos Fallanza Also thanks MINECO for the FPI fellowship.

“Progress in the recovery of gaseous olefins. The combined role of membranes, facilitated transport and ionic liquids.”

Marcos Fallanza Torices

Copyright© Marcos Fallanza Torices. Spain. 2013.

All rights reserved

*To my family,
who have taught me the most important things,
those that are not in the books.*

Acknowledgements

This thesis is the culmination of a stage of my life. In this moment I would like to look back and dedicate a few lines to all those people who are essential in my live and to whom I am enormously grateful.

First of all I would like to express my sincere gratitude to Prof. Inmaculada Ortiz, supervisor of this thesis and head of the Advanced Separation Processes research group. I admire her innovative and enthusiastic character which made possible the development of this thesis. I also thank her for believing in me and giving me the opportunity of joining her team.

I would like to give special thanks to Dr. Daniel Gorri for the patient guidance and the advices he gave me throughout these four years. I strongly appreciate his immense knowledge in many areas and his willingness to devote a while to teach me always something new which challenged and enriched my ideas. I could not have imagined having a better supervisor and mentor than Dani for my PhD.

Thanks to Dr. Alfredo Ortiz, who settled the basis for this work and helped me to complete this dissertation. Never matter how busy he was, he has been always there to meet, talk about my ideas and give me the best advices. Thanks for the invaluable assistance he provided me inside and outside the labs.

Besides my supervisors I would like to thank Prof. Angel Irabien for all the efforts he has been doing for years in the Department of Chemical Engineering and Inorganic Chemistry, to the administrative staff (Inma and Pili) and Félix for making easier our daily work. Thanks to Pablo, Germán and Juan who as graduates students, contributed to this project.

I want to express my gratitude to Prof. Kang Li for accepting me as a visiting student at Imperial College London. Thanks to Rami, Smith, Fran, George and Ivan for sharing with me those unforgettable three months.

Likewise thanks to Dr. Pepe Palomar for the time I spent in his group in the Universidad Autónoma de Madrid and for the personal lectures on molecular simulation. Special thanks to Maria, Elia and Jesús Lemus for making me feel at home.

I sincerely acknowledge to my colleagues during this years, especially to Javi, Juancho, Jorge, Rubén, Virginia, Gema, Raquel, Axel, Rosa, Antía, Elia, Vanesa and Gabi for their friendship and the great moments we have shared. To “Les Brokers” and my friends, especially to Chechu, Adri, Sara, Marina, Vitín, Luis Ángel, Yari and Blanco, thanks a lot for helping me to disconnect, always stealing me a smile.

Thanks to José Miguel, Amaya and Sandra for their kindness and affection. My heartfelt thanks go to my girlfriend Elisa, for always being there for me, for her love, devotion and unstinting support that makes me feel special. I could not have found a better travel partner.

Thanks to my uncles and aunts Fredi, Silvia, Leigh, Antonio and Chiqui for their love and believing in me. To my cousins Toñín, Belén and Andrea who are like siblings for me. Special mention to my grandparents Luisa and Alfredo for those magical moments every Christmas, and Balbina (“güela”) for being the most loving and kindest person in the world. Although they left too early, I'm sure wherever they are they feel very proud of me. Thanks to my grandpa Vicente (“güelo”), for the confidence he always had in me, I know he is even prouder of my success than I.

Special thanks to my parents, Marisa and Modesto, for their endless love, support and encouraging me to pursue my dreams. I owe to them everything that I have and who I am. I have no words, time and ways to thank them for all what they have done for me.

To all of you, **THANK YOU!**

A part of this is yours

Agradecimientos

Esta tesis es la culminación de una etapa de mi vida. En este momento me gustaría mirar atrás y dedicar unas líneas a todas aquellas personas que son esenciales en mi vida y a quienes estoy enormemente agradecido.

En primer lugar me gustaría expresar my más sincera gratitud a la Catedrática Inmaculada Ortiz, supervisora de esta tesis y cabeza del grupo de investigación Procesos Avanzados de Separación. Admiro su carácter innovador y entusiasta que ha hecho posible el desarrollo de esta tesis. Del mismo modo agradezco la confianza que siempre depositó en mí y la oportunidad de unirme a su equipo.

Me gustaría agradecer de manera especial al Dr. Daniel Gorri por orientarme pacientemente así como por los buenos consejos que me ha dado durante estos cuatro años. Aprecio enormemente su vasto conocimiento y su disposición para dedicarme siempre un momento y enseñarme algo nuevo que enriquecía mis ideas. No hubiera podido imaginar un mejor supervisor y mentor que Dani para my doctorado.

Gracias al Dr. Alfredo Ortiz, quien sentó las bases de este trabajo y me ayudó a completar esta tesis. Nunca importó lo ocupado que estaba, siempre tuvo un momento para reunarnos, hablar de mis ideas y darme los mejores consejos. Gracias por su inestimable ayuda tanto dentro como fuera de los laboratorios.

Además, me gustaría agradecer al Catedrático Ángel Irabien por todo el esfuerzo dedicado durante años al Departamento de Ingeniería Química y Química Inorgánica, al personal administrativo (Inma y Pili) y a Félix por hacer más fácil el trabajo diario. A Pablo, Germán y Juan quienes como estudiantes contribuyeron a la realización de este proyecto.

Quiero expresar mi gratitud al Catedrático Kang Li por aceptarme como estudiante visitante en el Imperial College de Londres. Gracias a Rami, Smith, Fran, George y Ivan por compartir conmigo esos tres meses

inolvidables. Del mismo, modo gracias al Dr. Pepe Palomar por el tiempo que pasé en su grupo en la Universidad Autónoma de Madrid y por las lecciones personales sobre simulación molecular. Un agradecimiento especial a María, Elia y Jesús Lemus por hacerme sentir como en casa.

Un sincero agradecimiento para mis compañeros durante estos años, especialmente a Javi, Juancho, Jorge, Rubén, Virginia, Gema, Raquel, Axel, Rosa, Antía, Elia, Vanesa y Gabi por su amistad y los grandes momentos compartidos. A “Les Brokers” y a mis amigos, de forma especial a Chechu, Adri, Sara, Marina, Vitín, Luis Ángel, Yari y Blanco, muchas gracias por ayudarme a desconectar y sacarme siempre una sonrisa.

Gracias a José Miguel, Amaya y Sandra por su cariño y su afecto. Mi más sentido agradecimiento para Elisa, por estar siempre ahí, por su cariño, dedicación y apoyo incondicional que me hacen sentir especial. No podría haber encontrado una mejor compañera de viaje.

Gracias a mis tíos Fredi, Silvia, Leigh, Antonio y Chiqui por su cariño y por desvivirse por mí. A mis primos Toñín, Belén y Andrea que son como hermanos para mí. Una mención especial para mis abuelos Luisa y Alfredo por todas esas Navidades mágicas, a Balbina (“güela”) por ser la persona más buena y cariñosa del mundo. A pesar de que se fueron demasiado pronto, estoy seguro de que estén donde estén se sienten orgullosos de mí. Gracias a mi abuelo Vicente (“güelo”) por la confianza que siempre ha tenido en mí, sé que está aún más orgulloso de mis éxitos que yo mismo.

Un agradecimiento muy especial para mis padres, Marisa y Modesto, por su cariño infinito, su apoyo incondicional y animarme siempre a perseguir mis sueños. A ellos les debo todo lo que tengo y lo que ahora mismo soy. No tengo palabras, tiempo ni maneras de agradecerles todo lo que han hecho por mí.

A todos ellos, ¡GRACIAS!

Una parte de esto es vuestra

Summary

Light olefins such as ethylene and propylene are key chemical building blocks that play an essential role in many chemical syntheses and industrial processes. Currently there are several technologies available for light olefin production. However, regardless of the olefin manufacturing route, the obtained product is always a gaseous stream mixture of olefins and paraffins that must be separated in further steps. This separation, which represents one of the most important but also the most challenging processes in the chemical industry usually relies upon energy intensive distillation-based technologies. The large capital investment required as well as the high energy cost associated to the conventional distillation process provides the incentive for ongoing olefin/paraffin separation technology research. Therefore the development of a more sustainable separation process is becoming increasingly important. Although in last years several technologies including extractive distillation, adsorption, absorption and membrane processes have been proposed, none of them has met the requirements to achieve their real application.

In this thesis, novel membrane-based separations have been considered as promising alternatives to intensify the conventional separation process in a modular, compact, robust and safe way. Moreover, the use of ionic liquids as more efficient reaction media has been evaluated. Room Temperature Ionic liquids (RTILs) are organic salts with melting points below 373 K. They usually consist on bulky and asymmetric organic cations combined with a wide range of anions. The use of room temperature ionic liquids has been considered because in addition to their lack of volatility that facilitates their use in gas separations without solvent losses or gas stream pollution, they are termed as “designer solvents” as their properties can be tuned by properly selecting the cation and anion moieties.

This work comprises the selection of the most suitable ionic liquid-silver salt system to carry out the separation process and evaluates the separation performance of different membrane technologies including membrane contactors, supported ionic liquid membranes (SILMs) and polymer/ionic liquid composite membranes.

First, a brief overview of the current light olefin industry and its increasing importance in the modern society is discussed, emphasizing the challenges in the propane/propylene separation.

The first step of this work was the selection of the best Ag^+ -RTIL reaction medium for the separation of propane/propylene mixtures. Absorption equilibrium isotherms of propane and propylene in 7 ILs with different structures were obtained at temperatures between 288 and 308 K, silver concentrations in the range 0-1 M and pressures up to 7 bar. Based on the experimental gas solubility measurements Henry's constants, standard solvation enthalpies, equilibrium constants and enthalpies of complexation are reported. Afterwards, a screening using the COSMO-RS methodology was applied to select the most effective ionic liquid-silver salt combination to carry out the separation of olefin/paraffin gas mixtures.

Having defined the ionic liquid-silver salt system, the implementation of the separation process in gas-liquid membrane contactors was addressed. First, the use of different types of fibers both, polymeric (PVDF and PTFE) and ceramic with different structures (symmetric and asymmetric) has been studied. Then two different commercial membrane contactors, a parallel flow membrane contactor with tubular configuration and a hollow fiber transverse flow membrane contactor have been evaluated. Furthermore, a mathematical model that satisfactorily predicts the obtained experimental results has been developed.

Last, novel facilitated transport membranes such as supported ionic liquid membranes (SILMs) and polymer/ionic liquid composite

membranes have been considered. In this part of the thesis the preparation method of the membranes as well as the effect of the membrane composition on the separation of propane/propylene gas mixtures are described. The separation performance of these membranes under different operational conditions, temperatures from 293 to 323 K and transmembrane pressures up to 5 bar, has been evaluated in terms of membrane stability, flux of gases across the membrane, membrane permeability and separation selectivity. Finally, the performance of these novel facilitated transport membranes was compared to a conventional distillation unit in order to gain insight about the feasibility of the industrial implementation of this type of membrane technology.

Resumen

Las olefinas ligeras como el etileno y el propileno son importantes precursores químicos que juegan un papel esencial en muchas síntesis químicas y procesos industriales. Actualmente hay varias tecnologías disponibles para la producción de olefinas ligeras. Sin embargo, independientemente de la ruta de fabricación, el producto obtenido es siempre una corriente gaseosa mezcla de olefinas y parafinas que deben ser separadas en etapas posteriores. Esta separación, que representa uno de los más procesos importantes y a la vez más difíciles de la industria química se realiza por lo general mediante tecnologías de destilación altamente intensivas en energía. La gran inversión de capital requerida así como el elevado coste energético asociado al proceso de destilación convencional proporciona un incentivo para la investigación de nuevas tecnologías de separación de mezclas olefina/parafina. Por lo tanto, el desarrollo de un proceso de separación más sostenible es cada vez más importante. Aunque en los últimos años se han propuesto una gran variedad de tecnologías alternativas incluyendo la destilación extractiva, adsorción, absorción y procesos de membrana, ninguno de ellos ha cumplido con los requisitos necesarios para lograr su aplicación real.

En esta tesis se proponen nuevos procesos de separación asistidos con membranas como alternativas prometedoras para intensificar el proceso de separación convencional de una forma modular, compacta, robusta y segura. Por otra parte, se ha evaluado el uso de líquidos iónicos como medio de reacción más eficaz. Los líquidos iónicos a temperatura ambiente (RTILs) son sales orgánicas con puntos de fusión por debajo de 373 K. Por lo general, consisten en cationes orgánicos asimétricos de gran tamaño combinados con una amplia gama de aniones. El uso de líquidos iónicos a temperatura ambiente se ha considerado ya que

además de su volatilidad prácticamente despreciable que facilita su uso en separaciones de gases sin pérdidas de disolvente o contaminación de la corriente de gaseosa, son designados como "disolventes de diseño" ya que sus propiedades se pueden modificar mediante la selección adecuada del catión y el anión que lo forman.

Este trabajo comprende la selección del sistema líquido iónico-sal de plata más adecuado para llevar a cabo el proceso de separación y evalúa el rendimiento de la separación de diferentes tecnologías de membrana, incluyendo contactores de membrana, membranas de líquido iónico soportadas (SILMs) y membranas compuestas polímero/líquido iónico.

En primer lugar se da una visión global de la industria de las olefinas ligeras en la actualidad y su creciente importancia en la sociedad moderna, haciendo hincapié en la problemática de la separación de mezclas propano/propileno.

La primera etapa de este trabajo fue la selección del medio de reacción Ag^+ -RTIL más adecuado para llevar a cabo la separación de mezclas de propano/propileno. Las isotermas de absorción de propano y propileno en 7 ILs con diferentes estructuras fueron obtenidas a temperaturas entre 288 y 308 K, para diferentes concentraciones de plata en el rango 0-1 M y presiones de hasta 7 bar. En base a los resultados experimentales obtenidos se determinaron los parámetros característicos como las constantes de Henry, las entalpías de solvatación estándar, las constantes de equilibrio y las entalpías de complejación. Posteriormente se realizó un barrido empleando la metodología COSMO-RS para seleccionar el sistema de líquido iónico-sal de plata más eficaz para llevar a cabo la separación de mezclas gaseosas olefina/parafina.

Definido el sistema de líquido iónico-sal de plata, se abordó la implementación del proceso de separación en contactores de membrana gas-líquido. En primer lugar, se realizó un estudio del uso de diferentes tipos de fibras tanto poliméricas (PVDF y PTFE) como cerámicas con diferentes estructuras (simétrica y asimétrica). A

continuación, se evaluaron dos contactores de membrana comerciales diferentes, un contactor de membrana tubular de flujo paralelo y un contactor de flujo transversal con configuración de fibras huecas. Por otra parte, se desarrolló un modelo matemático capaz de predecir satisfactoriamente los resultados experimentales obtenidos.

Por último, se desarrollaron nuevas membranas de transporte facilitado, como membranas de líquido iónico soportadas (SILMs) y membranas compuestas de polímero/líquido iónico. En este apartado, se describe el método de preparación de las membranas, así como el efecto de la composición de la membrana en la separación de mezclas gaseosas propano/propileno. Además, se ha evaluado la capacidad de separación de estas membranas bajo diferentes condiciones de operación, temperaturas entre 293 y 323 K, y presiones transmembrana de hasta 5 bar, en términos de estabilidad de la membrana, flujo de los gases a través de la misma, permeabilidad de la membrana y selectividad del proceso de separación. Por último, el rendimiento de estas nuevas membranas de transporte facilitado se comparó con una unidad de destilación convencional con el fin de avanzar en la viabilidad de la aplicación de este tipo de tecnología de membranas a nivel industrial.

Contents



ACKNOWLEDGEMENTS	i
SUMMARY	v
1. INTRODUCTION	1
1.1. Light olefins industry	2
1.2. Propane/propylene separation	5
1.3. Olefin π -complexation mechanism	8
1.4. Room temperature ionic liquids (RTILs)	9
1.5. Thesis scope and outline	11
1.6. References	13
2. SCREENING OF IONIC LIQUIDS	23
2.1. Introduction	24
2.2. Experimental methods	26
2.2.1. Materials	26
2.2.2. Synthesis of AgTf_2N	28
2.2.3. Gas solubility measurements	28
2.2.4. Computational details	31
2.3. Results and discussion	32
2.3.1. Physical solubility in RTILs	32
2.3.2. Gas solubility in Ag^+ -RTILs media	36
2.3.3. Optimization of COSMO-RS approach to predict the C_3H_8 and C_3H_6 solubility in ionic liquids	41
2.3.4. Screening of ionic liquids	45

2.3.5. Qualitative silver salt solubility in RTILs	51
2.4. Conclusions.....	54
2.5. Nomenclature.....	55
2.6. References.....	57
3. MEMBRANE CONTACTORS	63
3.1. Introduction.....	64
3.2. Experimental methods	66
3.2.1. Materials.....	66
3.2.2. Ceramic hollow fiber fabrication.....	68
3.2.3. Ceramic hollow fiber characterization	70
3.2.4. Methods	70
3.3. Model development.....	73
3.3.1. Mass balances	74
3.3.2. Mass transfer rate	76
3.3.3. Physical properties	80
3.3.4. Chemical reaction.....	82
3.4. Results and discussion.....	84
3.4.1. Comparison between different types of fibers	84
3.4.2. Parallel flow membrane contactor.....	93
3.4.3. Transverse flow membrane contactor	97
3.4.4. Mathematical model validation	104
3.4.5. Comparison between different contactors	109
3.5. Conclusions.....	112
3.6. Nomenclature.....	113
3.7. References.....	116
4. FACILITATED TRANSPORT MEMBRANES	121

4.1. Introduction.....	122
4.2. Experimental methods	124
4.2.1. Materials.....	124
4.2.2. Preparation of SILMs	125
4.2.3. Preparation of polymer/ionic liquid composite membranes	126
4.2.4. Characterization of polymer/ionic liquid composite membranes	126
4.2.5. Permeation cell.....	127
4.2.6. Methods	128
4.3. Results and discussion.....	130
4.3.1. Supported ionic liquid membranes (SILMs)	130
4.3.2. Polymer/ionic liquid composite membranes	141
4.3.3. Comparison with other membranes	155
4.3.4. Comparison with distillation	157
4.4. Conclusions.....	163
4.5. Nomenclature.....	164
4.6. References.....	165
5. CONCLUSIONS AND CHALLENGES FOR FUTURE RESEARCH	171
5.1. Conclusions.....	172
5.2. Challenges for future research.....	174
LIST OF SCIENTIFIC CONTRIBUTIONS	183
Publications in international journals	183
Contributions to international conferences	184
ABOUT THE AUTHOR	187



1

Introduction

Abstract

This thesis proposes innovative alternatives to the separation of olefin/paraffin gas mixtures based on the selective and reversible olefin-silver(I) reaction, using room temperature ionic liquids as favorable reaction medium and different membrane technologies including membrane contactors, supported liquid membranes and polymer/ionic liquid composite membranes. This preface chapter introduces an overview of the light olefins world market, current separation technologies and the drawbacks associated to the actual technical approaches. The olefin π -complexation mechanism is described and the main features of the ionic liquids are presented. Finally, the scope and outline of the thesis are summarized.

1.1. Light olefins industry

Light olefins such as ethylene and propylene are very important to petrochemical industries because they are used as main building blocks for many essential chemicals and products for industrial and domestic applications. Ethylene and propylene represent by far the largest output among all the petrochemical products. Thus, in 2010 the global market was estimated in 123.3 million metric tons for ethylene and 74.9 million metric tons for propylene. Moreover during the current decade it is expected a forecast to growth at an average of 3.5 % and 4.3 % per year respectively [1]. This growth is driven by the creation of new geographic and fast growth end-use markets mainly located in developing countries. Therefore in the last decade the world market of light olefins has been shifted from developed countries to fast emerging economies in Asia, especially in Middle East and China (figure 1.1) [2,3].

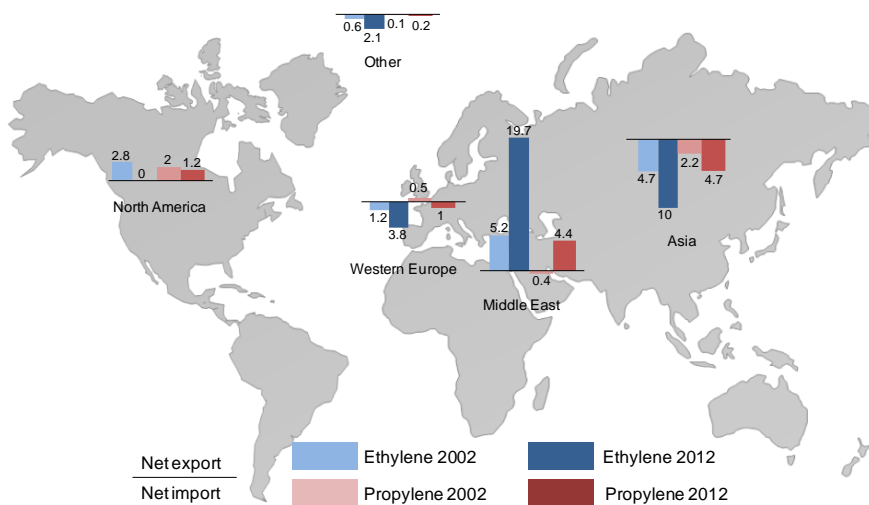


Figure 1.1. Evolution of the ethylene and propylene world equivalent trade in million metric tons.

Propylene is traded commercially in three grades: polymer grade (min. 99.5 % purity), chemical grade (90-95 % purity) and refinery grade (50-70 % purity). The main uses of refinery grade propylene are in liquefied petroleum gas (LPG) for thermal use or as an octane-enhancing component in motor gasoline. However the most significant market for refinery grade propylene is the conversion to chemical grade for use in the production of acrylonitrile, oxo-alcohols and propylene oxide while the main use of the polymer grade is the production of polypropylene [4]. In recent years the rising prices of light olefins are also driving downstream portfolio changes as many large producers increasingly focus on higher value derivatives, the production of polyolefins remain by far the largest derivative well accountings for more than half of the world light olefin consumption (figure 1.2) [5].

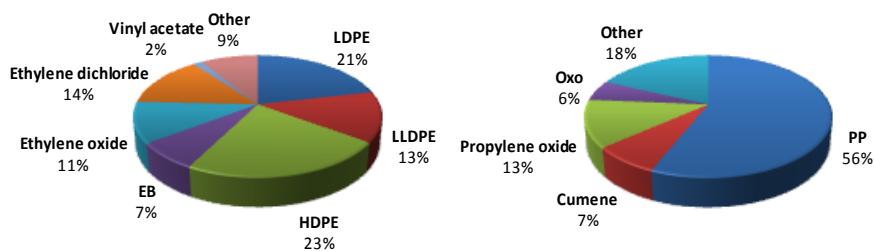


Figure 1.2. Distribution of ethylene and propylene consumption by derivatives in 2010 [6].

Commonly, most of the propylene consumed in the world was produced as a by-product of ethylene and gasoline in steam cracking and Fluidized Catalytic Cracking (FCC) in refineries respectively. However, currently steam crackers are shifting to lighter and cheaper feedstocks which together with the flat gasoline demand growth in some regions have tightened the propylene supplies. Thus, this by-product propylene production cannot satisfy the foreseeable future growth in the demand yielding a gap in the supply and demand of propylene. Consequently on-purpose propylene production technologies are becoming increasingly

important in order to meet the growth projections. Indeed it is expected that on-purpose propylene technologies will supply 20% of global propylene by 2020 (figure 1.3).

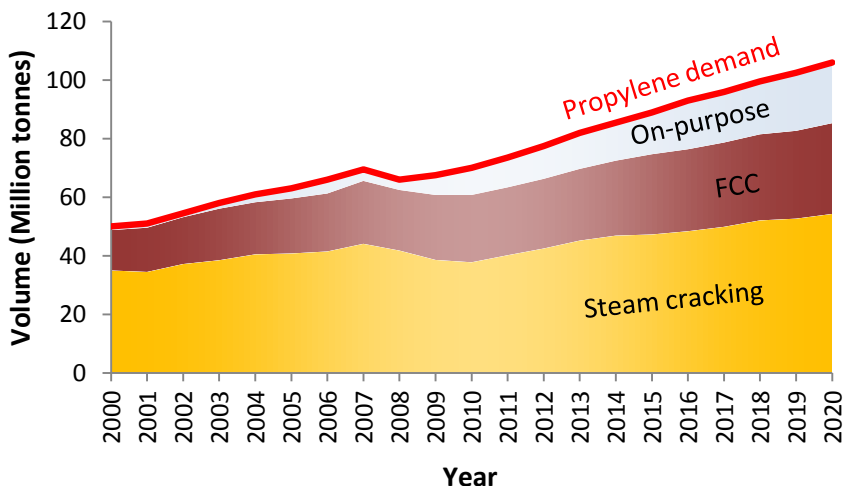


Figure 1.3. Propylene (chemical grade) supply and demand between 2000 and 2020 [7].

Currently the on-purpose propylene production technologies available are high severity FCC, propane dehydrogenation, olefin conversion by metathesis and methanol to olefins (MTO) [8]. The common feature of most of these technologies is that they are either based on longer chain molecules or olefinic feed stock, originally depending on natural gas or crude oil. In addition as the dehydrogenation of propane requires low cost source of propane, it is understood that this technology will be limited to the Middle East region only [9]. However, the propylene supply dependency on natural hydrocarbons is being broken up as olefins can be also produced from methanol capturing the carbon from coal or even from renewable resources like biomass [10]. The potential routes currently available for producing propylene are shown in figure 1.4 [11].

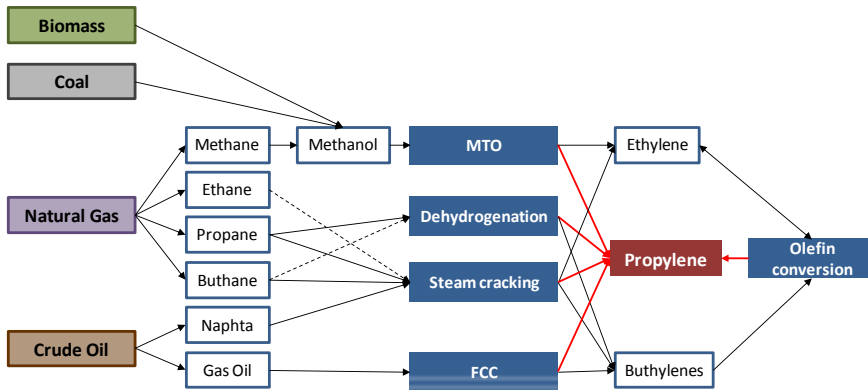


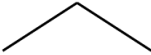
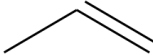
Figure 1.4. Different routes for propylene production from different feedstocks (adapted from [8]).

However, regardless of the propylene manufacturing route, the obtained product is always a propylene/propane mixture. Due to the difference in the applications and also in the prices between propane and propylene these mixtures must be separated in further steps.

1.2. Propane/propylene separation

The separation of olefins from paraffins is a task of primary importance in the petrochemical industry. Traditionally this separation is being performed by distillation in a single or double column with 150-200 trays. The columns usually operate at high pressures (16-26 bar) and room temperature or moderate pressures and low temperatures (183-233 K) working at high reflux ratios between 12 and 20. Therefore the process not only requires high capital investment, but also it is one of the most highly energy demanding processes in the petrochemical industry [12]. In fact, it was estimated that 0.12 Quads of energy (1 Quad = 10^{15} BTU) were used yearly only for olefin/paraffin distillation [13]. Thus, the conventional separation process certainly holds an enormous potential for capital and energy cost savings which provide an incentive to develop new separation technologies for olefin/paraffin separation.

Table 1.1. Propane and propylene physico-chemical properties [14].

Compound	 propane	 propylene
Molecular formula	C_3H_8	C_3H_6
CAS number	74-98-6	115-07-1
Molecular weight ($g \cdot mol^{-1}$)	44.09	42.08
Melting point (K)	85.45	87.85
Liquid density ($kg \cdot m^{-3}$) (1 bar at boiling point)	582	613.9
Normal boiling point (K)	231.05	225.35
Vapor pressure (bar) (293 K)	8.7	10.3
Critical temperature (K)	369.75	364.15
Critical pressure (bar)	42.5	46.1
Gas density ($kg \cdot m^{-3}$) (1 bar at boiling point)	2.423	2.365
Compressibility factor (1 bar and 288 K)	0.982	0.984
Specific gravity (air = 1) (1 bar and 293 K)	1.55	1.48
Solubility in water k_H^0 ($mol \cdot kg^{-1} \cdot bar^{-1}$) (298 K)	0.0015	0.0048

In the last few years several technologies have been surveyed including extractive distillation, adsorption, absorption and membrane processes. However, this separation is very difficult due to the similarities in physicochemical properties between olefins and their corresponding paraffins [15,16]. Extractive distillation requires the addition of a high-boiling polar compound which should dissolve the alkene facilitating the separation of the gas mixture [17]. However, the thermodynamic characteristics of the solvent had a major impact on the process economics and in most cases it was concluded that extractive distillation offers no advantage over traditional distillation [18]. Conventional

physical and chemical adsorption on zeolites and molecular sieves has been extensively investigated. Although, high product purities can be achieved adsorption systems suffer from low olefin loadings and complicated regeneration cycles [19-26]. Absorption processes either physical or chemical hold a great potential for cost and energy saving. Despite of suffering from instability carrier issues in some cases, reactive absorption has been found to be more suitable due to its higher olefin capacity as well as separation selectivity [27-31]. In this sense membrane contactors have been considered to implement gas-liquid absorption processes in a modular, small, robust and safe way avoiding the disadvantages associated to direct compact equipments like spray towers or packed columns such as emulsion formation, flooding, unloading, or foaming [32-37]. In gas-liquid membrane contactors, the membrane offers no selectivity, it acts as a physical barrier between both phases allowing mass transfer between gas and liquid without dispersing one phase into the other with a large contacting surface area [38]. On the other hand, the use of membranes that play an active role in the olefin/paraffin separation has been also evaluated. The separation mechanism is based either on selective physicochemical interactions between olefin and the membrane material, in molecular sieving effects or in a combination of both. These membrane technologies can be categorized into three main groups: polymeric, inorganic, and facilitated transport membranes. Literature shows that various polymers can potentially be used in the development of selective membranes for separating olefin/paraffin gas mixtures. However the tradeoff between permeability and selectivity is one of the biggest issues that must be faced by pure polymer membranes and greatly limits their further application [39-44]. Inorganic membranes such as carbon molecular sieves (CMS) and zeolites-based membranes have been also investigated [45-51]. Despite their higher tolerance to harsh environments, their typical poor mechanical resistance, combined with their expensive and complex preparation methods have limited their use in large-scale application. Thus alternative approaches using facilitated transport membranes (either in solid and liquid state) which provide high olefin

permeabilities as well as high separation selectivities are being explored [52-60].

1.3. Olefin π -complexation mechanism

The reactive absorption of olefins with transition metal cations in aqueous solutions has been extensively studied in literature [28,61-66]. The metal salts commonly used are selected from heavy metal ions such as Cu(I), Ag(I), Au(I), Ni(II), Pt(II) and Pd(II). Although the use of copper salts has been explored due to their low price [67], silver salts are particularly preferred since they have been proved to be the most effective [68]. The interaction is based on the formation of electron donor/acceptor complexes via π -complexation mechanism. The σ component of the bond results from overlapping of the vacant outermost s atomic orbital of the metal with the full π (bonding) molecular orbital of the olefin. The π component of the bond is formed by a backdonation of electrons from the d orbitals of the metal to the olefin's empty π antibonding (π^*) orbital [16].

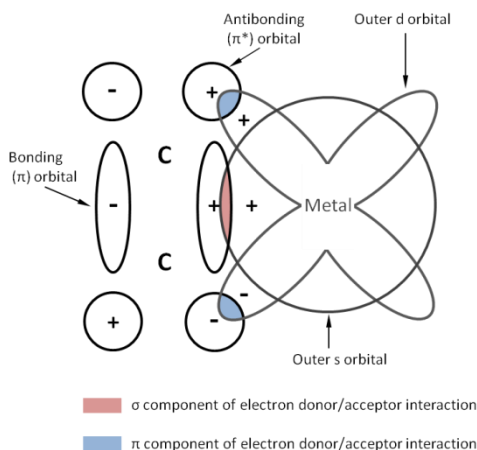


Figure 1.5. Dewar-Chatt model of π -bond Complexation (adapted from [16]).

The main advantage of chemical complexation of olefins with transition metal cations is that in contrast to distillation, which uses an energy separating agent, separations based upon reversible chemical complexation utilize a mass separating agent that potentially leads to more cost-effective processes and smaller equipments [64]. In addition the formed bonds are stronger than those due to Van der Waals forces alone. So it is possible to achieve high selectivity and high capacity for the component to be bounded and at the same time the bonds are still weak enough to be broken by temperature or pressure swings in an economically acceptable manner (figure 1.6).

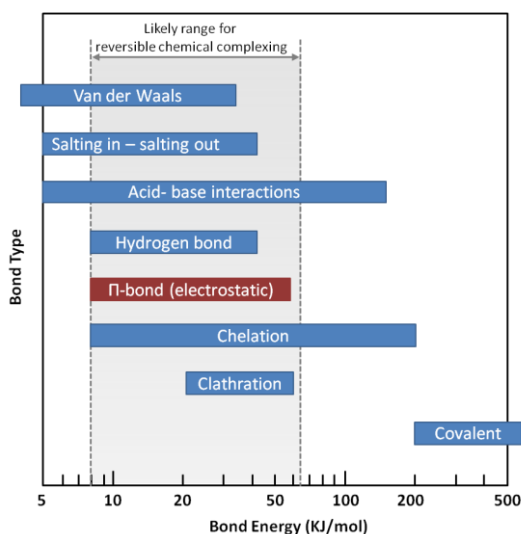


Figure 1.6. Bond energies of the different interactions (adapted from [64]).

1.4. Room temperature ionic liquids (RTILs)

Room Temperature Ionic liquids (RTILs) are organic salts with melting points below 373 K. In contrast to conventional ionic solutions were the

dissolved ions are solvated by the molecules of the solvent, ionic liquids are composed entirely by ions (figure 1.7).

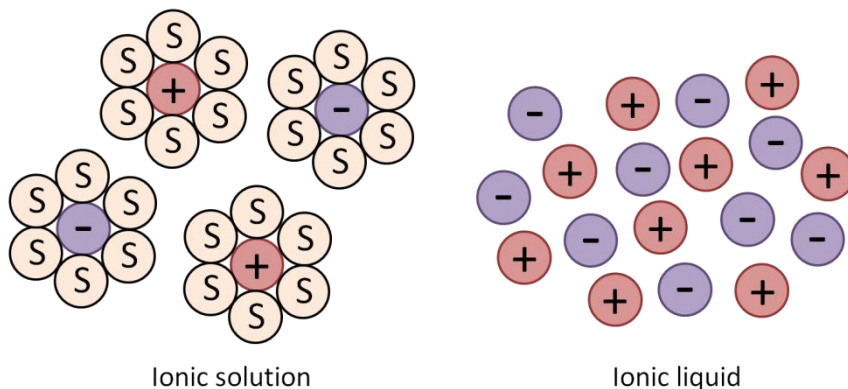


Figure 1.7. Schematic definition of ionic liquids and comparison with conventional ionic solutions.

They usually consist on bulky and asymmetric organic cations such as imidazolium, pyridinium, pyrrolidinium, ammonium and phosphonium combined with a wide range of anions that range from simple halides or small inorganic anions such as tetrafluoroborate and hexafluorophosphate to large organic anions like triflate or bis-trifluoromethylsulphonylimide. The radical groups of the cation are variable, although they typically are alkyl chains they can be also any of a wide variety of other functional groups. RTILs are compounds that present negligible vapor pressure, nonflammability, high thermal stability and chemical stability, wide liquid range, and solvating properties for diverse kinds of materials. Moreover, the variability of the anion, cation as well as the radical groups in the cation may be used to adjust the properties of the ionic liquids. Therefore, the possibility arises to optimize the ionic liquid for a specific application by stepwise tuning the relevant solvent properties. For this reason ionic liquids have been referred to as “designer solvents”. Currently, there are more than 10^3 different ionic liquids available, but it has been demonstrated that there is at least 10^6 simple ionic liquids which can be synthesized in the laboratory. There will be 10^{12} binary combinations of these and 10^{18}

ternary systems possible [69-72]. These remarkable properties make RTILs potential substitutes for organic solvents as separating agents and liquid media for reactions or electrochemical processes [73-81]. In the context of this work besides their lack of volatility that facilitates their role in gas separations without solvent losses or gas stream pollution, ionic liquids present stronger affinity for the olefinic compounds compared to saturated hydrocarbons and provide stability to the metal cation dissolved or suspended inside. Thus ionic liquids present unique properties as potential solvents to carry out the separation of olefin/paraffin gas mixtures [82-90].

1.5. Thesis scope and outline

This study focuses on the development of an alternative separation process of propane/propylene gas mixtures using ionic liquids and membrane technology. The work covers the selection of the most suitable ionic liquid to carry out the separation process and describe the separation performance of different membrane technologies including membrane contactors, supported ionic liquid membranes (SILMs) and polymer/ionic liquid composite membranes.

Chapter 2 reports and describes the selection procedure of the most suitable ionic liquid and silver salt to accomplish the separation process. Experimental propane and propylene solubility into 7 ionic liquids with different structures, containing different concentrations of silver salt as a function of temperature and pressure are reported. Based on the experimental gas solubility measurements Henry's constants, standard solvation enthalpies, C_3H_8/C_3H_6 absorption selectivity, equilibrium constants and enthalpies of reaction with Ag^+ are reported. Moreover a screening of RTILs for propane/propylene separation using the COSMO-RS methodology has been performed.

Chapter 3 aims at the implementation of the separation process in gas-liquid membrane contactors. The system was characterized in terms of

mass transfer performance. First of all a comparative analysis of different types of fibers including PVDF, PTFE and ceramic fibers with symmetric and asymmetric structure has been carried out. Afterwards two different contactors have been studied: a parallel flow membrane contactor with tubular configuration and a transverse flow membrane contactor with hollow fiber configuration. Furthermore the reactive absorption process has been described with a mathematical model based on the resistances in series approach.

Chapter 4 deals with the development of facilitated transport membranes such as supported ionic liquid membranes (SILMs) and polymer/ionic liquid composite membranes to carry out the separation process. In this part the preparation method of the membranes as well as their separation performance under different operational conditions are presented.

Finally, Chapter 5 collects the general conclusions of this thesis and an overview of the challenges and prospects for future research.

1.6. References

- [1] S. Davis, Petrochemical industry overview, , Chemical Engineering Handbooks- SRI Consulting, 2011.
- [2] M. Eramo, North America light olefins: competitive again, how long can it last? presented at Petrochemical Feedstock Association of the Americas, Texas, (November 2007).
- [3] M. Eramo, State of the global petrochemical industry. A perspective on the future, presented to VMA 2012 Market Outlook Workshop, Chicago, (August 2012).
- [4] Intratec, Propylene production via methatesis, Intratec Solutions, Intratec Report #TEC001A 2012.
- [5] IHS, Chemical World Analysis: Propylene, (2012).
- [6] Association of Petrochemicals Producers in Europe (APPE), www.petrochemistry.net, 28-2-2013.
- [7] T. Brookes, New Technology Developments in the Petrochemical Industry, presented at Egypt Petrochemicals Conference, (September 2012).
- [8] J.M. Houdek, "On-purpose" propylene technology developments, presented at ARTC 8th Annual Meeting, Kuala Lumpur, (November 2005).
- [9] T. Wurzel, H. Kömpel, M. Rothaemel, and W. Liebner, MTP[®]- The on-purpose propylene technology for a changing feedstock environment, presented at 19th Petroleum Congress, Madrid, (2008).
- [10] V. Venkataraman, Propy-LENE Supply! Go Green! On-Purpose technologies for the future! White paper. BEROE, (2012).
- [11] A. Aitani, Propylene production, in S. Lee (Ed.), Encyclopedia of Chemical Processing, New York, Taylor & Francis, 2006, pp. 2461-2466.

- [12] D.E. Gottschlich, D.L. Roberts, Energy minimization of separation processes using conventional/membrane hybrid systems., SRI International, Menlo Park, CA (USA), Report N° DOE/ID-10301 1990.
- [13] R.B. Eldridge. Olefin/paraffin separation technology: A review. *Ind. Eng. Chem. Res.*, 32 (1993) 2208.
- [14] Air liquide, encyclopedia.airliquide.com/encyclopedia.asp, 8-3-2013.
- [15] P.F. Bryan. Removal of propylene from fuel-grade propane. *Sep. Purif. Rev.*, 33 (2004) 157.
- [16] D.J. Safarik, R.B. Eldridge. Olefin/paraffin separations by reactive absorption: a review. *Ind. Eng. Chem. Res.*, 37 (1998) 2571.
- [17] V. Mokrushin, D. Assenbaum, N. Paape, D. Gerhard, L. Mokrushina, P. Wasserscheid, et al. Ionic liquids for Propene-Propane separation. *Chem. Eng. Technol.*, 33 (2010) 63.
- [18] R. Kumar, J.M. Prausnitz, and C.J. King, Process design considerations for extractive distillation: separation of propylene-propane, in D.P. Tassios (Ed.), *Extractive and Azeotropic Distillation*, Washington, DC, American Chemical Society, 1972, pp. 16.
- [19] S.U. Rege, J. Padin, and R.T. Yang. Olefin/Paraffin Separations by Adsorption: π -Complexation vs. Kinetic Separation. *AIChE J.*, 44 (1998) 799.
- [20] F.A. Da Silva, A.E. Rodrigues. Propylene/propane separation by vacuum swing adsorption using 13X zeolite. *AIChE J.*, 47 (2001) 341.
- [21] C.A. Grande, A.E. Rodrigues. Propane/propylene separation by Pressure Swing Adsorption using zeolite 4A. *Ind. Eng. Chem. Res.*, 44 (2005) 8815.
- [22] N. Lamia, L. Wolff, P. Leflaive, P.S. Gomes, C.A. Grande, and A.E. Rodrigues. Propane/propylene separation by simulated moving bed I. Adsorption of propane, propylene and isobutane in pellets of 13X zeolite. *Sep.Sci.Technol.*, 42 (2007) 2539.

- [23] G. Autie-Castro, M. Autie, E. Reguera, R. Moreno-Tost, E. Rodríguez-Castellón, A. Jiménez-López, et al. Adsorption and separation of propane and propylene by porous hexacyanometallates. *Appl.Surf.Sci.*, 257 (2011) 2461.
- [24] A.F.P. Ferreira, J.C. Santos, M.G. Plaza, N. Lamia, J.M. Loureiro, and A.E. Rodrigues. Suitability of Cu-BTC extrudates for propane-propylene separation by adsorption processes. *Chem.Eng.J.*, 167 (2011) 1.
- [25] M.G. Plaza, A.F.P. Ferreira, J.C. Santos, A.M. Ribeiro, U. Müller, N. Trukhan, et al. Propane/propylene separation by adsorption using shaped copper trimesate MOF. *Microporous Mesoporous Mater.*, 157 (2012) 101.
- [26] M.C. Campo, A.M. Ribeiro, A. Ferreira, J.C. Santos, C. Lutz, J.M. Loureiro, et al. New 13X zeolite for propylene/propane separation by vacuum swing adsorption. *Sep. Purif. Technol.*, 103 (2013) 60.
- [27] H.W. Quinn, Hydrocarbon separations with silver (I) systems, in E.S. Perry and C.J. van Oss (Ed.), New York, Wiley Interscience, 1971, pp. 133.
- [28] G.E. Keller, A.E. Marcinkowsky, S.K. Verms, and K.D. Williamson, Olefin recovery and purification via silver complexation, in N. Li and J.M. Calo (Ed.), *Handbook of Separation and Purification Technology*, New York, Marcel Dekker, 1992.
- [29] I.H. Cho, D.L. Cho, H.K. Yasuda, and T.R. Marrero. Solubility of propylene in aqueous silver nitrate. *J.Chem.Eng.Data*, 40 (1995) 102.
- [30] K. Nymeijer, T. Visser, W. Brilman, and M. Wessling. Analysis of the complexation reaction between Ag^+ and ethylene. *Ind. Eng. Chem. Res.*, 43 (2004) 2627.
- [31] P. Chilukuri, K. Rademakers, K. Nymeijer, L. Van Der Ham, and H.D. Van Berg. Propylene/propane separation with a gas/liquid membrane contactor using a silver salt solution. *Ind. Eng. Chem. Res.*, 46 (2007) 8701.
- [32] H. Kreulen, C.A. Smolders, G.F. Versteeg, and W.P.M. Van Swaaij. Microporous hollow fibre membrane modules as gas-liquid contractors.

Part 2. Mass transfer with chemical reaction. *J.Membr.Sci.*, 78 (1993) 217.

[33] B.W. Reed, M.J. Semmens, and E.L. Cussler, Membrane contactors, in R.D. Noble and S.A. Stern (Ed.), *Membrane science and technology*, Amsterdam, Elsevier, 1995.

[34] P.H.M. Feron, A.E. Jansen. CO₂ separation with polyolefin membrane contactors and dedicated absorption liquids: Performances and prospects. *Sep. Purif. Technol.*, 27 (2002) 231.

[35] V.Y. Dindore, G.F. Versteeg. Gas-liquid mass transfer in a cross-flow hollow fiber module: Analytical model and experimental validation. *Int.J.Heat Mass Transfer*, 48 (2005) 3352.

[36] R. Klaassen, P.H.M. Feron, and A.E. Jansen. Membrane contactors in industrial applications. *Chem.Eng.Res.Design*, 83 (2005) 234.

[37] K. Simons, K. Nijmeijer, and M. Wessling. Gas-liquid membrane contactors for CO₂ removal. *J.Membr.Sci.*, 340 (2009) 214.

[38] E. Drioli, A. Criscuoli, and E. Curcio, *Membrane Contactors: Fundamentals, Applications and Potentialities*, Amsterdam, Elsevier Science, 2006.

[39] R. Faiz, K. Li. Polymeric membranes for light olefin/paraffin separation. *Desalination*, 287 (2012) 82.

[40] M.L. Chng, Y. Xiao, T.-. Chung, M. Toriida, and S. Tamai. Enhanced propylene/propane separation by carbonaceous membrane derived from poly (aryl ether ketone)/2,6-bis(4-azidobenzylidene)-4-methyl-cyclohexanone interpenetrating network. *Carbon*, 47 (2009) 1857.

[41] K. Tanaka, A. Taguchi, J. Hao, H. Kita, and K. Okamoto. Permeation and separation properties of polyimide membranes to olefins and paraffins. *J.Membr.Sci.*, 121 (1996) 197.

[42] C. Staudt-Bickel, W.J. Koros. Olefin/paraffin gas separations with 6FDA-based polyimide membranes. *J.Membr.Sci.*, 170 (2000) 205.

- [43] M. Das, W.J. Koros. Performance of 6FDA-6FpDA polyimide for propylene/propane separations. *J.Membr.Sci.*, 365 (2010) 399.
- [44] R.L. Burns, W.J. Koros. Defining the challenges for C₃H₆/C₃H₈ separation using polymeric membranes. *J.Membr.Sci.*, 211 (2003) 299.
- [45] A.B. Fuertes, I. Menendez. Separation of hydrocarbon gas mixtures using phenolic resin-based carbon membranes. *Sep. Purif. Technol.*, 28 (2002) 29.
- [46] K.-I. Okamoto, S. Kawamura, M. Yoshino, H. Kita, Y. Hirayama, N. Tanihara, et al. Olefin/paraffin separation through carbonized membranes derived from an asymmetric polyimide hollow fiber membrane. *Ind. Eng. Chem. Res.*, 38 (1999) 4424.
- [47] M. Yoshino, S. Nakamura, H. Kita, K.-. Okamoto, N. Tanihara, and Y. Kusuki. Olefin/paraffin separation performance of carbonized membranes derived from an asymmetric hollow fiber membrane of 6FDA/BPDA-DDBT copolyimide. *J.Membr.Sci.*, 215 (2003) 169.
- [48] I.G. Giannakopoulos, V. Nikolakis. Separation of propylene/propane mixtures using faujasite-type zeolite membranes. *Ind. Eng. Chem. Res.*, 44 (2005) 226.
- [49] C. Zhang, Y. Dai, J.R. Johnson, O. Karvan, and W.J. Koros. High performance ZIF-8/6FDA-DAM mixed matrix membrane for propylene/propane separations. *J.Membr.Sci.*, 389 (2012) 34.
- [50] Y. Pan, T. Li, G. Lestari, and Z. Lai. Effective separation of propylene/propane binary mixtures by ZIF-8 membranes. *J.Membr.Sci.*, 390-391 (2012) 93.
- [51] S.M. Saufi, A.F. Ismail. Fabrication of carbon membranes for gas separation - A review. *Carbon*, 42 (2004) 241.
- [52] S.W. Kang, Y.S. Kang. Silver nanoparticles stabilized by crosslinked poly(vinyl pyrrolidone) and its application for facilitated olefin transport. *J.Colloid Interface Sci.*, 353 (2011) 83.
- [53] S.W. Kang, D.H. Lee, J.H. Park, K. Char, J.H. Kim, J. Won, et al. Effect of the polarity of silver nanoparticles induced by ionic liquids on

facilitated transport for the separation of propylene/propane mixtures. *J.Membr.Sci.*, 322 (2008) 281.

[54] H.S. Kim, J.Y. Bae, S.J. Park, H. Lee, H.W. Bae, S.O. Kang, et al. Separation of olefin/paraffin mixtures using zwitterionic silver complexes as transport carriers. *Chemistry - A European Journal*, 13 (2007) 2655.

[55] J.H. Lee, S.W. Kang, D. Song, J. Won, and Y.S. Kang. Facilitated olefin transport through room temperature ionic liquids for separation of olefin/paraffin mixtures. *J.Membr.Sci.*, 423–424 (2012) 159.

[56] M.T. Ravanchi, T. Kaghazchi, and A. Kargari. Separation of propylene-propane mixture using immobilized liquid membrane via facilitated transport mechanism. *Sep.Sci.Technol.*, 44 (2009) 1198.

[57] M. Teramoto, H. Matsuyama, T. Yamashiro, and Y. Katayama. Separation of ethylene from ethane by supported liquid membranes containing silver nitrate as carrier. *J.Chem.Eng.Japan*, 19 (1986) 419.

[58] S. Duan, A. Ito, and A. Ohkawa. Separation of propylene/propane mixture by a supported liquid membrane containing triethylene glycol and a silver salt. *J.Membr.Sci.*, 215 (2003) 53.

[59] F. Agel, F. Pitsch, F.F. Krull, P. Schulz, M. Wessling, T. Melin, et al. Ionic liquid silver salt complexes for propene/propane separation. *Phys. Chem. Chem. Phys.*, 13 (2011) 725.

[60] F. Pitsch, F.F. Krull, F. Agel, P. Schulz, P. Wasserscheid, T. Melin, et al. An adaptive self-healing ionic liquid nanocomposite membrane for olefin-paraffin separations. *Adv. Mater*, 24 (2012) 4306.

[61] B.B. Baker. The effect of metal fluoroborates on the absorption of ethylene by silver ion. *Inorg.Chem.*, 3 (1964) 200.

[62] H. Lawrence Clever, E.R. Baker, and W.R. Hale. Solubility of ethylene in aqueous silver nitrate and potassium nitrate solutions. Silver ion-ethylene association constant. *J.Chem.Eng.Data*, 15 (1970) 411.

- [63] J.V. Crookes, A.A. Woolf. Competitive interactions in the complexing of ethylene with silver(I) salt solutions. *J. Chem. Soc., Dalton Transactions*, (1973) 1241.
- [64] C.J. King, Separation processes based on reversible chemical complexation, in R.W. Rousseau (Ed.), *Handbook of Separation Process Technology*, New York, Wiley, 1987, pp. 760.
- [65] A.E. Wentink, N.J.M. Kuipers, A.B. De Haan, J. Scholtz, and H. Mulder. Synthesis and evaluation of metal-ligand complexes for selective olefin solubilization in reactive solvents. *Ind. Eng. Chem. Res.*, 44 (2005) 4726.
- [66] M. Azhin, T. Kaghazchi, and M. Rahmani. A review on olefin/paraffin separation using reversible chemical complexation technology. *J. Ind. Eng. Chem.*, 14 (2008) 622.
- [67] T.A. Reine, R.B. Eldridge. Absorption equilibrium and kinetics for ethylene-ethane separation with a novel solvent. *Ind. Eng. Chem. Res.*, 44 (2005) 7505.
- [68] C.L. Munson, L.C. Boudreau, M.S. Driver, and W.L. Schinski, Separation of olefins from paraffins using ionic liquid solutions, Chevron, USA, Patent US 6623659 B2, 2003.
- [69] M.J. Earle, K.R. Seddon. Ionic liquids. Green solvents for the future. *Pure Appl. Chem.*, 72 (2000) 1391.
- [70] J.F. Brennecke, E.J. Maginn. Ionic liquids: Innovative fluids for chemical processing. *AIChE J.*, 47 (2001) 2384.
- [71] R.D. Rogers, K.R. Seddon. Ionic Liquids - Solvents of the Future? *Science*, 302 (2003) 792.
- [72] G.W. Meindersma, M. Maase, and A.B. De Haan, Ionic liquids, *Ullman's Encyclopedia of Industrial Chemistry*, Wiley-VCH, 2007.
- [73] T. Welton. Ionic liquids in catalysis. *Coord.Chem.Rev.*, 248 (2004) 2459.

- [74] R.E. Baltus, R.M. Counce, B.H. Culbertson, H. Luo, D.W. DePaoli, S. Dai, et al. Examination of the potential of ionic liquids for gas separations. *Sep.Sci.Technol.*, 40 (2005) 525.
- [75] H. Zhao. Innovative applications of ionic liquids as "green" engineering liquids. *Chem.Eng.Commun.*, 193 (2006) 1660.
- [76] X. Han, D.W. Armstrong. Ionic liquids in separations. *Acc.Chem.Res.*, 40 (2007) 1079.
- [77] N.V. Plechkova, K.R. Seddon. Applications of ionic liquids in the chemical industry. *Chem.Soc.Rev.*, 37 (2008) 123.
- [78] P. Wasserscheid, T. Welton, *Ionic Liquids in Synthesis*, Weinheim, Wiley-VCH, 2008.
- [79] K. Haerens, E. Matthijs, A. Chmielarz, and B. Van der Bruggen. The use of ionic liquids based on choline chloride for metal deposition: A green alternative? *J.Environ.Manage.*, 90 (2009) 3245.
- [80] K. Haerens, E. Matthijs, K. Binnemans, and B. Van Der Bruggen. Electrochemical decomposition of choline chloride based ionic liquid analogues. *Green Chem.*, 11 (2009) 1357.
- [81] H. Olivier-Bourbigou, L. Magna, and D. Morvan. Ionic liquids and catalysis: Recent progress from knowledge to applications. *Appl. Catal. A-Gen.*, 373 (2010) 1.
- [82] S.W. Kang, K. Char, J.H. Kim, C.K. Kim, and Y.S. Kang. Control of ionic interactions in silver salt-polymer complexes with ionic liquids: Implications for facilitated olefin transport. *Chem. Mater.*, 18 (2006) 1789.
- [83] L.M. Galán, *Functionalized ionic liquids. Absorption solvents for carbon dioxide and olefin separation*. PhD dissertation. Eindhoven University of Technology, (2008).
- [84] A. Ortiz, A. Ruiz, D. Gorri, and I. Ortiz. Room temperature ionic liquid with silver salt as efficient reaction media for propylene/propane separation: Absorption equilibrium. *Sep. Purif. Technol.*, 63 (2008) 311.

- [85] L.M. Galán, G.W. Meindersma, and A.B. Haan. Potential of silver-based room-temperature ionic liquids for ethylene/ethane separation. *Ind. Eng. Chem. Res.*, 48 (2009) 10650.
- [86] A. Ortiz, D. Gorri, A. Irabien, and I. Ortiz. Separation of propylene/propane mixtures using Ag^+ -RTIL solutions. Evaluation and comparison of the performance of gas-liquid contactors. *J.Membr.Sci.*, 360 (2010) 130.
- [87] A. Ortiz, L.M. Galán, D. Gorri, A.B. De Haan, and I. Ortiz. Kinetics of reactive absorption of propylene in RTIL- Ag^+ media. *Sep. Purif. Technol.*, 73 (2010) 106.
- [88] A. Ortiz, L.M. Galán Sanchez, D. Gorri, A.B. De Haan, and I. Ortiz. Reactive ionic liquid media for the separation of propylene/propane gaseous mixtures. *Ind. Eng. Chem. Res.*, 49 (2010) 7227.
- [89] A. Ortiz, Process intensification in the separation of olefin/paraffin mixtures, PhD dissertation. Universidad de Cantabria, (2010).
- [90] S. Kasahara, E. Kamio, R. Minami, and H. Matsuyama. A facilitated transport ion-gel membrane for propylene/propane separation using silver ion as a carrier. *J.Membr.Sci.*, 431 (2013) 121.



Screening of ionic liquids

Abstract

The solubility of propane and propylene in 7 ionic liquids, EMImBF₄, HMImBF₄, OMImBF₄, BMImNO₃, BMImTf₂N, MOOONTf₂N and BMMMNTf₂N is evaluated in this chapter. The equilibrium isotherms of both pure gases were measured in the pure ionic liquids and in presence of a silver salt containing the same anion than the ionic liquid in a range of concentration of 0-1 M at temperatures between 288 and 308 K and pressures ranging from 0 to 7 bar. Henry's law constants values for physical solubility as well as the characteristic parameters for chemical solubility such as chemical equilibrium constants and enthalpies of the chemical reactions between silver cations and propylene are reported. Afterwards the predictive capability of COSMO-RS methodology was evaluated through a comparison of estimated values with the experimental solubility data. Finally the COSMO-RS approach was applied to do a screening of 696 RTILs and select the most suitable ionic liquid-silver salt for C₃H₆/C₃H₈ separation.

2.1. Introduction

The most common absorption solvents for selective separation of olefin from paraffin mixtures usually consist of aqueous solutions of a transition metal salt [1-3]. However, in a high polar solvent the affinity for the gas olefin is low and the high solvation degree is equivalent to a reduced availability of the metal cation to react with the olefin [4-8]. Also, the high degree of solvation is associated to higher metal cation instability. Moreover the water content of the treated stream must be removed, particularly if the olefin is sent to a polyolefin plant that requires olefin streams of high purity, which finally entails a negative impact in the energy and economic balance of the global process [1-3,9,10]. Therefore some authors have proposed the use of RTILs containing silver ions as reaction media in the separation process of olefins from paraffins [11-19]. ILs can be used to control the interaction between the silver cation (Ag^+) and its counteranion (X^-) in an IL/silver salt system, with the result that the silver cation becomes chemically more active in forming silver–olefin complexes and therefore the olefin capacity and selectivity can be synergetically enhanced [20,21]. The selection of the IL is basically affected by the solubility of the olefin. Camper et al. [22] reported the Henry's law constants of a group of hydrocarbons in BMImPF_6 , BMImBF_4 , EMImTf_2N , $\text{EMImCF}_3\text{SO}_3$ and EMImDca at 315 K. Mokrushin et al. [23] studied the use of several RTILs as entrainers in propene-propane separation. Munson et al. [11] tested the separation of n-butene/butane by ionic liquids containing a silver salt. Galán et al. [21,24] presented the effects of different cations and anions in Ag^+ -based ILs on the absorption of ethane and ethylene. Ortiz et al. [16,25-27] evaluated the solubility of propane and propylene in BMImBF_4 and BMPyBF_4 containing a silver salt. They reported the physicochemical characteristics of the reactive system, including thermodynamic and kinetic data of the complexation reaction between propylene and silver cations in the ionic liquids BMImBF_4 and BMPyBF_4 showing an improvement of the solvent capacity of ionic liquids compared to conventional aqueous solutions in terms of olefin uptake

as well as separation selectivity. This thesis corresponds to the continuation of the previous work done in a previous thesis by Ortiz [27].

Despite the number of publications on gas solubility in ionic liquids is steeply growing, the huge amount of ionic liquids that can be synthesized suggests the need of a tool to estimate the equilibrium solubility of a gas in different ionic liquids. Several methods have been reported to predict the thermodynamic behavior of different compounds in ionic liquids, ranging from molecular dynamics (MD) using atomistic force fields, over quantitative structure–property relationship (QSPR) models, to classical thermodynamic models such as NRTL, UNIQUAC or UNIFAC [28-32]. The main drawback is that most of the parameters of these models must be determined from a large amount of experimental data that are not available for the vast majority of ionic liquids [33]. On the contrary, the quantum chemistry based of the “conductor-like screening model for real solvents” (COSMO-RS) method has a small and general parameter set that does not need to be adjusted to specific ILs and therefore it can be applied in a predictive way to the full range of ILs. The COSMO-RS calculations are based on a unique combination of a quantum chemical treatment of solutes and solvents with an efficient statistical thermodynamics procedure for the molecular surface interactions which finally enables the efficient calculation of many properties that other methods can barely predict. Thus, in this sense COSMO-RS approach is a unique a priori computational tool which can be applied to predict the equilibrium solubility of a gas in a given ionic liquid based on the structural information of the compounds [34-38].

The main objective of this chapter is to develop a predictive procedure to select the optimum set of ionic liquids and silver salt to carry out the separation of olefin/paraffin gas mixtures by reactive absorption. For this purpose the gas-liquid equilibrium behavior of propane and propylene into 7 ionic liquids with different structures at pressures between 0 and 7 bar, temperatures in the range 288-308 K and silver concentrations from 0 to 1 M has been characterized. Afterwards the

COSMO-RS methodology has been validated and applied to predict the physical solubility and thermodynamic selectivity of propane and propylene in different ionic liquids. A computational screening of 696 ionic liquids was carried out, considering different structures by varying the types of anions and cations and also the number and length of radical substituents of the cation. In addition, a qualitative study of the solubility of 8 commercially available silver salts into ionic liquids that contain the same anion was performed in order to select the most suitable silver salt.

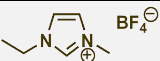
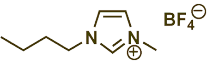
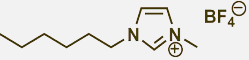
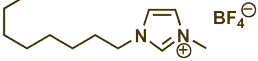
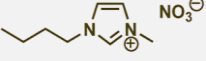
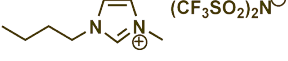
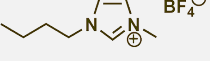
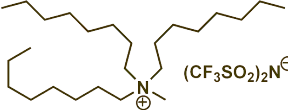
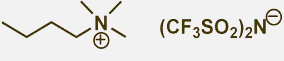
2.2. Experimental methods

2.2.1. Materials

Propylene and propane gas were purchased from Praxair with a minimum purity of 99.5 %. The ionic liquids selected in this work were 1-ethyl-3-methylimidazolium tetrafluoroborate (EMImBF₄) (CAS number 143314-16-3), 1-hexyl-3-methylimidazolium tetrafluoroborate (HMImBF₄) (CAS number 244193-50-8), 1-octyl-3-methylimidazolium tetrafluoroborate (OMImBF₄) (CAS number 244193-52-0), 3-methylimidazolium nitrate (BMImNO₃) (CAS number 179075-88-8), 1-butyl-3-methylimidazolium bis-(trifluoromethylsulphonylimide) (BMImTf₂N) (CAS number 174899-83-3), methyltrioctylammonium bis(trifluoromethylsulphonylimide) (MOOONTf₂N) (CAS number 375395-33-8) and butyltrimethylammonium bis(trifluoromethylsulphonylimide) (BMMMN Tf₂N) (CAS number 258273-75-5) supplied by Iolitec, with a minimum purity of 99 % and residual halide content less than 500 ppm. The silver salts used in this work are silver tetrafluoroborate (CAS number 14104-20-2) of 99 % purity purchased from Apollo Scientific Ltd., silver nitrate (CAS number 7761-88-8) of 99 % purity and silver bis(trifluoromethylsulphonylimide) prepared in our lab from the reaction between silver oxide (CAS number 20667-12-3) and bis(trifluoromethylsulphonylimide) (CAS number 82113-65-3) supplied by Sigma Aldrich.

The 7 different ILs studied in this chapter were selected to evaluate the effect of the different structures, including different types of cations, anions and number and length of alkyl substituents, in the propane and propylene solubility. The chemical structures of the 7 ionic liquids used in this work (and two previously reported by our research group) are collected in table 2.1.

Table 2.1. Chemical structures of the ionic liquids studied in this work

Chemical name	Abbreviation	Structure
1-ethyl-3-methylimidazolium tetrafluoroborate	EMImBF ₄	
1-butyl-3-methylimidazolium tetrafluoroborate	BMImBF ₄	
1-hexyl-3-methylimidazolium tetrafluoroborate	HMImBF ₄	
1-octyl-3-methylimidazolium tetrafluoroborate	OMImBF ₄	
1-butyl-3-methylimidazolium nitrate	BMImNO ₃	
1-butyl-3-methylimidazolium bis(trifluoromethylsulphonylimide)	BMImTf ₂ N	
1-butyl-3-methylpyridinium tetrafluoroborate	BMPyBF ₄	
methyltrioctylammonium bis(trifluoromethylsulphonylimide)	MOOONTf ₂ N	
Butyltrimethylammonium bis(trifluoromethylsulphonylimide)	BMMMNTf ₂ N	

2.2.2. Synthesis of AgTf₂N

The AgTf₂N salt was prepared in our laboratory from the reaction between silver oxide and bis-(trifluoromethylsulphonylimide) following a synthesis route which is rather similar to earlier literature procedures [39,40]. For this preparation route, pure silver oxide (Ag₂O) is dissolved in an aqueous solution of H[Tf₂N] and the reaction takes place under stirring at room temperature for 8 hours. Afterwards, the mixture was filtered in order to remove possible solid impurities or unreacted Ag₂O particles and subsequently the Ag[Tf₂N] silver salt was isolated as a white solid by evaporation under vacuum (P= 1 mbar) at room temperature and dark conditions.

2.2.3. Gas solubility measurements

Gas solubility of C₃H₈ and C₃H₆ in the ionic liquids EMImBF₄, HmImBF₄, OMImBF₄, BMImNO₃, BMImTf₂N, MOOONTf₂N and BMMMNTf₂N was determined using an autoclave and the isochoric saturation technique. This method calculates the amount of gas absorbed by subtracting the amount of gas that is in the vapor phase at the equilibrium from the total amount of gas introduced into the system.

In order to begin the absorption experiments 15 mL of the silver–ionic liquid mixture were added to the autoclave. The temperature of the system was controlled by fluid circulation in conjunction with computer controlled electric heating with a type K thermocouple (Assy) placed inside the lower chamber and automatically maintained within 0.1 K of the setpoint. Air was removed by applying vacuum (<2 mbar) to the gas cylinder and the stirred tank reactor by a vacuum pump Telstar 2P-3. The valve was closed, separating the two chambers. Then a gas sample was injected into the gas cylinder (V₀= 144 mL) to a desired pressure (p₀) which was measured by a digital pressure gauge (Omega Engineering DPG1000B-30V100G with an accuracy of ± 0.017 bar). Afterwards, the stirrer was turned on (1500 rpm) and the gas was introduced into the autoclave. The pressure of the system changed with time as the gas was

being absorbed into the liquid phase. The pressure and temperature readings were recorded over time until the pressure remained constant for 10 minutes. The autoclave pressure was measured with a pressure transducer (Hirsschmann12B-GDM0-25 bar with an accuracy of ± 0.001 bar). The final pressure (p_f) and the final volume ($V_f = 195$ mL), which is equal to the sum of the gas cylinder (144 mL) and the reactor (66 mL) minus the volume occupied by the liquid (15 mL) inside the reactor, were used to calculate the total amount of gas absorbed into the ionic liquid. Once the final equilibrium conditions were recorded, the stirrer was stopped, and the solution was regenerated by stirring under vacuum (<2 mbar) for a subsequent absorption experiment. Figure 2.1 shows a schematic diagram of the experimental set up.

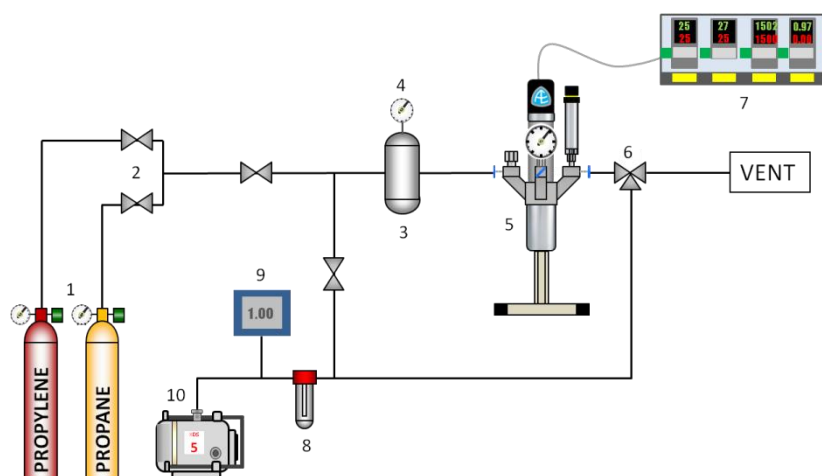


Figure 2.1. Experimental set up for gas solubility measurements.

1-Gas bottles, 2-Two-way valves, 3-Gas cylinder, 4-Pressure gauge, 5-Stirred tank reactor, 6-Three-way valve, 7-Control box, 8-Liquid trap, 9-Vacuometer, 10-Vacuum pump.

Gas solubilities were obtained for the pure ionic liquids at different pressures between 0 and 7 bar and temperatures ranging from 288 to

318 K. Furthermore, the effect of the addition of a suitable silver salt (with the same anion as the ionic liquid) in the range 0-1 M on the solubility of both gases has been analyzed and the reaction parameters (equilibrium constants and enthalpies of reaction) between the silver cations and propylene were determined.

Each experiment was performed twice and the experimental error was determined. The weighted standard deviation, defined by eq. 2.1 was calculated leading to values of $\sigma_{\text{EXP}} < 0.02$ concluding that the experiments were replicable.

$$\sigma_{\text{EXP}} = \sqrt{\frac{\sum_{i=1}^n \left(\frac{C_{\text{exp}} - C'_{\text{exp}}}{C_{\text{exp}}} \right)^2}{n-1}} \quad (2.1)$$

For the gas solubility calculation the following assumptions were undertaken:

- i. The absorption liquid was non-volatile at the absorption conditions.
- ii. The amount of initial gas absorbed in the ionic liquid is negligible.
- iii. No volume change of the liquid was observed.
- iv. Ideal gas behavior is observed.

The total moles of gas introduced into the system are:

$$n_0 = p_0 \cdot V_0 / R \cdot T \quad (2.2)$$

The mass of gas present in the pure gas phase at equilibrium is:

$$n_f = p_f \cdot V_f / R \cdot T \quad (2.3)$$

Then the gas solubility in the ionic liquid is:

$$C_i = (n_0 - n_f) / V_{\text{IL}} \quad (2.4)$$

where C_i ($\text{mol}\cdot\text{L}^{-1}$) is the gas solubility in the ionic liquid, p_0 (bar) and p_f (bar) are the initial gas pressure and the gas pressure at the equilibrium respectively, T (K) is the temperature of the system and R ($\text{bar}\cdot\text{L}\cdot\text{mol}^{-1}\cdot\text{K}^{-1}$) is the universal gas constant.

2.2.4. Computational details

This study was performed in collaboration with the Departamento de Química Física Aplicada of the Universidad Autónoma de Madrid. The COSMO-RS calculations were carried out following a multistep procedure. First, the software Gaussian03 was used for the quantum-chemical calculation to generate the COSMO files for each of the studied compounds [41]. For this purpose, the molecular geometries of the gaseous solutes and the ILs were optimized at the B3LYP/6-31++G** computational level, while the molecular geometries of the silver salts were optimized at the B3LYP/DGDZVP computational level. The optimization of the molecular geometry of every compound was performed considering a gas phase environment. In each case, vibrational frequency calculations were checked to confirm the presence of an energy minimum state. Two different molecular models, [C+A] and [CA], were used to simulate IL solvents in COSMO-RS calculations, that consider the ionic liquid as independent counterions, [C+A], and ion-paired structures, [CA], respectively. To perform the molecular model of independent counterions in COSMO-RS calculations, ILs were treated as equimolar mixtures of cations and anions. The COSMO files include the ideal screening charges on the molecular surface of each species, calculated by the COSMO continuum solvation model using theory level BVP86/TZVP/DGA1. Subsequently, COSMO files were used as an input in the COSMOthermX [42] code to calculate the Henry's law constant of propane and propylene and excess enthalpies of silver cations in different ILs. Henry's law constants were estimated attending to the expression:

$$H'_i = \gamma^\infty \cdot p_i \quad (2.5)$$

where γ^∞ is the activity coefficient of the propane or propene solute in the IL at infinite dilution and p_i is the vapor pressure of pure propane or propene (MPa) at the studied temperature. According to this chosen quantum method, the functional, and the basis set, we used the corresponding parametrization (BP_TZVP_C21_0111) that is required for the calculation of physicochemical data and contains intrinsic parameters of COSMOtherm, as well as specific parameters. The errors in the Henry's constants of both hydrocarbons in the different ionic liquids calculated using the implemented COSMO-RS approach against experimental data previously obtained were determined by calculating the mean prediction error (MPE) and the standard deviation (eqs. 2.6 and 2.7):

$$\text{MPE} = \frac{1}{N} \sum_{i=1}^N \frac{|H'_{\text{EXP}} - H'_{\text{COSMO-RS}}|}{H'_{\text{EXP}}} \cdot 100 \quad (2.6)$$

$$\sigma_{\text{COSMO-RS}} = \sqrt{\frac{\sum_{i=1}^n \left(\frac{H'_{\text{EXP}} - H'_{\text{COSMO-RS}}}{H'_{\text{EXP}}} \right)^2}{n-1}} \quad (2.7)$$

where n is the total number of data used, $H_{\text{COSMO-RS}}$ is the Henry's constant of propane or propylene obtained by COSMO-RS and H_{EXP} is the corresponding value experimentally determined.

2.3. Results and discussion

2.3.1. Physical solubility in RTILs

To further examine the role of physical solubility in the absorption equilibrium curves, silver-free ionic liquids were used as absorption media. In previous works carried out by our research group it was observed that the equilibrium curves for propylene and propane generated with the silver-free ionic liquids showed an ideal Henry's law behavior in the studied range of pressures [16]. Furthermore, solubility

data showed that RTILs showed higher affinity for propylene than for propane. As representative, Figure 2.2 shows solubility values obtained in this work using pure EMImBF₄ as absorbing liquid. Results obtained with this ionic liquid follow the general observed trend, where the gas solubility increases with pressure (linearly), decreases with temperature and propylene is slightly more soluble than propane.

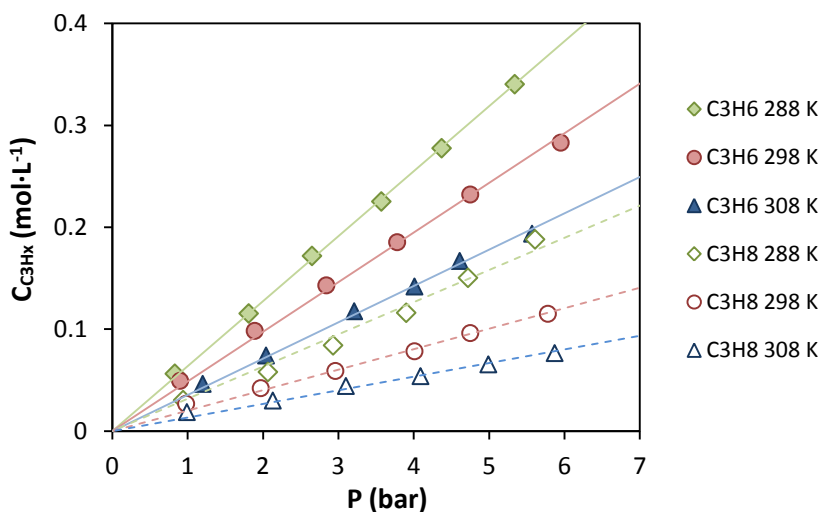


Figure 2.2. Physical solubility of C₃H₈ and C₃H₆ in EMImBF₄.

The Henry's law is defined by the following equation:

$$H_i = \frac{C_i}{p_i} \quad (2.8)$$

where H_i is the Henry's law constant in mol·L⁻¹·bar⁻¹, C_i is the concentration of the gas in the liquid phase in mol·L⁻¹ and p_i is the gas partial pressure in bar. The Henry's law constants for both gases at different temperatures are collected in table 2.2. In this table we include some data previously published by our research group [25] to facilitate the analysis and comparison.

Table 2.2. Henry's constants ($\text{mol}\cdot\text{L}^{-1}\cdot\text{bar}^{-1}$) of C_3H_8 and C_3H_6 in the ionic liquids under study at different temperatures.

	T = 288 K		T = 298 K		T = 308 K	
	C_3H_8	C_3H_6	C_3H_8	C_3H_6	C_3H_8	C_3H_6
EMImBF ₄	0.032	0.064	0.020	0.049	0.013	0.036
BMImBF ₄ [25]	0.045	0.103	0.028	0.069	0.011	0.055
HMImBF ₄	0.090	0.155	0.064	0.125	0.048	0.088
OMImBF ₄	0.104	0.167	0.085	0.125	0.070	0.096
BMImNO ₃	0.045	0.077	0.028	0.063	0.022	0.042
BMImTf ₂ N	0.108	0.146	0.074	0.094	0.056	0.074
BMPyBF ₄ [25]	0.047	0.103	0.034	0.079	0.024	0.064
MOOONTf ₂ N	0.329	0.329	0.224	0.239	0.156	0.169
BMMMNTf ₂ N	0.103	0.169	0.070	0.129	0.054	0.092

It is observed that in the 9 ionic liquids and for both gases the gas solubility decreases with increasing the temperature of the system. This dependence with temperature can be described using an Arrhenius type equation (eq. 2.9) [43].

$$H(T) = H_0 e^{\frac{-\Delta H_{\text{sol}}}{RT}} \quad (2.9)$$

where H is the Henry's constant at a given temperature ($\text{mol}\cdot\text{L}^{-1}\cdot\text{bar}^{-1}$), H_0 is the pre-exponential factor, ΔH_{sol} is the solvation enthalpy ($\text{kJ}\cdot\text{mol}^{-1}$), R is the gas constant ($\text{kJ}\cdot\text{mol}^{-1}\cdot\text{K}^{-1}$) and T is the temperature (K). Therefore, the logarithm of the H values of propylene and propane were plotted against the reciprocal of the temperature (figure 2.3), showing a linear relationship. From this linearization, parameters that characterize the solubility such as the pre-exponential factor (H_0) and the standard solvation enthalpy for every IL were obtained (table 2.3).

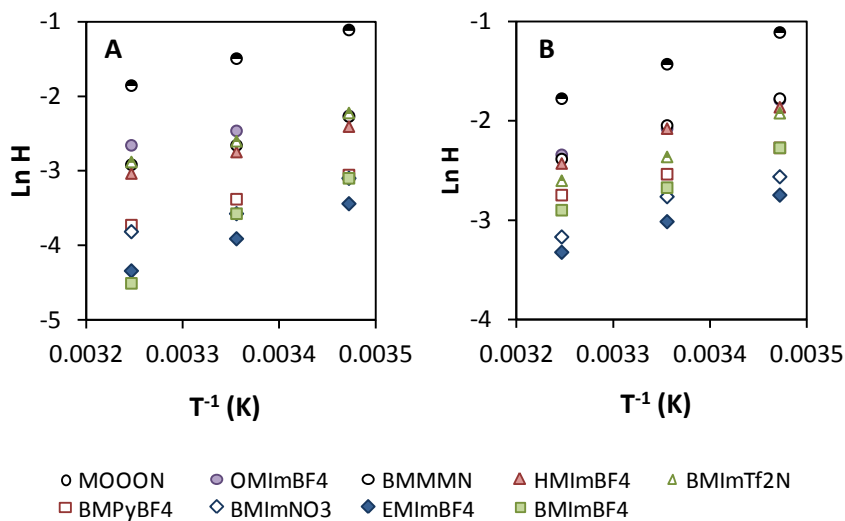


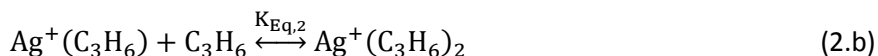
Figure 2.3. (A) C_3H_8 and (B) C_3H_6 Henry's constants as a function of the temperature.

Table 2.3. Solubility parameters of C_3H_8 and C_3H_6 in pure ionic liquids.

	C_3H_8		C_3H_6	
	H_0 ($\text{mol} \cdot \text{L}^{-1} \cdot \text{bar}^{-1}$)	ΔH_{sol} ($\text{kJ} \cdot \text{mol}^{-1}$)	H_0 ($\text{mol} \cdot \text{L}^{-1} \cdot \text{bar}^{-1}$)	ΔH_{sol} ($\text{kJ} \cdot \text{mol}^{-1}$)
EMImBF ₄	$5.75 \cdot 10^{-8}$	-31.6	$8.52 \cdot 10^{-6}$	-21.4
BMImBF ₄ [25]	$1.84 \cdot 10^{-7}$	-29.5	$4.28 \cdot 10^{-6}$	-24.1
HMIImBF ₄	$5.51 \cdot 10^{-6}$	-23.2	$2.79 \cdot 10^{-5}$	-20.7
OMImBF ₄	$2.59 \cdot 10^{-4}$	-14.3	$3.14 \cdot 10^{-5}$	-20.5
BMImNO ₃	$1.16 \cdot 10^{-5}$	-21.6	$2.88 \cdot 10^{-6}$	-24.5
BMImTf ₂ N	$4.14 \cdot 10^{-6}$	-24.3	$4.21 \cdot 10^{-6}$	-25.0
BMPyBF ₄ [25]	$1.52 \cdot 10^{-6}$	-24.8	$6.14 \cdot 10^{-5}$	-17.8
MOOONTf ₂ N	$3.52 \cdot 10^{-6}$	-27.4	$1.19 \cdot 10^{-5}$	-24.5
BMMMNTf ₂ N	$3.93 \cdot 10^{-6}$	-24.3	$1.49 \cdot 10^{-5}$	-22.4

2.3.2. Gas solubility in Ag⁺-RTILs media

In order to improve the absorption capacity for propylene and the thermodynamic selectivity, silver cations as complexation agent were added to the ionic liquid and the effect of temperature, silver concentration and pressure in the separation performance were analyzed. In π -complexation systems, although in most cases only complexes with a 1:1 silver–olefin stoichiometry are formed in significant amounts, under certain conditions (high silver loading, high propylene partial pressure, and low temperature), complexes with different stoichiometries like the secondary complex with 1:2 silver–olefin stoichiometry can exist. The reversible formation of organometallic complexes of olefin-silver in the reactive phase proceeds according to reactions 2.a and 2.b [8,44].



The isotherms of propylene solubility with the silver reactive media exhibited nonlinear profiles with pressure as shown in figure 2.4 for the case of EMImBF₄-AgBF₄ mixtures. As previously expected, the data showed positive influences of both, the gas pressure as well as the silver concentration on the solubility of propylene. However, for the system BMImNO₃-AgNO₃ the propylene solubility showed a linear dependence with pressure, providing the same solubility values as the pure BMImNO₃. This fact indicates that the system containing NO₃⁻ resulted ineffective to carry out the reactive absorption of propylene, which is in good agreement with the results obtained by Galán et al. [24] for ethylene absorption.

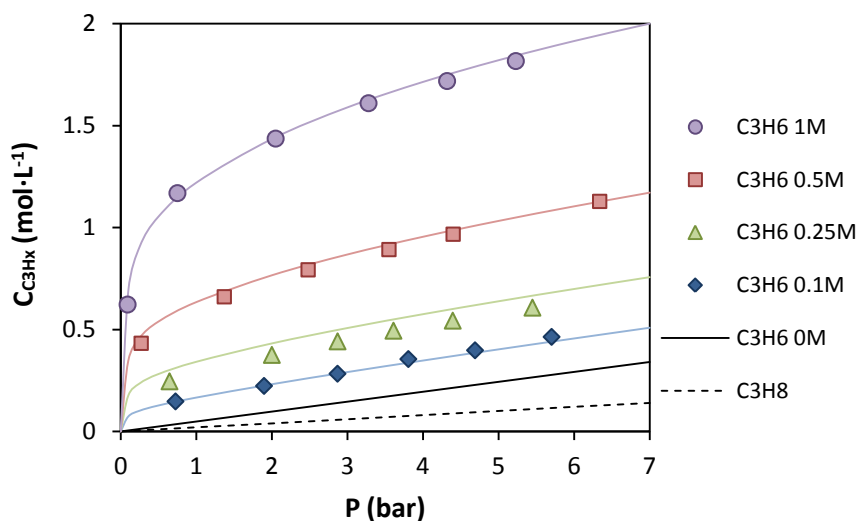


Figure 2.4. Equilibrium isotherms of C_3H_8 and C_3H_6 at 298K in EMImBF₄. (markers) experimental; (lines) calculated.

However, the solubility of propylene increases with decreasing the temperature, showing that the absorption of propylene is an exothermic process which can be enhanced at low temperatures (figure 2.5). The equilibrium constants ($K_{Eq,1}$ and $K_{Eq,2}$) for the complexation reactions depend on temperature and can be described by the Van't Hoff equation [45].

$$\frac{d \ln K_{Eq}}{d(1/T)} = -\frac{\Delta H_r}{R} \quad (2.10)$$

where K_{Eq} is the equilibrium constant in $L \cdot mol^{-1}$, T is the temperature (K), ΔH_r is the enthalpy of reaction ($kJ \cdot mol^{-1}$) and R is the gas constant ($kJ \cdot mol^{-1} \cdot K^{-1}$).

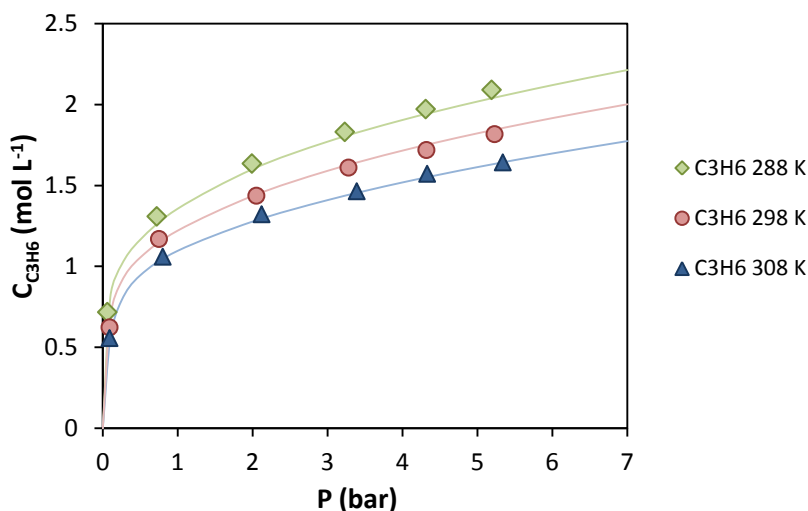


Figure 2.5. Equilibrium isotherms of C_3H_6 in EMImBF₄ with 1 M AgBF₄ (markers) experimental; (lines) calculated.

In order to successfully describe the absorption process an equilibrium model based on the formation of two organometallic complexes between silver cations and propylene was proposed [16]. The unknown parameters such as the enthalpies of reactions ($\Delta H_{r,1}$ and $\Delta H_{r,2}$) as well as the equilibrium constants at 298 K ($K_{\text{Eq},1}$ (298 K), $K_{\text{Eq},2}$ (298 K)) were estimated using the experimental data series and the parameter estimation tool of the software Aspen Custom Modeler. A comparison was made between simulated and experimental values (as representative, see figures 2.4 and 2.5). The weighted standard deviation between experimental and simulated values of the reactive gas absorption was calculated as $\sigma < 0.03$. The accuracy of the simulation is presented in the parity graph shown in figure 2.6 where predicted concentration values (C_{sim}) are plotted versus experimental data (C_{exp}) obtained under the conditions studied in this work. All the results of C_{sim} fall within the interval $C_{\text{exp}} \pm 10 \% C_{\text{exp}}$, showing a good agreement between experimental and simulated results.

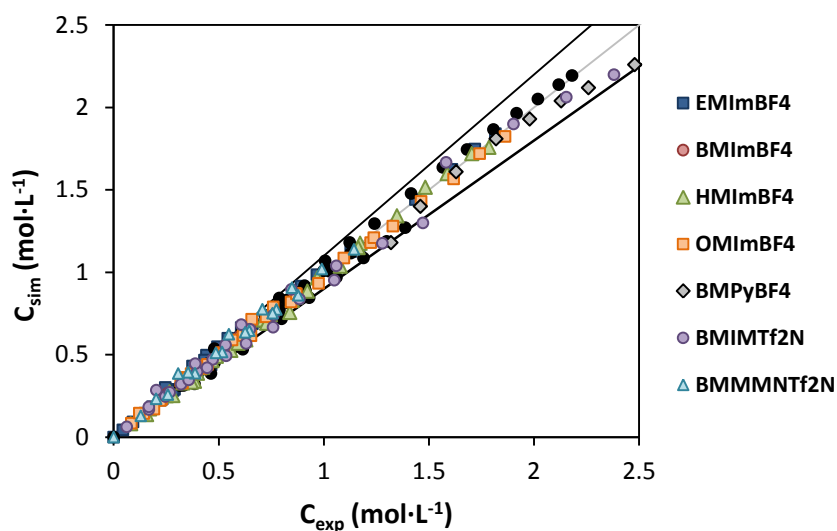


Figure 2.6. Parity graph of propylene for simulated and experimental equilibrium values.

The values of the estimated model parameters are shown in table 2.4.

Table 2.4. Complexation enthalpies and equilibrium constants at 298 K.

	$K_{Eq,1}$ (298K) (L·mol ⁻¹)	$K_{Eq,2}$ (298K) (L·mol ⁻¹)	$\Delta H_{r,1}$ (kJ·mol ⁻¹)	$\Delta H_{r,2}$ (kJ·mol ⁻¹)
EMImBF ₄	398	5.71	-16.1	-18.2
BMImBF ₄ [25]	338	4.90	-13.1	-40.8
HMImBF ₄	48.2	0.50	-64.8	-149
OMImBF ₄	49.3	0.70	-80.1	-64.4
BMIMTf ₂ N	130	5.90	-18.4	-47.5
BMPyBF ₄ [25]	166	26.3	-21.3	-51.6
BMMMNTf ₂ N	27.8	7.50	-29.4	-38.9

With the equilibrium constants of the systems based on the BMIm cation shown in table 2.4 it is possible to assess the effect of the anion in the separation performance. As previously discussed, the system based on the NO_3^- anion did not offer any enhancement when adding the silver salt to the IL. On the other hand, although the system based on the Tf_2N^- anion showed an important increase in the solubility of propylene in presence of the silver salt AgTf_2N , the ionic liquid BMImBF₄ combined with AgBF_4^- provided the best results in terms of propylene capacity and thermodynamic selectivity (eq. 2.11).

$$\text{Selectivity} = \frac{\left(\frac{C_{\text{C}_3\text{H}_6}^T}{C_{\text{C}_3\text{H}_8}^T} \right)}{\left(\frac{P_{\text{C}_3\text{H}_6}}{P_{\text{C}_3\text{H}_8}} \right)} \quad (2.11)$$

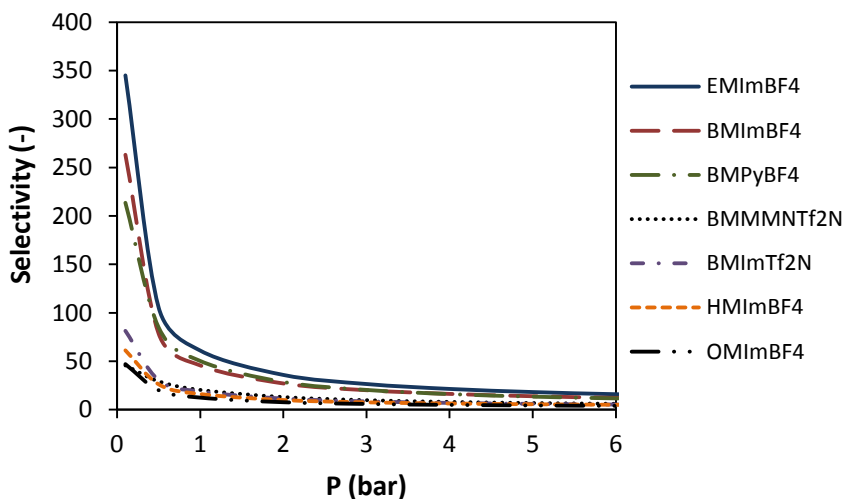


Figure 2.7. Effect of pressure on the thermodynamic selectivity with $[\text{Ag}^+] = 1 \text{ M}$ and 298 K .

Figure 2.7 shows the effect of pressure on the thermodynamic selectivity. The selectivity reached the highest value at the lowest gas partial pressure because the physical solubility effects were dominated by the chemical complexation effects. On the contrary, at partial pressures above 3 bar, the selectivity starts to level out because under

these conditions the silver sites are becoming saturated. As it can be seen in figure 2.7, for the ionic liquids containing the same anion (EMImBF₄, BMImBF₄, HMImBF₄ and OMImBF₄) the selectivity increases when the length of the alkyl substituents in the cation decreases. This is because shorter alkyl chains provide lower physical solubility of both gases, and therefore the separation process is dominated by the effect of the chemical reaction. Therefore, based upon the experimental results, ionic liquids based on imidazolium cations with less and shorter alkyl substituents improve the selective separation of these mixtures. Regarding the structure of the anion it was gathered that ionic liquids with BF₄⁻ anion, combined with the AgBF₄ silver salt provided the best results in terms of olefin capacity and selectivity.

2.3.3. Optimization of COSMO-RS approach to predict the C₃H₈ and C₃H₆ solubility in c liquids

It was experimentally observed that the solubility of propane and propylene in different silver-free ionic liquids exhibited an ideal behavior. Hence the physical solubility of the individual gas component at moderate pressures can be described by the Henry's law. In this section the Henry's law is used in the form described by COSMO-RS (eq. 2.12).

$$H_i' = \frac{p_i}{x_i} \quad (2.12)$$

where H_i' is the Henry's constant, p_i is the partial pressure of the gas in MPa and x_i is the molar fraction of the gas in the ionic liquid.

Thus, assuming an ideal behavior of these mixtures the equilibrium selectivity ($\alpha_{i/j}$) can be determined as the ratio between the Henry's constant of each gas in the ionic liquid (eq. 2.13).

$$\alpha_{i/j} = \frac{H_j'}{H_i'} \quad (2.13)$$

In order to evaluate the capability of COSMO-RS to predict the Henry's law constants of propane and propylene in the considered ionic liquids, the Henry's constants predicted by COSMO-RS were compared against a set of experimental data previously obtained. The comparison included values of the Henry's constants of both propane and propylene in different ionic liquids varying the nature of the cation, the alkyl chain length of the cation and the anion at temperatures in the range of 278–318 K (figures 2.8 A and 2.8 B). The linear regressions obtained between experimental and computed H data (eqs. 2.14 and 2.15) suggest the capability of the COSMO-RS approach to predict qualitatively the trend of the Henry's constants of propane and propylene in ionic liquids. However in order to calculate the solubility of both hydrocarbons in different ionic liquids more accurately the computational method was improved by calibrating against a limited set of experimental data (figures 2.8 A and 2.8 B).

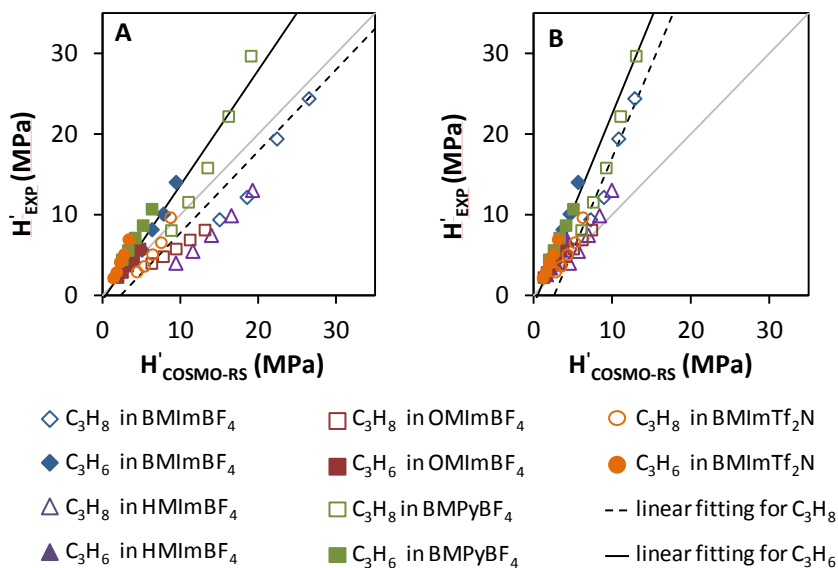


Figure 2.8. Comparison between experimental and predicted C_3H_8 and C_3H_6 Henry's constants in different ionic liquids at temperatures between 278 and 318 K by standard COSMO-RS using A) [C+A] approach and B) [CA] approach.

Figures 2.8 A and 2.8 B show that although the COSMO-RS approach is suitable to predict general trends in the solubility of propane and propylene in ionic liquids it is not accurate enough to predict quantitative values of the Henry's constants. Moreover, in the comparison between experimental and calculated data the slopes of the linear regression fittings for both methods, [CA] (eqs. 2.14 and 2.15) and [C+A] (eqs. 2.16 and 2.17) show a systematic underestimation of the Henry's constants of both gases.

$$H'_{C_3H_8,EXP} = 2.31 \cdot H'_{C_3H_8,COSMO-RS [CA]} - 6.05 \quad (2.14)$$

$$H'_{C_3H_6,EXP} = 2.37 \cdot H'_{C_3H_6,COSMO-RS [CA]} - 1.24 \quad (2.15)$$

$$H'_{C_3H_8,EXP} = 1.01 \cdot H'_{C_3H_8,COSMO-RS [C+A]} - 2.37 \quad (2.16)$$

$$H'_{C_3H_6,EXP} = 1.43 \cdot H'_{C_3H_6,COSMO-RS [C+A]} - 0.61 \quad (2.17)$$

This difference between calculated and experimental data was corrected using the linear fittings shown in eqs. 2.14 to 2.17, and therefore an optimization of the methodology was carried out providing an enhanced tool for the estimation of the propane and propylene solubility in any ionic liquid. The results plotted in figures 2.9 A and 2.9 B show that although the optimized [C+A] model is suitable to predict the trend in the solubility of propane and propylene in different ionic liquids, the [CA] model generally provides higher accuracy in the quantitative prediction of H coefficients in ILs (MPE < 22,9 %); thus proving the potential of the optimized COSMO-RS methodology developed in this work to predict accurately the solubility of propane and propylene in different ionic liquids with imidazolium and pyridinium cations.

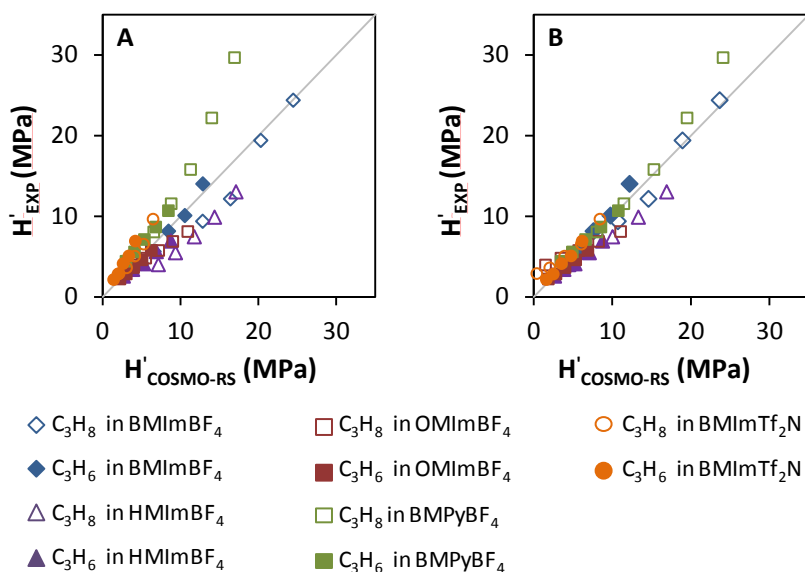


Figure 2.9. Comparison between experimental and predicted C_3H_8 and C_3H_6 Henry's constants in different ionic liquids at temperatures between 278 and 318 K by optimized COSMO-RS using A) [C+A] approach and B) [CA] approach.

It must be highlighted that the major error source in this study corresponds to the Henry's constant values obtained at higher temperatures, near 318 K, where the solubility of both hydrocarbons is very low. This is in agreement with the results previously obtained by Palomar et al. [37] where they observed that although four different COSMO-RS computational approaches were able to provide a qualitative description of the solubility-temperature trend of CO_2 in the ionic liquid HmImTf₂N in the 283-343 K temperature range, the COSMO-RS methodology was not suitable to carry out a quantitative analysis of the CO_2 solubility at different temperatures. The obtained results show that the [C+A] approach can predict the trend in the solubility of both gases into ionic liquids. Moreover, the optimized COSMO-RS methodology using the [CA] method predicts experimental results accurately enough allowing to carry out a quantitative analysis. Therefore the best way to proceed would result from a first screening of a large number of ILs

using the [C+A] method in order to select those ILs having better performance for olefin/paraffin separation, and afterwards applying the [CA] method, that involves more tedious calculations to achieve a higher accuracy in the solubility results. The detailed statistical analysis for the [C+A] and [CA] models before and after the optimization are compiled in table 2.5.

Table 2.5. Statistical results obtained from the comparison of experimental and predicted Henry's law constants of C_3H_8 and C_3H_6 in ILs at different temperatures using different COSMO-RS computational approaches.

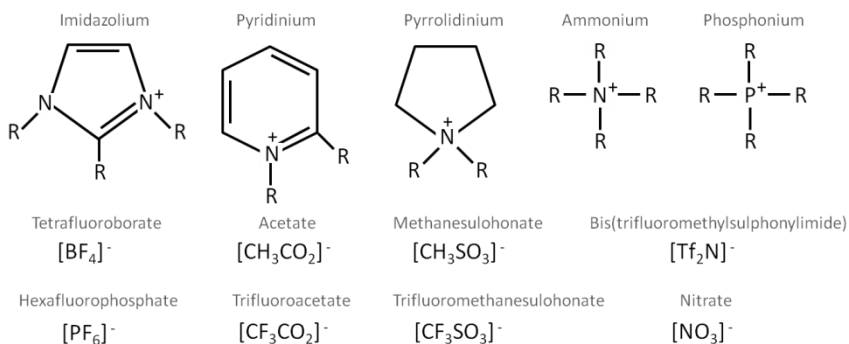
Model	Method	Gas	Slope	y-intercept	R^2	σ	MPE (%)
COSMO-RS	[C+A]	C_3H_8	1.01	-2.37	0.66	0.59	47.4
		C_3H_6	1.43	-0.61	0.85	0.29	23.6
	[CA]	C_3H_8	2.31	-6.05	0.90	0.31	24.4
		C_3H_6	2.37	-1.24	0.93	0.48	45.9
Optimized COSMO-RS	[C+A]	C_3H_8	0.76	2.07	0.66	0.37	30.9
		C_3H_6	0.93	0.64	0.81	0.25	21.3
	[CA]	C_3H_8	0.80	1.60	0.90	0.31	22.9
		C_3H_6	1.00	0.00	0.93	0.15	11.6

2.3.4. Screening of ionic liquids

Once the optimized COSMO-RS approach that is useful to evaluate the gas solubility of propane and propylene in different ionic liquids has been developed, the main objective of this work is to apply this methodology as a tool to select the most suitable ionic liquid for the selective separation of propane/propylene gas streams. In order to minimize the experimental effort to be performed, a computational

screening using COSMO-RS and the [C+A] model was carried out for 696 ionic liquids based on different cations (imidazolium, pyridinium, pyrrolidinium, ammonium and phosphonium) and anions (BF_4^- , PF_6^- , NO_3^- , Tf_2N^- , CH_3CO_2^- , CF_3CO_2^- , CH_3SO_3^- , CF_3SO_3^-). Table 2.6 compiles the cation and anion structures of the ionic liquids studied in this work.

Table 2.6. Molecular structures of the cations and anions studied in this work.



Figures 2.10 and 2.11 show the calculated solubility (as Henry's constant) of propane and propylene respectively in some of the most common ionic liquids. In general the solubility of propane and propylene follow the same trend according to the changes in the molecular structure of the ionic liquid. However, the physical selectivity increases as the solubility of both gases decreases (figure 2.12). These results are in good agreement with previous results obtained by Palomar et al. [33] working with CO_2 and N_2 . These results point to the important role that the structure of both, the anion and also the cation moieties of the ionic liquid play on the physical solubility of both hydrocarbons as well as on the separation selectivity. Generally, anions with more electron donor character such as CH_3CO_2^- or CH_3SO_3^- present higher solubilities for propylene and also for propane but at the same time lower separation selectivities. On the other hand, small anions with disperse charge like BF_4^- or PF_6^- result in lower solubilities and higher physical selectivities.

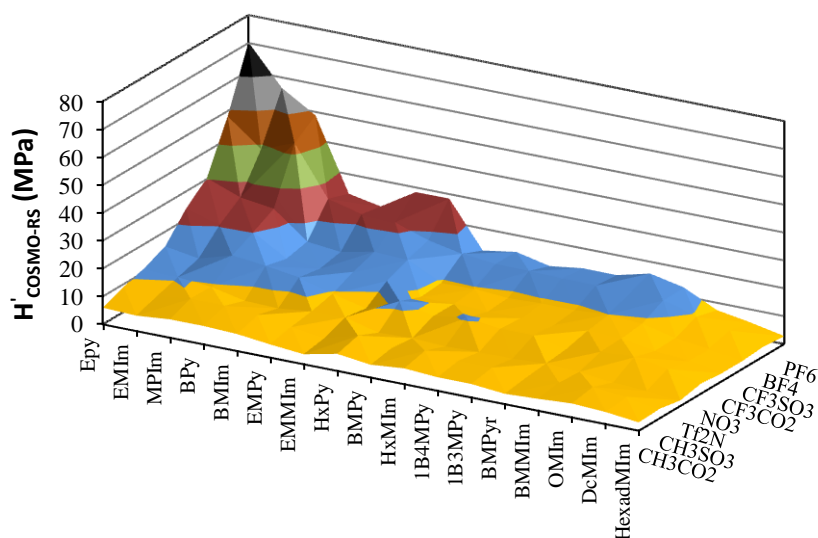


Figure 2.10. Screening of C_3H_8 solubility in the most common ionic liquids at 298 K calculated by optimized COSMO-RS approach.

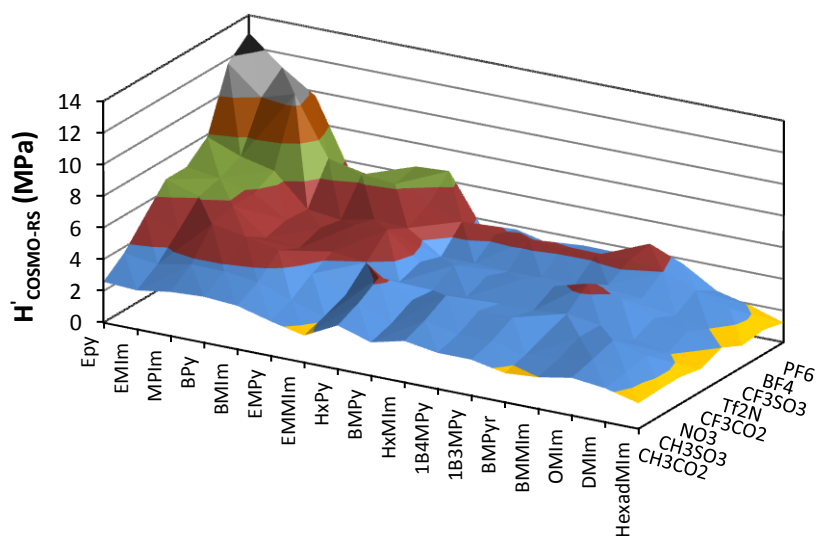


Figure 2.11. Screening of C_3H_6 solubility in the most common ionic liquids at 298 K calculated by optimized COSMO-RS approach.

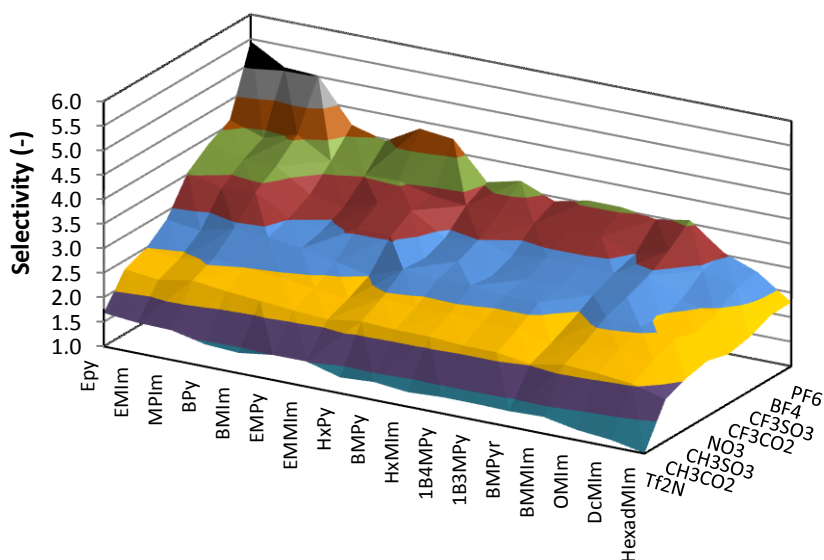


Figure 2.12. Screening of C_3H_6/C_3H_8 selectivity in some of the most common ionic liquids at 298 K calculated by optimized COSMO-RS approach.

Figures 2.10, 2.11 and 2.12 also highlight the importance of the structure of the cation in the physical solubility of both hydrocarbons and also in the thermodynamic selectivity. In order to study in more depth this influence, further studies were carried out analyzing the influence of the nature of the cation, the alkyl chain length and the number of substituents in the cation. Figure 2.13 shows the influence of the alkyl chain length of the ionic liquid in the range from 1 to 10 carbon atoms for the 1-methylimidazolium tetrafluoroborate family. The highest solubility of both gases was obtained for the cation with the longest alkyl chain (C10) because increasing the number of carbon atoms of the aliphatic substituent provides more organic character to the ionic liquid, showing more affinity for both hydrocarbons. Once more, the selectivity follows the opposite trend, increasing from 0.7 to 4.5 when the radical chain length was reduced from C10 to C1.

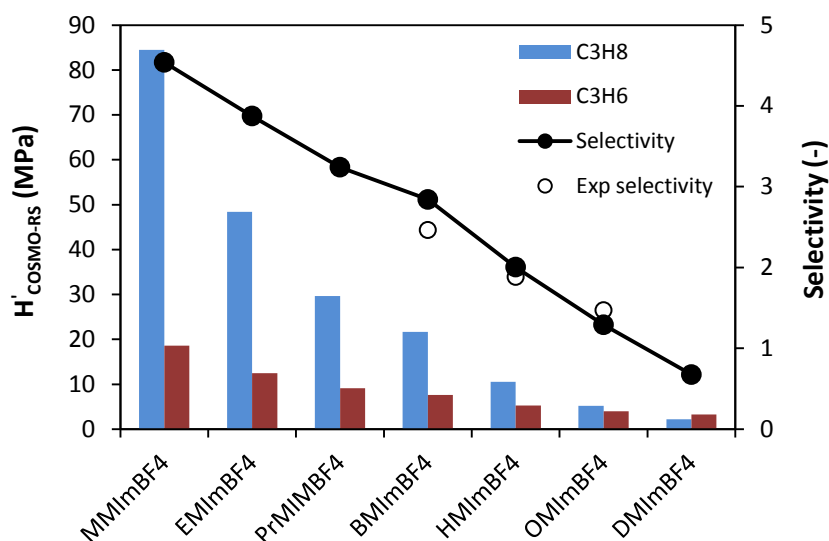


Figure 2.13. Effect of the length of the alkyl chain of the ionic liquid cation on the solubility of C_3H_8 and C_3H_6 and equilibrium selectivity.

Figure 2.14 shows the influence of the number of substituents in the cation on the gas solubility. They were analyzed both the solubility of propane and propylene as well as the separation selectivity as a function of the number of methyl groups included in the cation structure of the 1-ethyl imidazolium tetrafluoroborate family (EmBF₄). The results show that the solubility of propane and propylene slightly decreased when the number of methyl groups was reduced from 2 to 1; however the solubility was almost 7 times lower for propane and 4.6 times lower for propylene when the number of methyl substituents in the cation decreased from 1 to 0. At the same time the separation selectivity is increased from 2.6 for EMMImBF₄ to 5.1 using EmBF₄.

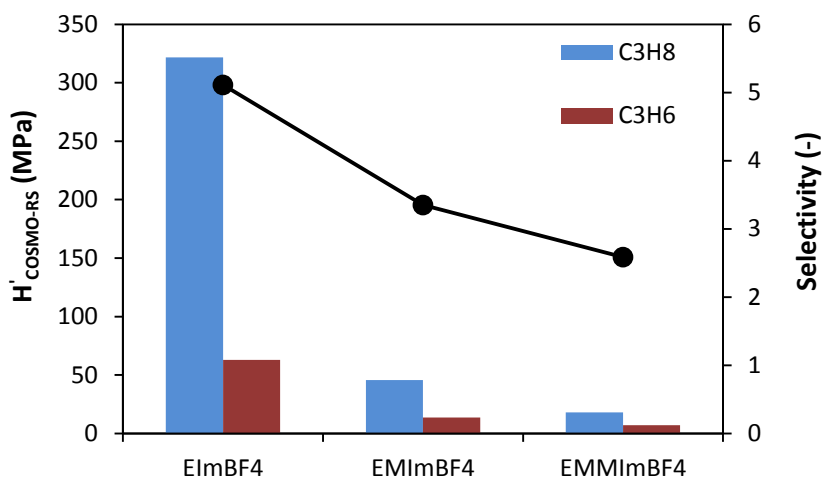


Figure 2.14. Effect of the number of substituents of the ionic liquid cation in the solubility of C₃H₈ and C₃H₆ and equilibrium selectivity.

The last variable in the ionic liquid structure under study is the type of cation. 5 different types of the most common cations (ammonium, pyridinium, pyrrolidinium, imidazolium and phosphonium) were analyzed. Figure 2.15 plots the calculated solubility of propane and propylene and the separation selectivity as a function of the type of cation of the ionic liquid at 298 K with the tetrafluoroborate anion in all cases. It shows a strong dependence of the gas solubility and with the nature of the cation. The highest solubility is obtained with phosphonium-based ionic liquids. This is because commonly phosphonium-based ionic liquids have several and long substituents that provide high affinity for both hydrocarbons, leading at the same time to the lowest separation selectivity (2.3). On the other hand imidazolium, pyridinium and pyrrolidinium-based ionic liquids provide similar results, with lower gas solubilities and separation selectivity around 3. This comparable behavior can be attributed to the similar structure of these 3 cations. However imidazolium-based ionic liquids generally have the lowest viscosities of these three families, leading to a better performance in the gas absorption process where the mass transfer in

the liquid side is often the controlling step of the process kinetics. On the other hand, ionic liquids based on monosubstituted butyl ammonium (BN^+) cation provide the lowest affinity for both gases due to the presence of the polar acidic hydrogen groups linked to nitrogen. This results in ILs with a low solubility of non-polar hydrocarbons such as C_3H_6 and C_3H_8 leading to the highest physical selectivity both gases (5.4) for the ionic liquid buthylammonium tetrafluoroborate). However, ammonium-based ionic liquids with low number of substituents usually remain in solid state at room temperature which limits their application in this field.

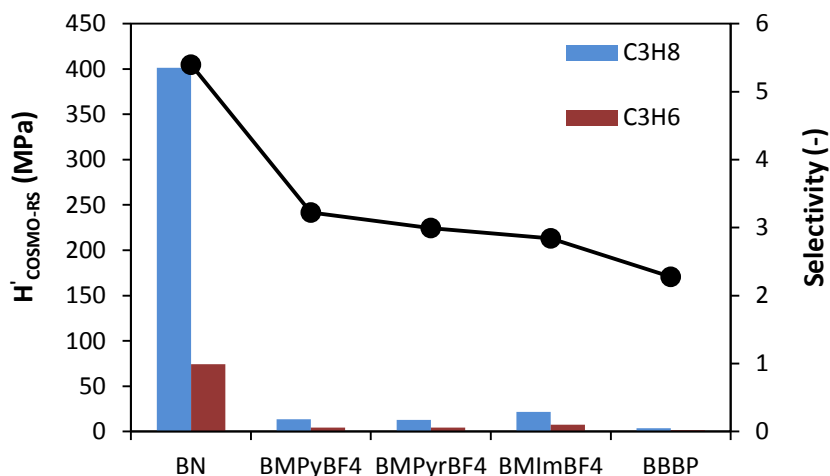


Figure 2.15. Effect of the nature of the cation in the solubility of C_3H_8 and C_3H_6 and selectivity.

2.3.5. Qualitative silver salt solubility in RTILs

Since the absorption of propylene in a given ionic liquid is enhanced by the addition of a silver salt, it is crucial to find out the most suitable silver salt to be dissolved in a specific ionic liquid. Due to the huge amount of combinations between silver salts and ionic liquids it is interesting to develop a computational approach able to predict a

qualitative trend in the solubility of different silver salts. In previous works Palomar et al. found that gas-liquid [33,36,37], liquid-liquid [46] and solid-liquid [47] equilibrium data for favorable separation processes based on IL solvents were associated to a higher exothermicity of the mixing process. This methodology was applied in this case to analyze the solubility of different silver salts in ionic liquids containing the same anion. Figure 2.16 shows the relationship between the lattice energy of 8 commercially available silver salts reported in literature [48] and the calculated excess enthalpies of the mixture IL-silver salt (H^E) for the BMIm cation family containing the same anion as the silver salt under study.

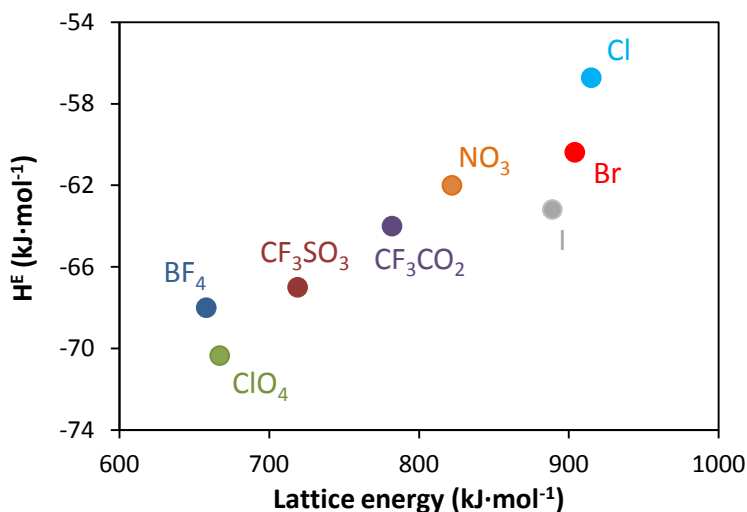


Figure 2.16. Comparison of the lattice energy of 8 commercially available silver salts with the excess molar enthalpies of Ag^+ -ILs mixtures at 298 K, calculated by the COSMO-RS/[CA] computational approach.

It can be seen that there exists a relationship between the lattice energy and the excess enthalpy of the silver salt-ILs mixture. This trend is in good agreement with the previous knowledge about the behavior of silver salts solutions. It is well known that silver halides have a negligible solubility in ILs. Previous studies also reveal that silver nitrate is not as

easy to dissolve in ILs, for instance in BMImNO₃, as in water. On the other hand AgBF₄, which has the lowest lattice energy, is soluble in different ionic liquids containing the BF₄⁻ anion such as BMImBF₄ or BMPyBF₄. COSMO-RS method anticipates that silver salts with PF₆⁻ and ClO₄⁻ should also present high solubility in ILs with common anion.

2.4. Conclusions

The selection of the most suitable Ag^+ -RTIL reaction medium for the separation of propane/propylene mixtures by reactive absorption is crucial to achieve the optimum separation performance. In this chapter equilibrium data of the absorption of propane and propylene gases in 7 ILs with different structures were obtained and the characteristic parameters of the physical and chemical solubility are reported. Afterwards a screening using the COSMO-RS methodology was applied to select the most effective ionic liquid-silver salt system to carry out the separation of olefin/paraffin gas mixtures by reactive absorption. In most cases the solubility of propane and propylene follow the same trend according to the changes in the structure of the ionic liquid. Therefore, since the absorption of olefins can be greatly enhanced by the addition of silver cations the most appropriate ionic liquid to perform the separation process is the one that shows the lowest propane solubility and at the same time is suitable to dissolve a silver salt. Concerning the anion selection, smaller symmetric anions such as BF_4^- provide the lowest solubility of both hydrocarbons and also the highest thermodynamic selectivity. Regarding the structure of the cation, ionic liquids based on imidazolium, pyridinium and pyrrolidinium presented a similar behavior in terms of physical solubility and selectivity. However, the use of imidazolium-based ionic liquids is preferred since on the whole they have the lowest viscosities of these three families, leading to a better performance in gas absorption processes where the mass transfer in the liquid side is the controlling step. Additionally, the relation between the excess enthalpy calculations and the lattice energy of 8 commercially available silver salts it was found that AgBF_4 seems to be the most suitable silver salt to be dissolved in ionic liquids containing the same anion. Thus, based upon these results it can be concluded that the most suitable system to carry out the separation of propane/propylene gas mixtures by reactive absorption should be based on an ionic liquid with the BF_4^- anion and an imidazolium-based cation with the less number and shortest alkyl groups as possible and silver tetrafluoroborate (AgBF_4) as a silver salt.

2.5. Nomenclature

C ($\text{mol}\cdot\text{L}^{-1}$)	concentration
H_i ($\text{mol}\cdot\text{L}^{-1}\cdot\text{bar}^{-1}$)	Henry's constant
H'_i (MPa)	Henry's constant
H_0 ($\text{mol}\cdot\text{L}^{-1}\cdot\text{bar}^{-1}$)	Henry's law preexponential factor
ΔH_r ($\text{kJ}\cdot\text{mol}^{-1}$)	enthalpy of reaction
ΔH_{sol} ($\text{kJ}\cdot\text{mol}^{-1}$)	standard solvation enthalpy
K_{eq} ($\text{L}\cdot\text{mol}^{-1}$)	equilibrium constant
H^E ($\text{kJ}\cdot\text{mol}^{-1}$)	excess enthalpy of the mixture
MPE (%)	mean prediction error
n (mol)	number of moles
p_i (bar)	gas partial pressure
R ($\text{kJ}\cdot\text{mol}^{-1}\cdot\text{K}^{-1}$)	universal gas constant
T (K)	temperature
V (L)	volume
x (-)	molar fraction of a gas into the liquid phase

Greel symbols

α (-)	thermodynamic selectivity
γ^∞ (-)	activity coefficient at infinite dilution
σ (-)	standard deviation

Superscripts/subscripts

COSMO-RS	computed results using COSMO-RS
EXP	experimental results
IL	ionic liquid

Ionic liquids

Cations

Im	Imidazolium
Py	Pyridinium
Pyr	Pyrrolidinium
N	Ammonium
P	Phosponium

Anions

BF_4^-	Tetrafluoroborate
PF_6^-	Hexafluorophosphate
NO_3^-	Nitrate
Tf_2N^-	Bis-(trifluoromethylsulphonylimide)
CH_3CO_2^-	Acetate
CF_3CO_2^-	Trifluoroacetate
CH_3SO_3^-	Methanesulphonate
CF_3SO_3^-	Trifluoromethanesulphonate

Alkyl chains

M	Methyl
Pr	Propyl
B	Buthyl
Hx	Hexyl
O	Octyl
D	Decyl
Hexad	Hexadecyl

2.6. References

- [1] R.B. Eldridge. Olefin/paraffin separation technology: A review. *Ind. Eng. Chem. Res.*, 32 (1993) 2208.
- [2] D.J. Safarik, R.B. Eldridge. Olefin/paraffin separations by reactive absorption: a review. *Ind. Eng. Chem. Res.*, 37 (1998) 2571.
- [3] T.A. Reine, R.B. Eldridge. Absorption equilibrium and kinetics for ethylene-ethane separation with a novel solvent. *Ind. Eng. Chem. Res.*, 44 (2005) 7505.
- [4] A. Sahgal, H.M. La, and W. Hayduk. Solubility of ethylene in several polar and non-polar solvents. *Can.J.Chem.Eng.*, 56 (1978) 354.
- [5] W.S.W. Ho, G. Doyle, D.W. Savage, and R.L. Pruett. Olefin separations via complexation with cuprous diketonate. *Ind. Eng. Chem. Res.*, 27 (1988) 334.
- [6] I.H. Cho, D.L. Cho, H.K. Yasuda, and T.R. Marrero. Solubility of propylene in aqueous silver nitrate. *J.Chem.Eng.Data*, 40 (1995) 102.
- [7] A.E. Wentink, Functionalised solvents for olefin isomer purification by reactive extractive distillation. PhD dissertation. University of Twente, (2004).
- [8] A.E. Wentink, N.J.M. Kuipers, A.B. De Haan, J. Scholtz, and H. Mulder. Synthesis and evaluation of metal-ligand complexes for selective olefin solubilization in reactive solvents. *Ind. Eng. Chem. Res.*, 44 (2005) 4726.
- [9] D. Parkash, *Refining Processes Handbook*, Amsterdam, Gulf Professional Publishing, 2003.
- [10] K. Nymeijer, Gas-liquid membrane contactors for olefin/paraffin separation. PhD dissertation. University of Twente, (2003).
- [11] C.L. Munson, L.C. Boudreau, M.S. Driver, and W.L. Schinski, Separation of olefins from paraffins using ionic liquid solutions, Chevron, USA, US Patent 6623659 B2, 2003.

- [12] S.W. Kang, K. Char, J.H. Kim, C.K. Kim, and Y.S. Kang. Control of ionic interactions in silver salt-polymer complexes with ionic liquids: Implications for facilitated olefin transport. *Chem. Mater.*, 18 (2006) 1789.
- [13] H.S. Kim, J.Y. Bae, S.J. Park, H. Lee, H.W. Bae, S.O. Kang, et al. Separation of olefin/paraffin mixtures using zwitterionic silver complexes as transport carriers. *Chem. Eur. J.*, 13 (2007) 2655.
- [14] S.W. Kang, K. Char, J.H. Kim, and Y.S. Kang. Ionic liquid as a solvent and the long-term separation performance in a polymer/silver salt complex membrane. *Macromol. Res.*, 15 (2007) 167.
- [15] J.-F. Huang, H. Luo, C. Liang, D.-. Jiang, and S. Dai. Advanced liquid membranes based on novel ionic liquids for selective separation of olefin/paraffin via olefin-facilitated transport. *Ind. Eng. Chem. Res.*, 47 (2008) 881.
- [16] A. Ortiz, A. Ruiz, D. Gorri, and I. Ortiz. Room temperature ionic liquid with silver salt as efficient reaction media for propylene/propane separation: Absorption equilibrium. *Sep. Purif. Technol.*, 63 (2008) 311.
- [17] S.W. Kang, D.H. Lee, J.H. Park, K. Char, J.H. Kim, J. Won, et al. Effect of the polarity of silver nanoparticles induced by ionic liquids on facilitated transport for the separation of propylene/propane mixtures. *J. Membr. Sci.*, 322 (2008) 281.
- [18] D.-E. Jiang, S. Dai. First principles molecular dynamics simulation of a task-specific ionic liquid based on silver-olefin complex: Atomistic insights into a separation process. *J Phys Chem B*, 112 (2008) 10202.
- [19] H.R. Mortaheb, M. Mafi, B. Mokhtarani, A. Sharifi, M. Mirzaei, N. Khodapanah, et al. Experimental kinetic analysis of ethylene absorption in ionic liquid [Bmim]NO₃ with dissolved AgNO₃ by a semi-continuous process. *Chem. Eng. J.*, 158 (2010) 384.
- [20] J. Won, B.K. Dong, S.K. Yong, K.C. Dai, S.K. Hoon, K.K. Chan, et al. An ab initio study of ionic liquid silver complexes as carriers in facilitated olefin transport membranes. *J. Membr. Sci.*, 260 (2005) 37.

- [21] L.M. Galán, G.W. Meindersma, and A.B. Haan. Potential of silver-based room-temperature ionic liquids for ethylene/ethane separation. *Ind. Eng. Chem. Res.*, 48 (2009) 10650.
- [22] D. Camper, C. Becker, C. Koval, and R. Noble. Low pressure hydrocarbon solubility in room temperature ionic liquids containing imidazolium rings interpreted using regular solution theory. *Ind. Eng. Chem. Res.*, 44 (2005) 1928.
- [23] V. Mokrushin, D. Assenbaum, N. Paape, D. Gerhard, L. Mokrushina, P. Wasserscheid, et al. Ionic liquids for Propene-Propane separation. *Chem. Eng. Technol.*, 33 (2010) 63.
- [24] L.M. Galán, Functionalized ionic liquids. Absorption solvents for carbon dioxide and olefin separation. PhD dissertation. Eindhoven University of Technology, (2008).
- [25] A. Ortiz, L.M. Galán Sanchez, D. Gorri, A.B. De Haan, and I. Ortiz. Reactive ionic liquid media for the separation of propylene/propane gaseous mixtures. *Ind. Eng. Chem. Res.*, 49 (2010) 7227.
- [26] A. Ortiz, L.M. Galán, D. Gorri, A.B. De Haan, and I. Ortiz. Kinetics of reactive absorption of propylene in RTIL- Ag^+ media. *Sep. Purif. Technol.*, 73 (2010) 106.
- [27] A. Ortiz, Process intensification in the separation of olefin/paraffin mixtures, PhD dissertation. Universidad de Cantabria, (2010).
- [28] R. Kato, J. Gmehling. Systems with ionic liquids: Measurement of VLE and $\gamma \infty$ data and prediction of their thermodynamic behavior using original UNIFAC, mod. UNIFAC(Do) and COSMO-RS(OI). *J. Chem. Thermodyn.*, 37 (2005) 603.
- [29] Z. Lei, B. Chen, C. Li, and H. Liu. Predictive molecular thermodynamic models for liquid solvents, solid salts, polymers, and ionic liquids. *Chem. Rev.*, 108 (2008) 1419.
- [30] M. Diedenhofen, A. Klamt. COSMO-RS as a tool for property prediction of IL mixtures-A review. *Fluid Phase Equilib.*, 294 (2010) 31.

- [31] L.F. Vega, O. Vilasecaa, F. Llorell, and J.S. Andreua. Modeling ionic liquids and the solubility of gases in them: Recent advances and perspectives. *Fluid Phase Equilib.*, 294 (2010) 15.
- [32] A.A. Oliferenko, P.V. Oliferenko, K.R. Seddon, and J.S. Torrecilla. Prediction of gas solubilities in ionic liquids. *Phys. Chem. Chem. Phys.*, 13 (2011) 17262.
- [33] M. Gonzalez-Miquel, J. Palomar, S. Omar, and F. Rodriguez. CO₂/N₂ selectivity prediction in supported ionic liquid membranes (SILMs) by COSMO-RS. *Ind. Eng. Chem. Res.*, 50 (2011) 5739.
- [34] M. Miltner, A. Miltner, and A. Friedl. Calculation of physical gas solubilities in various solvents using the COSMO-RS method. *Chemie-Ingenieur-Technik*, 78 (2006) 1087.
- [35] K.Z. Sumon, A. Henni. Ionic liquids for CO₂ capture using COSMO-RS: Effect of structure, properties and molecular interactions on solubility and selectivity. *Fluid Phase Equilib.*, 310 (2011) 39.
- [36] J. Palomar, M. Gonzalez-Miquel, J. Bedia, F. Rodriguez, and J.J. Rodriguez. Task-specific ionic liquids for efficient ammonia absorption. *Sep. Purif. Technol.*, 82 (2011) 43.
- [37] J. Palomar, M. Gonzalez-Miquel, A. Polo, and F. Rodriguez. Understanding the physical absorption of CO₂ in ionic liquids using the COSMO-RS method. *Ind. Eng. Chem. Res.*, 50 (2011) 3452.
- [38] J.-G. Rosenboom, W. Afzal, and J.M. Prausnitz. Solubilities of some organic solutes in 1-ethyl-3-methylimidazolium acetate. Chromatographic measurements and predictions from COSMO-RS. *J. Chem. Thermodyn.*, 47 (2012) 320.
- [39] A. Vij, Y.Y. Zheng, R.L. Kirchmeier, and J.M. Shreeve. Electrophilic addition and substitution reactions of bis((trifluoromethyl)sulfonyl)amide and its N-chloro derivative. *Inorg.Chem.*, 33 (1994) 3281.

- [40] F. Agel, F. Pitsch, F.F. Krull, P. Schulz, M. Wessling, T. Melin, et al. Ionic liquid silver salt complexes for propene/propane separation. *Phys. Chem. Chem. Phys.*, 13 (2011) 725.
- [41] Gaussian Inc., Gaussian 03, Revision C.02 (2004).
- [42] GmbH&CoKG, COSMOtherm C2.1 Release 01.11, G. Leverkusen 2010. <<http://www.cosmologic.de>>.
- [43] K.C. Hansen, Z. Zhou, C.L. Yaws, and T.M. Aminabhavi. Determination of Henry's law constants of organics in dilute aqueous solutions. *J.Chem.Eng.Data*, 38 (1993) 546.
- [44] A.E. Wentink, D. Kockmann, N.J.M. Kuipers, A.B. De Haan, J. Scholtz, and H. Mulder. Effect of C6-olefin isomers on π -complexation for purification of 1-hexene by reactive extractive distillation. *Sep. Purif. Technol.*, 43 (2005) 149.
- [45] K.G. Denbigh, *The Principles of Chemical Equilibrium: With Applications in Chemistry and Chemical Engineering*, 4th edition, Cambridge, Cambridge University Press, 1981.
- [46] A. Navas, J. Ortega, R. Vreekamp, E. Marrero, and J. Palomar. Experimental thermodynamic properties of 1-butyl-2-methylpyridinium tetrafluoroborate [b2mpy][BF₄] with water and with alkan-1-ol and their interpretation with the COSMO-RS methodology. *Ind. Eng. Chem. Res.*, 48 (2009) 2678.
- [47] J. Palomar, J. Lemus, M.A. Gilarranz, and J.J. Rodriguez. Adsorption of ionic liquids from aqueous effluents by activated carbon. *Carbon*, 47 (2009) 1846.
- [48] Y.S. Kang, J.O. Won, H.H. Park, and S.G. Oh, Solid state polymer electrolyte facilitated transport membranes containing surfactants, Korea, US Patent 6645276 B2, 2003.



3

Membrane contactors

Abstract

The first part of this chapter deals with the comparison in the separation performance between the four different membranes of different nature (PVDF, PTFE and ceramic membranes with asymmetric and symmetric structures). In the second part, the performance of two commercial membrane contactors with tubular configuration and different flow patterns of the fluid phases, i) parallel flow and ii) transverse flow has been evaluated. The improved fluid-dynamics of the transverse flow membrane contactor led to an overall mass transfer coefficient 17.6 times higher than that reported using a parallel flow contactor and a process intensification by a factor of 17.4 in terms of mass transfer per specific area compared to a conventional stirred tank reactor. Finally, a detailed mathematical model that satisfactorily predicts the experimental behaviour has been developed.

3.1. Introduction

Among a number of alternative separation processes for olefin/paraffin gas mixtures, reactive absorption using a silver salt solution has been considered an attractive alternative to conventional distillation processes. A wide range of gas-liquid contactors are commercially available: stirred tanks, bubble columns, packed-bed columns, plate columns, static or dynamic mixers and membrane equipment. Therefore the choice of the best absorption process is difficult, taking into account the high number of variables that have to be considered [1,2]. Direct compact equipments like spray towers or packed columns present many disadvantages such as emulsion formation, flooding, unloading, or foaming. In this respect non-dispersive gas-liquid contact offers an alternative technology that overcomes these disadvantages providing high operational flexibility, large specific area, and the capacity to control the gas as well as the liquid flow rates and pressures independently. Thus, membrane contactors constitute a unique way to accomplish gas-liquid absorption processes in a modular, small, robust and safe way. Moreover, membrane gas absorption processes provide several economical advantages including low investment costs, low pumping power consumption and for their installation no expensive civil engineering work is required [3]. Kreulen et al. [4] also found that membrane contactors were more advantageous over conventional devices such as bubble columns when viscous liquids were used. This is because in conventional contactors increasing the viscosity of the fluid decreases the interfacial area and the mass transfer coefficient, whereas when using membrane contactors the mass transfer coefficient is only affected. Usually, the three most common module configurations employed are parallel flow, cross flow and transverse flow. Many authors [5-10] have reported that the transverse flow module offers significant advantages over both, parallel flow and cross flow configuration, which finally lead to higher shell side mass transfer coefficients. This is because the liquid flowing perpendicular to the fibers creates local turbulence increasing the local liquid mass transfer coefficient in the shell side. The uniform fiber to fiber distance and the

presence of a central baffle also contribute to minimize flow channeling in the shell side. Furthermore, the improved fluid-dynamics facilitate process scale-up and allow for a more precise performance prediction.

One of the major issues associated with the use of conventional polymeric membrane contactors is the long-term stability of the membranes due to wetting or chemical incompatibility with the solvent. Barbe et al. [11] observed that polypropylene membranes presented changes in their surface morphology after being exposed to water for 72 h. Kamo et al. [12] reported solvent-induced morphological changes of microporous polyethylene hollow fiber membranes as a function of the surface tension of solvents. In addition, Rangwala [13] found that the membrane mass transfer coefficients for CO₂ absorption were much lower than those theoretically calculated for completely non-wetted pores of polypropylene membranes in aqueous NaOH and DEA solutions, indicating that the pores were partially wetted. Thus, the appropriate selection of the absorbents and membrane materials for a given gas separation process must take into account the possible interactions between the membrane and the solvent in the long term, since the compatibility of the membranes and the absorbents is a real concern in membrane-based processes [14].

Several authors have studied the use of gas-liquid membrane contactors to carry out gas separations. Nymeijer et al. [15] studied the separation of ethane/ethylene gas mixtures using a gas-liquid membrane contactor with a dense polymer coated on the porous support and an aqueous silver nitrate solution as absorbent. Luis et al. [16] reported promising results using membrane contactors and ionic liquids to develop a zero solvent emission process to recover SO₂. Moreover, Ortiz et al. [17] proved the viability of the separation of propane/propylene gas mixtures using Ag⁺-BMImBF₄ as reaction medium in a parallel flow membrane contactor.

In this chapter, the performance of different membrane materials including PVDF and PTFE polymeric membranes and ceramic membranes with symmetric and asymmetric structures has been evaluated. Next,

the separation process has been analyzed using two different commercial membrane contactors, a parallel flow membrane contactor with tubular configuration and a transverse flow membrane contactor with hollow fiber configuration. The mass transfer rate has been experimentally characterized through the evaluation of the overall mass transfer coefficient as a function of the operational conditions, which will allow to expand the comparison of the performance of these new devices with other contactors. Finally, a mathematical model has been developed in order to describe and predict the experimental behaviour.

3.2. Experimental methods

3.2.1. Materials

Propylene and propane with 99.5 % purity were purchased from Praxair. The RTIL used in this study was 1-butyl-3-methylimidazolium tetrafluoroborate (CAS number: 174501-65-6) purchased from Iolitec, with a minimum purity of 99 % and residual halide content less than 500 ppm. Silver tetrafluoroborate (AgBF_4) of 99 % purity was supplied by Apollo Scientific Ltd. All chemicals were used as received.

Regarding the hollow fibers used in the first part of this chapter, the polymeric membranes (PTFE and PVDF) were provided by Jiraratananon research group in Thailand. On the other hand, the ceramic hollow fiber membranes, both with symmetric and asymmetric structures were prepared in the Department of Chemical Engineering and Chemical Technology at Imperial College of London.

In the second part of this chapter, the performance of two commercial membrane contactors is evaluated. The membrane contactors under study are a parallel flow MD020 TP 2N membrane contactor with tubular configuration supplied by Enka-Microdyn and a transverse flow membrane contactor Liqui-Cel® 2.5 x 8 Extra-flow module commercialized by Celgard LLC (Charlotte, USA) equipped with

microporous polypropylene hollow fibers Celgard® X50. The main characteristics of the membrane modules are collected in table 3.1.

Table 3.1. Characteristics of the commercial membrane modules Enka-Microdyn MD020 TP 2N and Liqui-Cel® 2.5 x 8 Extra-flow.

	Enka-Microdyn MD020 TP 2N	Liqui-Cel® 2.5 x 8 Extra-flow
Flow pattern	Parallel flow	Transverse flow
Inner diameter of the shell (m)	0.02	0.05
Inner diameter of the fibers (m)	$5.5 \cdot 10^{-3}$	$220 \cdot 10^{-6}$
Outer diameter of the fibers (m)	$8.6 \cdot 10^{-3}$	$300 \cdot 10^{-6}$
Wall thickness (m)	$1.55 \cdot 10^{-3}$	$40 \cdot 10^{-6}$
Nominal pore diameter (m)	$0.2 \cdot 10^{-6}$	$0.04 \cdot 10^{-6}$
Porosity (%)	75	40
Number of hollow fibers	3	10200
Module length (m)	0.75	0.16
Effective membrane area (m ²)	0.036	1.4
Packing density	0.55	0.45
Tortuosity ^a	1.4	1.4

^a Assumed as $1/\epsilon$ [18]

Figure 3.1 shows a schematic view of the structure and flow patterns of the two commercial membrane modules studied in this chapter.

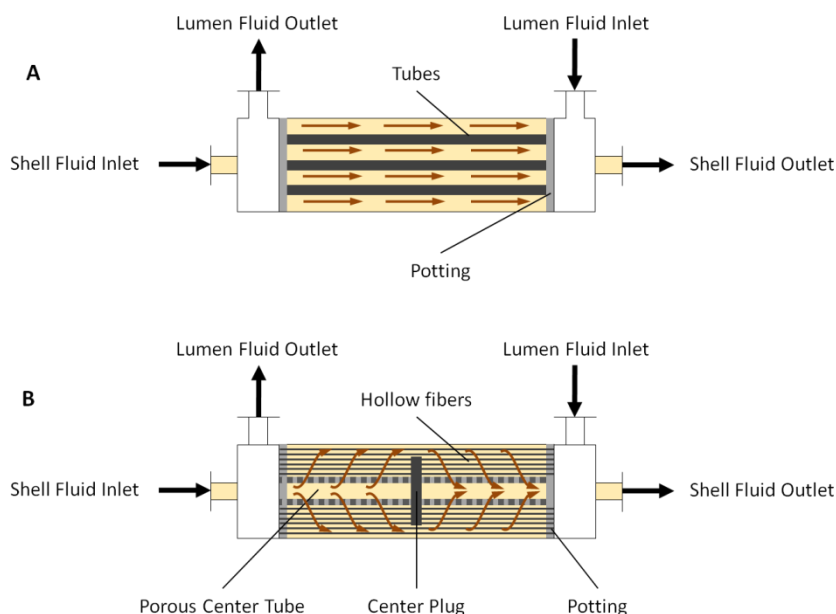


Figure 3.1. Schematic view of A) parallel flow MD020 TP 2N membrane contactor and B) transverse flow fiber module Liqui-Cel® 2.5 x 8 Extra flow.

3.2.2. Ceramic hollow fiber fabrication

Ceramic hollow fiber membranes were fabricated using a spinning/sintering technique [19]. More details about the fabrication procedures and protocols can be found elsewhere [20,21]. Firstly, the dispersant (Arlacel P135) was dissolved in NMP/water solution where different particle sizes of Al_2O_3 powders ($0.01\ \mu\text{m}$: $0.05\ \mu\text{m}$: $1\ \mu\text{m}$) were added afterwards at a ratio of 1:2:7. The suspension was rolled with 20 mm agate milling balls for 48 h and milling was continued for a further 48 h period after the addition of polyethersulfone (6.1 % w/w) as polymer binder. The suspension was then transferred and degassed under vacuum for a few hours to ensure no bubbles were trapped in the suspension before spinning. The presence of bubbles usually results in defects and holes on the membrane surface when fabricated, and

therefore it is desired to obtain a homogenous and smooth suspension to obtain defect-free fibers. Immediately after degassing, the spinning suspension was transferred to a syringe pump where it was extruded through a tube-in-orifice spinneret (OD 3 mm, ID 1.2 mm) into tap water with an air-gap of 15 cm. The fiber precursors were left in an external coagulation bath overnight and then they were taken out to be straightened for few days. Finally, the precursors were calcined in air (Carbolite furnace). The temperature was increased from room temperature to 873 K at a rate of 2 K·min⁻¹ and held for 2 h, then increasing to 1273 K at a rate of 5 K·min⁻¹ and held for 2 h and finally to 1723 K at a rate of 5 K·min⁻¹ and held for 4 h. The temperature was then reduced to room temperature at a rate of 3 K·min⁻¹. Originally, the fabricated ceramic hollow fibers membranes present a highly hydrophilic character due to the presence of hydroxyl (OH⁻) groups on the surface; however, the hydrophobicity of ceramic membranes can be promoted by surface modification [22]. Although several methods and types of surface modifying agents can be used fluoroalkylsilanes (FAS) were selected in this study. FAS solutions are organosilanes which have hydrolysable groups and other hydrophobic ends in their structures. The hydrolysable groups are coupled with the hydroxyl groups (OH⁻) on the ceramic surface, forming a chemically bound hydrophobic layer. Several factors including the number of functional groups in the FAS structure, the length of hydrophobic tails, grafting time, and grafting temperature play important roles in the surface grafting process. The saline solution used in this work was 1H, 1H, 2H, 2H-perfluorooctylethoxysilane purchased from Sigma Aldrich. The sintered hollow fibers were immersed into a 0.01 M of FAS in hexane solution at room temperature. The fibers were left in the solution for 2 h to allow the coupling reaction to occur. After the immersion, the fibers were rinsed with hexane to remove any unreacted chemicals from the membrane surface and dried in an oven at 373 K for 12 h.

3.2.3. Ceramic hollow fiber characterization

Prior to the olefin/paraffin separation experiments the hollow fiber membranes used in this study were characterized by scanning electron microscopy (SEM), mercury porosimetry, and contact angle measurements. First of all the membrane morphology was evaluated by scanning electron microscopy. The ceramic fibers were flexed at ambient temperature until a fracture occurred. However, due to the flexible character of polymeric fibers, these were previously immersed in liquid nitrogen to promote a fragile fracture. Afterwards, the samples were coated with gold particles under vacuum for 3 min at 20 mA (Emitech Model K550) and SEM images at varying magnifications were collected (JEOL JSM-5610 LV). For the Hg intrusion analysis, the Al_2O_3 hollow fiber substrates were broken into sections of approximately 3mm length. Then the pore size distribution of the Al_2O_3 hollow fiber substrates was measured using Hg porosimetry. Hg intrusion data were collected at absolute pressures between 0.01 and 2280 bar with an equilibrium time of 10 s (Micromeritics Autopore IV). However this technique is not suitable for polymeric membranes since pores with a diameter lower than 2 μm can not be reliably detected [18]. Therefore the mean pore size and pore size distribution of the PVDF and PTFE polymeric membranes were measured by the flow porosimetry technique using a capillary flow porosimeter (Porous Materials Inc., model CFP-1500A). Contact angle measurements were carried out using the goniometry method. Although this method is commonly used to measure the contact angles of flat-sheet surfaces, due to the high outer diameter of the ceramic hollow fibers (≈ 2 mm), this method can be also applicable. The contact angle was measured using a high resolution camera and software to capture and analyze the contact angle.

3.2.4. Methods

As explained in chapter 2 the ionic liquid BMImBF_4 was used in the experiments because it is able to dissolve a suitable silver salt (AgBF_4),

showing a high absorption capacity for propylene as well high separation selectivity. In addition, BMImBF₄-silver salt mixtures are hydrophilic, so that it is possible to operate in non-wetting mode of the fibers. The compatibility of the absorbing mixtures with module housing and membrane material of polypropylene was also checked. In gas-liquid membrane contactors, the membrane offers no selectivity, it only acts as a physical barrier between both fluid phases allowing mass transfer between gas and liquid without dispersing one phase into the other providing a large contacting surface area. During operation the interface between phases must be carefully controlled. Non wetting mode is preferred because with liquid-filled pores the membrane resistance is much higher than for gas-filled pores mode. Generally, a liquid does not pass through the pores as long as the pressure is kept below a critical threshold value known as breakthrough pressure which can be estimated using the Young- Laplace equation [18]:

$$\Delta P = - \frac{4\phi\sigma_L \cos \theta}{d_p} \quad (3.1)$$

where ΔP , is the breakthrough pressure, ϕ is a form factor equal to 1 for cylindrical pores, σ_L is the surface tension of the liquid, θ is the contact angle between the liquid phase and the membrane and d_p is the maximum membrane pore diameter.

A diagram of the experimental setup is shown in figure 3.2. First of all the flow rate of the feed gas mixture is controlled by a mass flow controller (Brooks Instrument SLA 5850). The gas phase circulates through the lumen side of the fibers while the liquid solvent is pumped from the storage tank through the shell side of the module in a closed circuit by a gear pump (Cole Parmer MicroPump 75211-35) because the cost of pumping a liquid with high viscosity through the lumen of the fibers becomes excessive when the hydrophobic fibers have small diameter [23,24]. The pressure of the gas phase is adjusted by means of a pressure controller (Brooks Instrument 5866) located at the outlet of the membrane module. Since the membrane used is hydrophobic, the

liquid pressure should be slightly higher than the gas pressure in order to prevent spreading of gas into the liquid phase. At the same time, the pressure of the liquid must not exceed the breakthrough pressure for this system calculated using Young-Laplace equation, in order to minimize the wetting phenomena of the membrane pores. This pressure is controlled by a needle valve placed between the membrane module and the storage tank. The gas flow rate at the outlet of the module is measured using a volumetric flowmeter equipped with a micro turbine (McMillan 113 series). When the liquid absorbent becomes saturated, the desorption step is carried out applying vacuum, pressure ≤ 0.01 bar, to the lumen of the fibers. The desorbed gas is accumulated in the gas cylinder, and using a micrometric valve the gas flow rate can be controlled and then it is measured using again a volumetric flowmeter (McMillan 113 series). Two liquid traps were placed in the gas circuit at the inlet and outlet of the module to check both the possible entrainment of fluid inside the fibers and to prevent the wetting of the electronic devices in the absorption and desorption steps.

In order to check the reliability of the obtained results each experiment was performed twice and the standard deviation (defined according to eq. 3.2) has been calculated.

$$\sigma = \sqrt{\frac{\sum_{i=1}^n \left(\frac{I_{C_3H_6} - I'_{C_3H_6}}{I_{C_3H_6}} \right)^2}{n-1}} \quad (3.2)$$

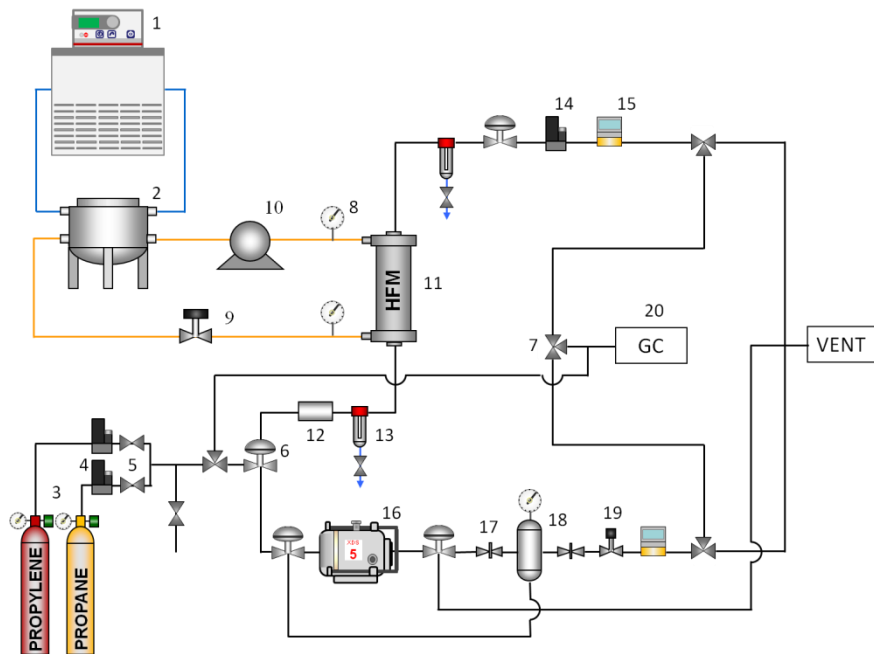


Figure 3.2. Experimental set up.

1-Thermostatic bath, 2-Storage tank, 3-Gas bottles, 4-Mass flow controllers, 5-Two way valves, 6-Solenoid valves, 7-Three way valve, 8-Pressure gauges, 9-Needle valve, 10-Gear pump, 11-Membrane module, 12-Pressure transducer, 13-Liquid trap, 14-Pressure controller, 15-Volumetric flowmeter, 16-Vacuum pump, 17-Check valve, 18-Gas cylinder, 19-Micrometric valve, 20-Gas chromatograph.

3.3. Model development

The design of multiphase equipments such as membrane contactors for gas-liquid absorption is a difficult task due to its highly complex nature [25]. Moreover, among the many different types of multiphase chemical processes, reactive absorption is regarded as one of the most complex systems due to interactions between chemical reaction and mass transfer taking place between the gas and liquid phases. Figure 3.3 shows a schematic diagram of the reactive absorption process of gas “i”

into a liquid using a membrane contactor with gas and liquid phases flowing in countercurrent.

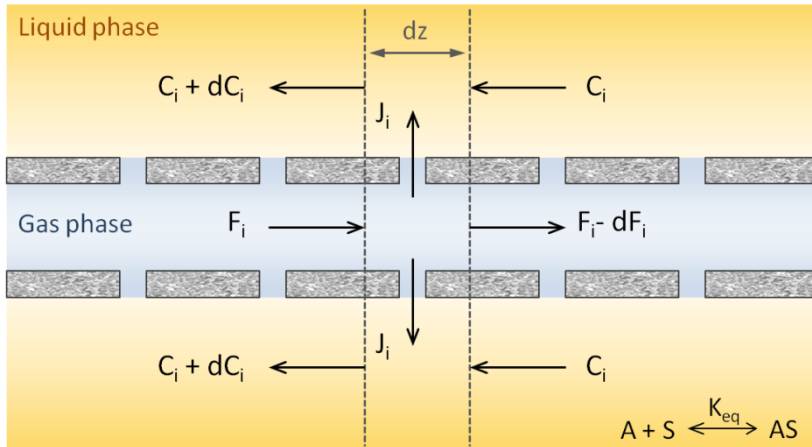


Figure 3.3. Schematic diagram of the gas-liquid reactive absorption process implemented in a membrane contactor with gas and liquid phases in countercurrent flow.

3.3.1. Mass balances

In order to develop the mass balances for all the species involved in the gas-liquid absorption process using membrane contactors the following assumptions were undertaken:

- Plug flow and negligible axial diffusion in both phases.
- Each fiber has identical specifications.
- Hollow fibers are hydrophobic, so the pores are completely filled by the gas phase.
- Ideal gas behavior is imposed.
- The system is under isothermal operation.

The mass balance for the gas “ i ” in the gas phase is given by eq. 3.3:

$$\frac{dF_i}{dz} = -\frac{A}{L} \cdot J_i \quad (3.3)$$

With boundary condition:

$$z = 0 \Rightarrow F_i = F_{i,in}$$

where F_i is the molar flow rate of the gas i , z is the axial position in the module, A is the membrane total area and L is the effective fiber length.

The mass balance for the gas “ i ” in the liquid phase can be expressed as:

$$\frac{V}{Q_{iL}L} \cdot \frac{\partial C_i}{\partial t} + \frac{\partial C_i}{\partial z} = \frac{A}{Q_{iL}L} \cdot J_i \quad (3.4)$$

With initial and boundary conditions:

$$t = 0 \Rightarrow C_i = 0$$

$$z = 0 \Rightarrow C_i = 0 \quad \text{for gas and liquid flowing in co-current flow}$$

$$z = L \Rightarrow C_i = 0 \quad \text{for gas and liquid flowing counter-currently}$$

where V is the volume of the liquid side of the membrane contactor, Q_{iL} is the ionic liquid flow rate and C_i is the concentration of gas dissolved in the liquid flowing through the module. The material balances are coupled by the flux of gas across the membrane, which can be expressed as a function of the driving force (difference in gas concentrations between the gas phase and the liquid bulk) and the overall mass transfer coefficient (eq. 3.5):

$$J_i = K_{overall} \left(\frac{P \cdot y_i}{R \cdot T} - \frac{C_i}{H_i \cdot R \cdot T} \right) \quad (3.5)$$

where J_i is the gas flux across the membrane ($\text{mol} \cdot \text{m}^2 \cdot \text{s}^{-1}$), $K_{overall}$ is the overall mass transfer coefficient ($\text{m} \cdot \text{s}^{-1}$), P is the total pressure of the gas

phase (bar), y_i is the molar fraction of the gas in the gas phase, R is the constant of ideal gases ($\text{bar}\cdot\text{m}^3\cdot\text{mol}^{-1}\cdot\text{K}^{-1}$), T is the temperature of the system (K), H_i is the Henry's constant ($\text{mol}\cdot\text{L}^{-1}\cdot\text{bar}^{-1}$) and C_i is the concentration of the gas in the liquid phase ($\text{mol}\cdot\text{L}^{-1}$).

3.3.2. Mass transfer rate

In membrane gas-liquid contacting processes the gas solute has to diffuse from the bulk of the gas phase across the membrane to the bulk of the liquid phase. So that there are three main resistances to mass transfer located in the gas phase, membrane and liquid phase boundary layers that must be considered [18,26,27]. In this case, the resistances-in-series approach can be used to describe the mass transfer kinetics (figure 3.4). Taking into account that the mass transfer between gas and liquid takes place in the gas-liquid interface, and considering hydrophobic membranes, the resistances-in-series can be written for: a) the liquid flowing through the shell side, and b) liquid flowing through the lumen of the fibers, as eqs. (3.6) and (3.7) respectively:

$$\frac{1}{K_{\text{overall}}} = \frac{d_{\text{out}}}{k_g d_{\text{in}}} + \frac{d_{\text{out}}}{k_{\text{mg}} d_{\text{lm}}} + \frac{1}{k_l H_{\text{di}} E_A} \quad (3.6)$$

$$\frac{1}{K_{\text{overall}}} = \frac{d_{\text{in}}}{k_g d_{\text{out}}} + \frac{d_{\text{in}}}{k_{\text{mg}} d_{\text{lm}}} + \frac{1}{k_l H_{\text{di}} E_A} \quad (3.7)$$

where K_{overall} is the overall mass transfer coefficient and k_g , k_{mg} , k_l are the individual mass transfer coefficients of the gas phase, the membrane (when the pores are filled with gas) and the liquid phase respectively. H_{di} represents the dimensionless Henry's constant while d_{out} , d_{in} and d_{lm} are the outer, inner and logarithmic mean diameters of the fibers, and E_A is the enhancement factor which takes into account the improvement in the overall mass transfer rate due to the chemical reaction.

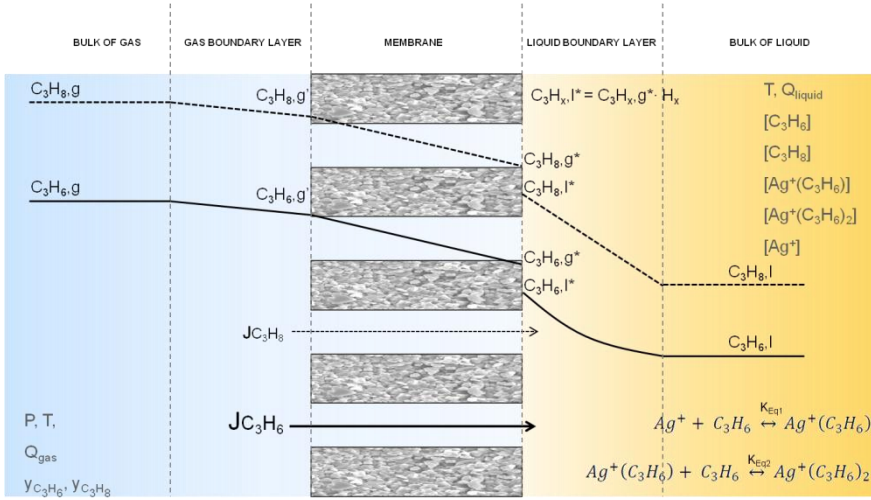


Figure 3.4. Absorption mechanism of propane and propylene with the resistances in series approach in a non wetted membrane contactor.

Mass transfer coefficient in the lumen side

The local mass transfer coefficient in the lumen side can be calculated using different correlations available in literature. The expression developed by L  v  que in the restricted range of laminar flow inside the fibers has been widely used (eq. 3.8) [28].

$$Sh = 1.62 + Gz^{0.33} \quad (3.8)$$

However, the mass transfer rate can be underestimated for low Graetz numbers. Another correlation proposed by Hausen for laminar flow and low Gz number can also be used (eq. 3.9) [28,29]:

$$Sh = 3.66 + \frac{0.0668Gz}{1+0.04Gz^{2/3}} \quad (3.9)$$

Membrane mass transfer coefficient

The mass transfer coefficient in the hydrophobic microporous membrane depends on the diffusion coefficient of the gas in the gas phase inside the pores and on the characteristics of the membrane (eq. 3.10) [1]:

$$k_{mg} = \frac{D_{i,g}\epsilon}{\tau\delta} \quad (3.10)$$

where ϵ , ζ and δ are the porosity, tortuosity and thickness of the membrane respectively. $D_{i,g}$ is the diffusion of species in the gas phase inside the pores of the membrane.

Mass transfer coefficient in the shell side

For membrane contactors with parallel or transverse flow the mass transfer coefficient in the shell side can be estimated using several correlations available in literature (tables 3.2 and 3.3), being d_h the hydraulic diameter defined in eqs. 3.11 and 3.12 for parallel flow membrane contactors and for transverse flow membrane contactors respectively; $D_{i,l}$ is the diffusion coefficient of species i in the liquid, L is the fiber length, ν is the kinematic viscosity of the liquid, u is the liquid linear velocity, ϕ_F is the membrane packing factor and N is the number of fibers.

$$d_h = \frac{d_{cin}^2 - Nd_{out}^2}{N \cdot d_{out}} \quad (3.11)$$

$$d_h = \frac{d_{cin}^2 - d_{co}^2 - Nd_{out}^2}{N \cdot d_{out}} \quad (3.12)$$

Table 3.2. Correlations to calculate the mass transfer coefficient in the shell side for parallel flow membrane contactors.

Reference	Correlation	
Yang and Cussler [30]	$Sh = 1.25 \left(\frac{d_h^2 u}{Lv} \right)^{0.93} \left(\frac{v}{D_{i,l}} \right)^{1/3}$	(3.13)
Prasad and Sirkar [31]	$Sh = 5.8 \left[(1 - \phi_F) \frac{d_h}{L} \right] \left(\frac{d_h u}{v} \right)^{0.6} \left(\frac{v}{D_{i,l}} \right)^{1/3}$	(3.14)
Wu and Chen [32]	$Sh = (0.3045\phi_F^2 - 0.3421\phi_F + 0.15) \left(\frac{d_h u}{v} \right)^{0.9} \left(\frac{v}{D_{i,l}} \right)^{1/3}$	(3.15)
Costello et al. [33]	$Sh = (0.53 - 0.58\phi_F) \left(\frac{d_h u}{v} \right)^{0.53} \left(\frac{v}{D_{i,l}} \right)^{1/3}$	(3.16)
Li et al. [34]	$Sh = 1.164 \left(\frac{d_h^2 v}{Lv} \right)^{0.967} \left(\frac{v}{D_{i,l}} \right)^{1/3}$	(3.17)

Table 3.3. Correlations to calculate the mass transfer coefficient in the shell side for transverse flow membrane contactors.

Reference	Correlation	
Zheng et al.[9]	$Sh = 2.15 \left(\frac{d_h u}{v} \right)^{0.42} \left(\frac{v}{D_{i,l}} \right)^{1/3}$	(3.18)
Fouad et al. (mod.) [35]	$Sh = 0.41 \left(\frac{d_h u}{v} \right)^{0.36} \left(\frac{v}{D_{i,l}} \right)^{1/3}$	(3.19)
Schöner et al. [5]	$Sh = 1.76 \left(\frac{d_h u}{v} \right)^{0.82} \left(\frac{v}{D_{i,l}} \right)^{1/3}$	(3.20)
Baudot et al. [36]	$Sh = 0.56 \left(\frac{d_h u}{v} \right)^{0.62} \left(\frac{v}{D_{i,l}} \right)^{1/3}$	(3.21)
Shen et al. [37]	$Sh = 0.055 \left(\frac{d_h u}{v} \right)^{0.72} \left(\frac{v}{D_{i,l}} \right)^{1/3}$	(3.22)

3.3.3. Physical properties

The estimation of the physical properties involved in the absorption process such as solubility and diffusivity is one of the most important factors for the mathematical modeling of the gas absorption with chemical reaction.

Physical solubility

When a gas contacts with a liquid, it is dissolved until gas-liquid equilibrium is established. The concentration at equilibrium of the gas into a liquid is related to its partial pressure by the Henry's constant:

$$H_i = \frac{C_i}{p_i} \quad (3.23)$$

The Henry's constant has an important dependence with temperature which can be described using a van't Hoff-type equation [38]:

$$H = H_0 \cdot e^{(-\Delta H_{\text{sol}}/RT)} \quad (3.24)$$

where the parameters H_0 and $-\Delta H_{\text{sol}}$ depend on the gas to be absorbed and the liquid solvent.

Diffusivities

The molecular diffusion coefficient of a gas into another ($D_{A,b}$) can be calculated by the Fuller's equation (eq. 3.25) [39]:

$$D_{A,b} = \frac{0.01013 \cdot T^{1.75} \cdot \left(\frac{1}{M_A} + \frac{1}{M_B}\right)^{0.5}}{P \cdot \left[(\sum \vartheta_A)^{1/3} + (\sum \vartheta_B)^{1/3}\right]^2} \quad (3.25)$$

where the units of T and P are K and Pa respectively, with the resulting diffusivity in $\text{m}^2 \cdot \text{s}^{-1}$. M_A and M_B are the molecular weights in $\text{g} \cdot \text{mol}^{-1}$.

$\sum \vartheta_A$ and $\sum \vartheta_B$ are the summation of atomic diffusion volumes for gases A and B.

However, the diffusion coefficient of the gas A into the gas B inside the pores of the membrane depends not only on the molecular diffusion, but also on the Knudsen diffusion, which takes into account the fact that the gas molecules frequently collide with the pore wall. Thus, the diffusivity of a gas inside the membrane pores filled by gas is a combination between molecular diffusion and Knudsen diffusion that can be calculated as follows [40]:

$$\frac{1}{D_{A,g}} = \frac{1}{D_{A,b}} + \frac{1}{D_{A,Kn}} \quad (3.26)$$

where the Knudsen diffusion depends on the pore diameter, the temperature and the molecular weight of the gas [41]:

$$D_{Kn} = \frac{1}{3} d_p \sqrt{\frac{8RT}{\pi \cdot M_A}} \quad (3.27)$$

where d_p is the pore diameter (m), R is the gas constant ($J \cdot kmol^{-1} \cdot K^{-1}$), T is temperature (K) and M_A is the molecular weight of the gas ($g \cdot mol^{-1}$). Diffusivity is obtained in $m^2 \cdot s^{-1}$.

The diffusion coefficient of a gas into a common solvent can be estimated using the Wilke Chang correlation [42].

$$D_{A,B} = \frac{7.4 \cdot 10^{-8} (\phi_B \cdot M_B)^{1/2} \cdot T}{\mu_B \cdot V_A^{0.6}} \quad (3.28)$$

where A and B refer to the gas and the absorption liquid respectively. ϕ_B is the association factor for the solvent; M_B is the molecular weight of the solvent ($g \cdot mol^{-1}$); T is temperature (K); μ_B is the solvent viscosity (cP); V_A is the molar volume of the gas at its normal boiling temperature ($cm^3 \cdot mol^{-1}$). Diffusivity is obtained in $cm^2 \cdot s^{-1}$.

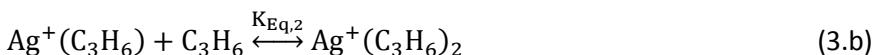
Although the Wilke-Chang equation provides good results in the estimation of diffusion coefficients in common solvents, it is not suitable to calculate diffusion coefficients in more complex solvents such as ionic liquids. In that case the diffusion coefficient of a gas can be estimated using the correlation developed by Scovazzo and co-workers for imidazolium-based ionic liquids [43].

$$D_{AB} = 2.66 \cdot 10^{-3} \frac{1}{\mu_B^{0.66 \pm 0.03} \cdot V_A^{1.04 \pm 0.08}} \quad (3.29)$$

where A and B refer to solute and solvent, respectively. μ_B is viscosity in cP, V_A is the molar volume of the gas in $\text{cm}^3 \text{mol}^{-1}$ and the diffusivity is obtained in $\text{cm}^2 \text{s}^{-1}$.

3.3.4. Chemical reaction

Once the gas is absorbed into the liquid according to Henry's law, propylene is able to react with the silver cations present in the liquid phase (reactions 3.a and 3.b) [44].



Therefore, the equilibrium constants can be defined as follows:

$$K_{\text{Eq},1} = \frac{[\text{Ag}^+(\text{C}_3\text{H}_6)]}{[\text{C}_3\text{H}_6][\text{Ag}^+]} \quad (3.30)$$

$$K_{\text{Eq},2} = \frac{[\text{Ag}^+(\text{C}_3\text{H}_6)_2]}{[\text{Ag}^+(\text{C}_3\text{H}_6)][\text{C}_3\text{H}_6]} \quad (3.31)$$

Considering all the species that can coexist at the same time in the liquid phase, the total concentration of propylene dissolved in the reaction medium is the sum of the free gas dissolved in the liquid and the gas molecules which have been bounded by the chemical reaction.

$$[C_3H_6]^T = [C_3H_6] + [Ag^+(C_3H_6)] + 2[Ag^+(C_3H_6)]_2 \quad (3.32)$$

Similarly a mass balance for the silver cations can be established.

$$[Ag^+]^T = [Ag^+] + [Ag^+(C_3H_6)] + [Ag^+(C_3H_6)]_2 \quad (3.33)$$

The dependence of the equilibrium constant with temperature can be described in most cases by the Van't Hoff equation (eq. 3.34).

$$\frac{d \ln K}{d(1/T)} = -\frac{\Delta H_r}{R} \quad (3.34)$$

where T is the temperature in K, ΔH_r is the enthalpy of reaction ($\text{kJ} \cdot \text{mol}^{-1}$) and R is the gas constant ($\text{kJ} \cdot \text{mol}^{-1} \cdot \text{K}^{-1}$).

Moreover, the chemical reaction that takes place between the gas and the solvent can enhance the absorption flux through the enhancement factor which increases the overall mass transfer coefficient. This enhancement factor (E_A) is defined as the ratio of the absorption flux of a gas in the liquid in the presence of a chemical reaction to the absorption flux in the absence of a reaction referring these fluxes to the same driving force.

$$E_A = \frac{J_{C_3H_6} \text{ with reaction}}{J_{C_3H_6} \text{ without reaction}} \quad (3.35)$$

In this work the enhancement factor has been calculated using the approximated solution proposed by DeCoursey for absorption with irreversible second order reaction [45].

$$E_A = -\frac{Ha^2}{2 \cdot (E_{A\infty} - 1)} + \sqrt{\frac{Ha^2}{4 \cdot (E_{A\infty} - 1)^2} + \frac{E_{A\infty} \cdot Ha^2}{(E_{A\infty} - 1)}} + 1 \quad (3.36)$$

where Ha is the Hatta number which relates the maximum conversion in the film and the maximum mass transport through the film and $E_{A\infty}$ is the infinite enhancement factor which can be calculated using the asymptotic solution proposed by Danckwerts (eqs. 3.37 and 3.38) [46].

$$Ha^2 = \frac{\frac{2}{n+1} k_{1,1} \cdot (C_{C_3H_6}^{int,IL})^{n-1} \cdot C_{Ag^+}^m \cdot D_{C_3H_6,l}}{k_l^2} \quad (3.37)$$

$$E_{A\infty} = \left(1 + \frac{D_{Ag^+} C_{Ag^+}}{D_{C_3H_6,l} C_{C_3H_6}^{int,IL}} \right) \left(\frac{D_{C_3H_6,l}}{D_{Ag^+}} \right)^{0.5} \quad (3.38)$$

where $k_{1,1}$ is the kinetic constant of the chemical reaction, $C_{C_3H_6}^{int,IL}$ is the concentration of propylene at the interface, $C_{Ag^+}^m$ is the concentration of silver ions in the liquid bulk phase, $D_{C_3H_6,l}$ is the diffusion coefficient of propylene in the liquid phase, and k_l is the liquid side mass transfer coefficient.

3.4. Results and discussion

3.4.1. Comparison between different types of fibers

Fiber characterization

The morphology of the polymeric and ceramic hollow fiber membranes used in this work is shown in figure 3.5.

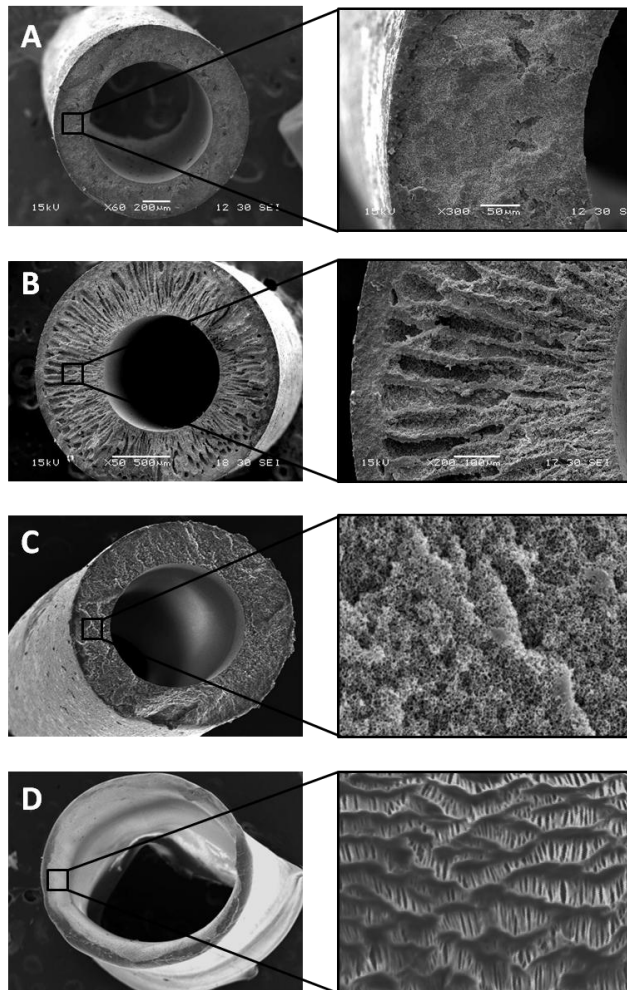


Figure 3.5. SEM images of the hollow fiber membranes used in this work A) symmetric ceramic, B) asymmetric ceramic, C) PVDF, and D) PTFE.

It can be seen that the asymmetric structure of the ceramic membranes consists of approximately 80 % finger-like region and 20 % sponge-like region, whereas the symmetric structure consists entirely of a sponge-like region. On the other hand, for the polymeric membranes such as PTFE and PVDF, the appearance of the pores on the cross section of the hollow fiber seems to be more obvious than the ceramic membranes. This is due to the fabrication methods of polymeric membranes such as thermally induced phase separation, non-solvent induced phased

separation or melting and stretching methods. These techniques usually results in the development of large and wide pores as recently shown by several authors [47,48]. On the other hand, since the ceramic hollow fiber membranes were obtained by a sintering technique at high temperatures, the pores on the outer surface of the membranes could be diminished significantly, and the membrane could become dense depending on the sintering temperature and dwelling time, as explained by Kingsbury and Li [20]. Nevertheless, the ceramic membranes used in this study were classified as permeable and microporous as confirmed by gas permeation and mercury intrusion analysis as follows.

The pore size distribution of the polymeric and ceramic hollow fiber membranes are shown in figure 3.6. It can be seen that the polymeric membranes present only one peak around 0.2 μm for PVDF and 0.4 μm for PTFE. Also symmetric ceramic membranes have only one pore size around 0.2 μm . However the asymmetric ceramic membranes present two peaks. One is around 10 μm which corresponds to the finger-like region of the membrane and the other peak is around 0.1 μm corresponding to the sponge-like layer of the membrane.

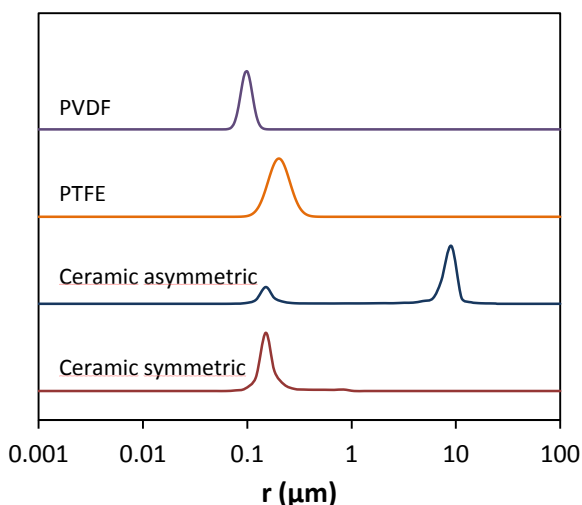


Figure 3.6. Pore size distribution of the ceramic and polymeric membranes used in this work.

Finally, to ensure that the hollow fiber membranes were hydrophobic enough to be utilized in membrane contactor experiments under non-wetting conditions, the contact angles of these fibers were determined. The observed contact angles are shown in figure 3.7 for the ceramic membrane with asymmetric structure, PVDF and PTFE hollow fibers. The contact angle of the ceramic membrane with symmetric structure is not shown because it was confirmed that these membranes have the same hydrophobicity as the ceramic membranes with asymmetric structures due to the similar procedures and experimental protocols used in the preparation of the ceramic membranes.

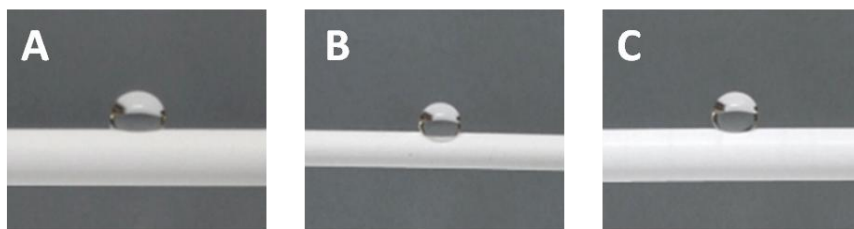


Figure 3.7. Contact angle measurements of the A) asymmetric ceramic, B) PVDF and C) PTFE hollow fiber membranes.

The obtained contact angles of these fibers were 111° , 93.9° and 112.9° for the ceramic, PVDF, and PTFE, respectively. The characteristics and the properties of the ceramic and polymeric hollow fiber membranes obtained after characterization are summarized and collected in Table 3.4.

Table 3.4. Main characteristics of the hollow fibers used in this work.

	CERAMIC asymmetric	CERAMIC symmetric	PTFE	PVDF
d_{in} (mm)	0.9	1	1.5	0.752
d_{out} (mm)	2.2	1.5	1.9	1.268
Contact angle ($^\circ$)	111.1	111.1	112.9	93.9
r_p (μm)	0.10/10	0.15	0.40	0.20
$r_{p,max}$ (μm)	20	0.35	0.65	0.30

Gas absorption experiments

Once the hollow fiber membranes were characterized, membrane modules were prepared by using 5 hollow fibers of 22 cm in length. Gas absorption experiments were carried out using a solution of 0.2 M AgNO_3 in water as absorbent, with different feed gas compositions in the range 0-50 % v/v $\text{C}_3\text{H}_6/\text{C}_3\text{H}_8$ at 1 bar and 298 K. These experiments were performed at liquid flow rates between 100 and 400 mL min^{-1} while the total gas flow rate was kept constant at 20 mL min^{-1} . The experimental molar fluxes of propylene and the overall mass transfer coefficients for all the experiments were obtained assuming negligible propane absorption in water according to eqs. 3.39 and 3.40 [49].

$$J_{\text{C}_3\text{H}_6} = \frac{1}{A} (F_{\text{in}} \cdot y_{\text{C}_3\text{H}_6,\text{in}} - F_{\text{out}} \cdot y_{\text{C}_3\text{H}_6,\text{out}}) \quad (3.39)$$

$$J_{\text{C}_3\text{H}_6} = K_{\text{overall}} \frac{\Delta y_{\text{C}_3\text{H}_6,\text{lm}} \cdot P}{R \cdot T} \quad (3.40)$$

P is the pressure in the gas (bar), F is the gas molar flow rate ($\text{mol} \cdot \text{s}^{-1}$) and $\Delta y_{\text{C}_3\text{H}_6,\text{lm}}$ is the logarithmic mean of the driving force based on gas phase molar fractions and taking into account the propylene concentration at the inlet ($y_{\text{C}_3\text{H}_6,\text{in}}$) and outlet ($y_{\text{C}_3\text{H}_6,\text{out}}$) of the contactor.

Figure 3.8 shows the propylene molar flux across the membrane using the asymmetric ceramic membrane module at 298 K as a function of the propylene logarithmic mean molar fraction. The results show that the flux of propylene increases with increasing the partial pressure of propylene in the gas phase following a linear trend. Then, the values of the overall mass transfer coefficients were obtained from the slope as previously reported Luis et al. [16] and Ortiz et al. [17].

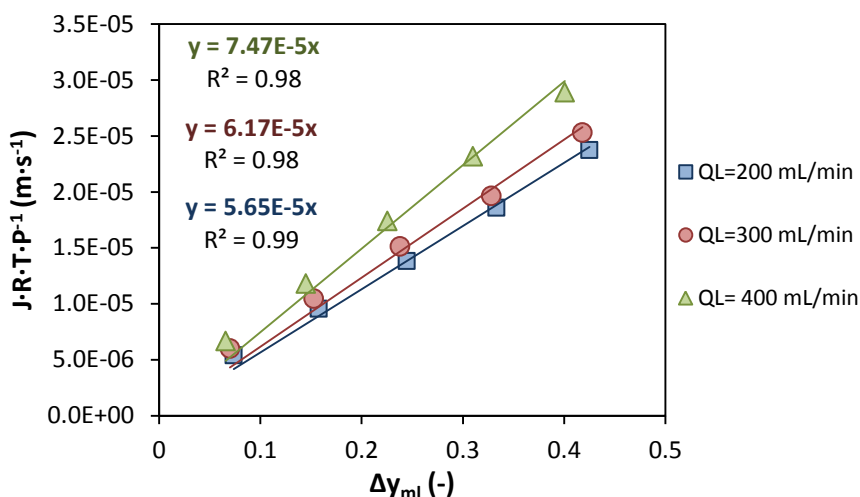


Figure 3.8. Absorption flux of propylene as a function of the propylene logarithmic mean molar fraction in the asymmetric ceramic membrane contactor using 0.2 M $AgNO_3$ in water as absorption medium at 1 bar and 298 K.

It can be seen that the overall mass transfer coefficient increases from $5.65 \cdot 10^{-5}$ to $7.47 \cdot 10^{-5} m \cdot s^{-1}$ as the liquid flow rate is increased from 200 to 400 $mL \cdot min^{-1}$. The same procedure was carried out for the rest of the membrane modules under study and the overall mass transfer coefficient was determined as a function of the liquid velocity. In order to compare the individual membrane mass transfer resistances occurring in the membrane modules, the experimental results were analyzed using the Wilson plot method. The Wilson plot method provides an outstanding tool for the analysis and design of mass transfer processes. It deals with the determination of the dependence of the mass transfer coefficients with the operational conditions based on measured experimental data and the resistance-in-series model [50,51]. $K_{overall}^{-1}$ versus $u^{-\alpha}$ is plotted and the value of the empirical parameter, α , is chosen from the best fitting to a straight line. In the gas-liquid membrane contacting process, if the resistance in the gas phase is much smaller than the total resistance it becomes negligible. Thus, the y-

intercept of the Wilson plot represents the value of membrane mass transfer resistance.

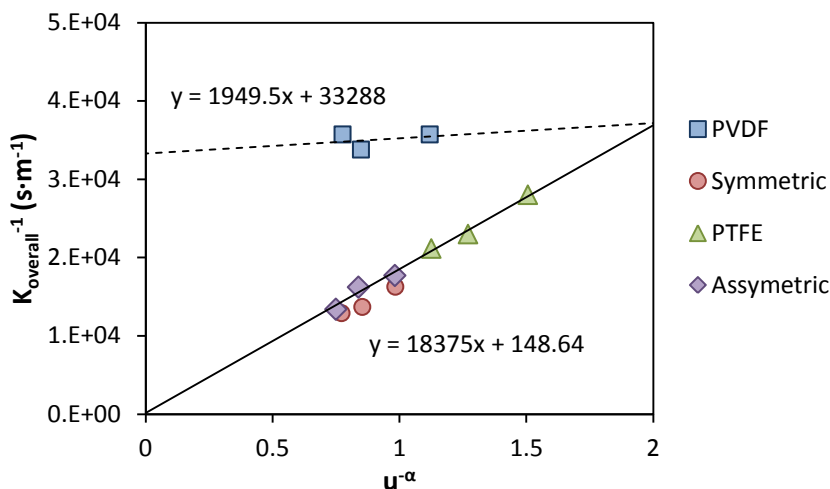


Figure 3.9. Wilson-plot of the experimental mass transfer resistance in the absorption of propylene in 0.2 M AgNO_3 aqueous solution in the different membrane modules used in this work at 293 K and a gas flow rate of $20 \text{ mL}\cdot\text{min}^{-1}$.

From figure 3.9 it can be seen that the PVDF membrane exhibited the highest membrane mass transfer resistance of the 4 types of membranes under study. This is because the membrane pores of PVDF were partially wetted by the absorbing solution, which finally results in a much higher mass transfer resistance in the membrane. On the other hand, it can be noticed that the membrane mass transfer resistances for the PTFE, symmetric and asymmetric ceramic membranes were negligible in comparison with the overall mass transfer resistance. This confirms that these membranes did not exhibit any wetting phenomena due to their higher hydrophobic character. Moreover, these findings demonstrate that the performance of ceramic membranes were similar to PTFE membranes, which is considered one of the polymers with best performance that could be promoted to be used in commercial applications.

Long-term assessment

Although a comparison at short times between the different types of fibers is useful to make a first choice, in order to implement an industrial process that can be operated for an extended period of time, it is necessary to conduct a long-term assessment of the fibers performance. For this reason, the different membrane modules were operated under the same experimental conditions for 60 days, and the overall mass transfer coefficient was experimentally determined every 15 days. Figure 3.10 plots the dimensionless overall mass transfer coefficient defined as ($K_{\text{overall } t=t} / K_{\text{overall } t=0}$) over 2 months of operation.

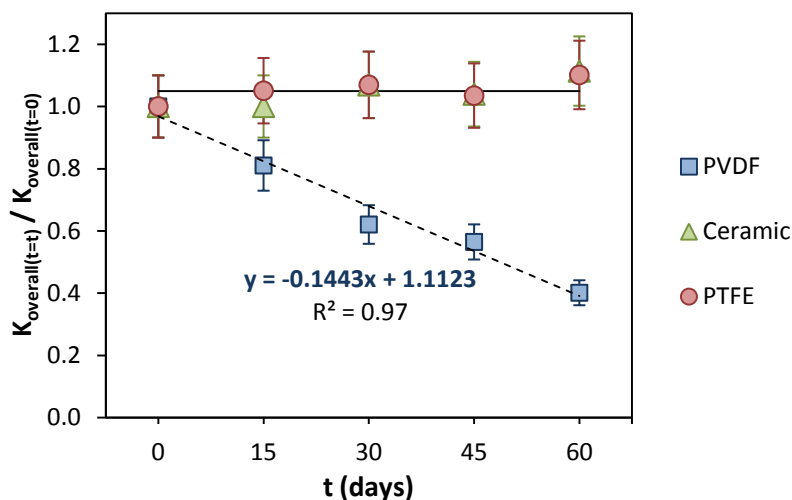


Figure 3.10. Dimensionless overall mass transfer coefficient in the different membrane modules used in this work for the absorption of propylene in 0.2 M AgNO_3 aqueous solution at 293 K, gas flow rate of $20 \text{ mL}\cdot\text{min}^{-1}$ and liquid flow rate of $200 \text{ mL}\cdot\text{min}^{-1}$.

It can be noted that for the PTFE and ceramic membranes, the overall mass transfer coefficient remained constant over the operating period indicating that these materials did not wet or degrade within this investigation stage. However, the performance for the PVDF membrane

decreased continuously with time following a linear trend, achieving a value after 2 months that was 60 % lower than the initial overall mass transfer coefficient value. This decline can be attributed to an increase in the pore volume wetted with time, resulting in higher mass transfer resistance in the membrane that is the controlling step when using PVDF membranes. Furthermore, after 2 months contact with the solvent, the PVDF fibers turned from white to transparent, which reveals that a wetting phenomenon was occurring. On the other hand the appearance of the PTFE and ceramic membranes remained unaffected. Figure 3.11 shows the pictures of the different fibers after being immersed in the reactive media for 2 months.

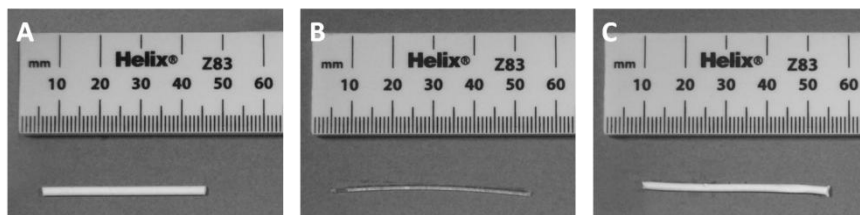


Figure 3.11. Pictures of fibers after 2 months immersion in the solvent. A) Ceramic with asymmetric structure, B) PVDF, C) PTFE.

Therefore it has been demonstrated that ceramic fibers can be an alternative to overcome the instability and durability problems associated with the use of traditional polymeric membranes. However they typically present poor mechanical resistance and suffer from expensive and complex preparation methods that limit their use in industrial applications. Thus in the separation of propane/propylene gas mixtures by reactive absorption the use of highly hydrophobic polymeric membranes (such as PTFE or polyolefins) is still preferred. Therefore, in next sections the use of two different commercial contactors equipped with polyolefin membranes are considered to carry out the separation process avoiding the wetting phenomena.

3.4.2. Parallel flow membrane contactor

This section continues and report progresses on a previous work carried out in our research group [17]. First of all the influence of the liquid flow rate in the separation performance was evaluated. Figure 3.12 shows the effect of the absorbing liquid flow rate on the change in the gas stream composition between the inlet and outlet of the membrane module versus time working with constant inlet gas flow rate (50/50 % v/v C_3H_6/C_3H_8) and $Ag^+-BMImBF_4$ [0.25 M] as reactive medium at 298 K.

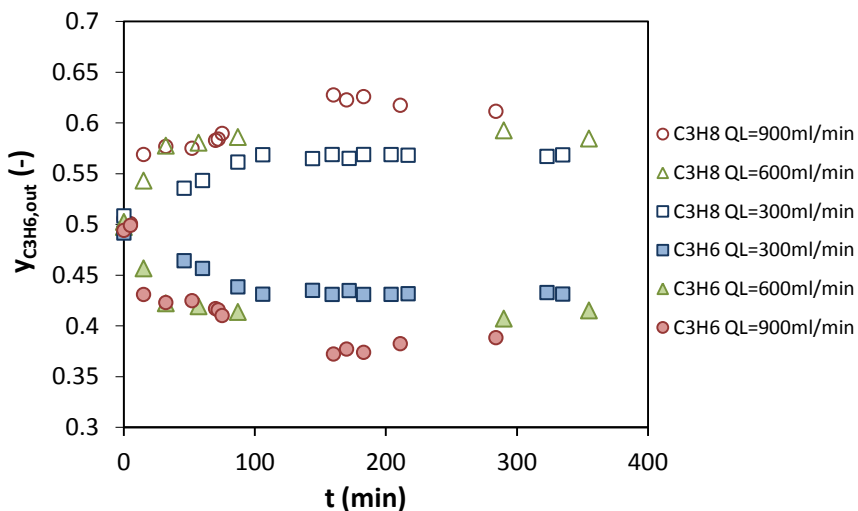


Figure 3.12. Evolution of the outlet gas stream composition in the membrane module versus time for constant inlet gas flow rate (50/50 % v/v C_3H_6/C_3H_8) at 298 K and different liquid volumetric flow rate.

As a large amount of liquid was being continuously recycled into the process, the reactive medium is very far from saturation and therefore a pseudo-steady state is reached where the outlet composition in the gas phase and mass transfer flux of propylene remained practically constant. The experimental molar fluxes of absorbed propylene and overall mass transfer coefficients for all the experiments performed at different liquid

volumetric flow rate at 298 K were obtained assuming negligible propane absorption according to eqs. 3.39 and 3.40.

Figure 3.13 shows that for a feed composition of 50/50 % v/v of C_3H_6/C_6H_8 , the propylene flux is enhanced from $4.1 \cdot 10^{-5}$ to $1.12 \cdot 10^{-4}$ $\text{mol} \cdot \text{m}^{-2} \cdot \text{s}^{-1}$ when the liquid flow rate increases from 300 to 900 $\text{mL} \cdot \text{min}^{-1}$ showing a remarkable improvement in the overall mass transfer coefficient.

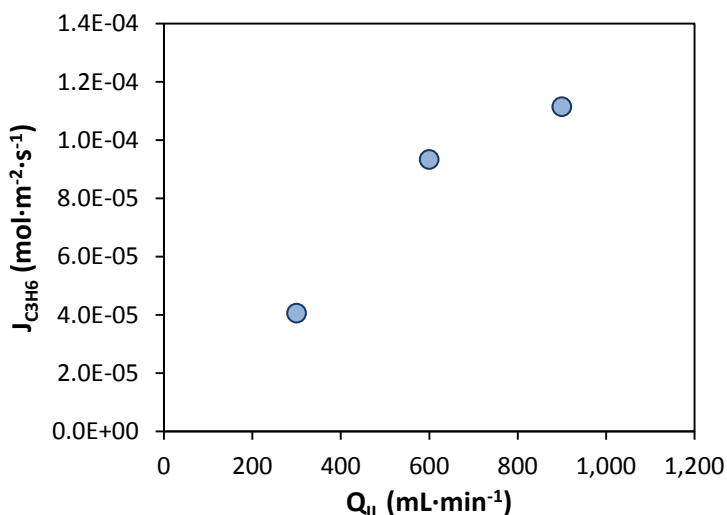


Figure 3.13. Effect of the liquid flow rate in the flux of propylene for constant inlet gas flow rate (50/50 % v/v C_3H_6/C_3H_8) at 298 K and silver concentration of 0.25 M.

The absorption rate increased with increasing the liquid flow rate. This is because an increase in the liquid flow rate results in the decrease of the boundary layer thickness on the liquid side. Hence, this leads to the decrease of the resistance of the liquid phase, and the increase in the mass transfer rate. The experimental evaluation of the mass transfer resistances in the system was carried out through the Wilson plot (figure 3.14). For the tubular membrane contactor Enka-Microdyn MD020 TP 2N with the liquid absorbent flowing through the shell side the value of the empirical parameter α was 0.54. Equation 3.41 correlates the overall

mass transfer resistance to the mean superficial velocity of the liquid phase.

$$\frac{1}{K_{\text{Overall}}} = 86583u_e^{-0.54} + 2873 \quad (3.41)$$

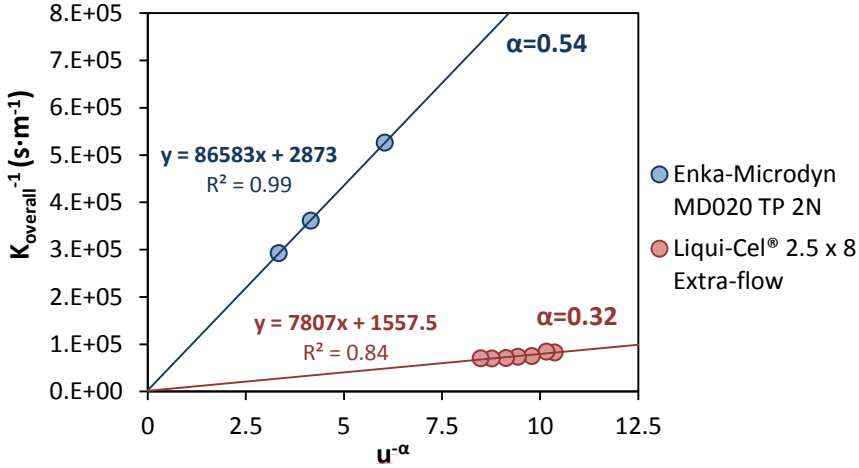


Figure 3.14. Wilson plot of the experimental mass transfer coefficient in the absorption of propylene in BMImBF_4 in the Enka-Microdyn MD020 TP 2N and Liqui-Cel® 2.5 x 8 Extra flow membrane contactor at 293 K.

According to the above equation, the mass transfer resistance of the membrane ($d_o/k_{\text{mg}} d_{\text{lm}}$) can be obtained from the y-intercept value, 2873 s·m^{-1} , which represents less than 1 % of the overall mass transfer resistance, indicating that the resistances of the gas film and the membrane are negligible and therefore the system is controlled by the diffusional resistance in the liquid film.

In general, the flow pattern in the shell side is not clearly understood. Several correlations have been proposed in the literature over the past few years, but none is applicable to a wide range of systems. Equations

that include geometrical dependence have been used successfully to describe the mass transfer coefficient outside the fibers (table 3.2).

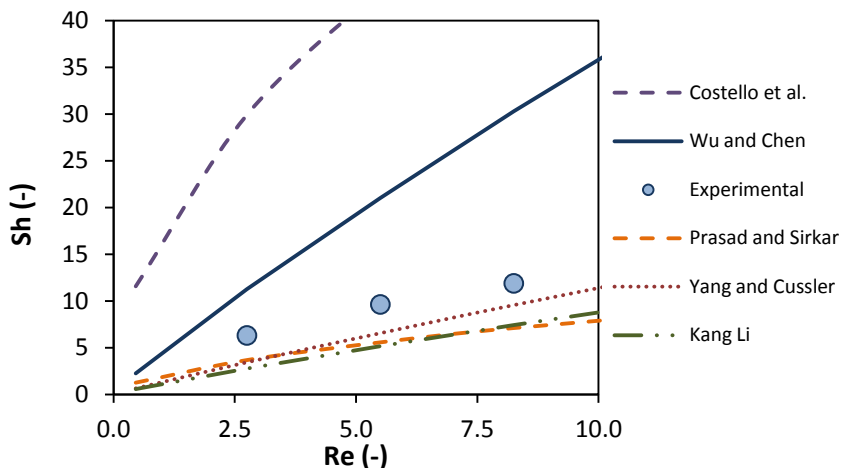


Figure 3.15. Comparison between experimental results and reported correlations.

Figure 3.15 shows values of the Sherwood number obtained from experimental data together with values estimated from literature correlations. The correlations reported by Yang & Cussler [30], Prasad & Sirkar [31] and Li et al. [34] predicted closer values to the experimental Sh number than the correlations proposed by Wu and Chen [32] and Costello et al. [33]. The reason for the larger deviation using the 2 latter correlations may be the different range of Reynolds numbers used in this study with respect to that used in the other works where the proposed correlations were obtained. Although turbulent flow can also be achieved in a membrane contactor, unfortunately in practice it may not be economically and operationally viable. In the first place, to maintain a turbulent flow, larger power consumption is needed and secondly under high liquid pressures the membrane might be wetted by the liquid. In this case, the mass-transfer will be greatly reduced because of the presence of a stagnant liquid film in the membrane pores. Next section deals with the use of cross-flow membrane contactors with improved design to reduce the liquid boundary layer resistance.

3.4.3. Transverse flow membrane contactor

A pure propylene gas stream was flowed at 1 bar into the membrane contactor operating isothermally at 293 K. The gas flow rate at the outlet of the contactor was measured along time in experiments performed at different liquid flow rates obtaining non linear profiles as displayed in figure 3.16. The improved fluid-dynamics of the transverse flow membrane contactor provided higher values of the overall mass transfer coefficient which combined with the high interfacial area leads to enhanced rate of mass transfer. Thus the absorption kinetics were fast leading to saturation of the liquid absorbent after short operational times between 8 and 15 minutes.

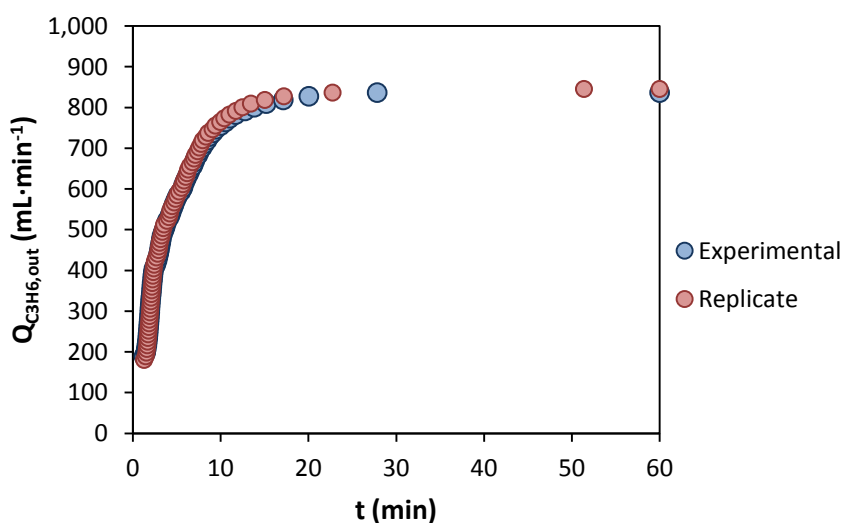


Figure 3.16. Evolution of the module outlet gas flow rate with time for an inlet gas flow rate of 860 mL·min⁻¹ and a liquid flow rate of 714 mL·min⁻¹ at 293 K.

The experimental values of the molar flux of propylene across the membrane during the absorption step were calculated by performing an overall mass balance to propylene in the contactor (eq. 3.42).

$$J_{C_3H_6} = \frac{(F_{C_3H_6,in} - F_{C_3H_6,out})}{A} \quad (3.42)$$

Under the operating conditions used in this study, the pressure drop due to the gas flow through the lumen of the hollow fibers was very low and thus it can be safely neglected. Many authors reported that for transverse flow membrane contactors the pressure drop in the shell side was much lower than in the lumen side. However, in our study the liquid flowing through the shell side is the ionic liquid BMImBF₄ which presents a relative high viscosity (0.105 Pa·s at 293 K). Just because of the high viscosity of the ionic liquid the pressure drop in the shell side could be important.

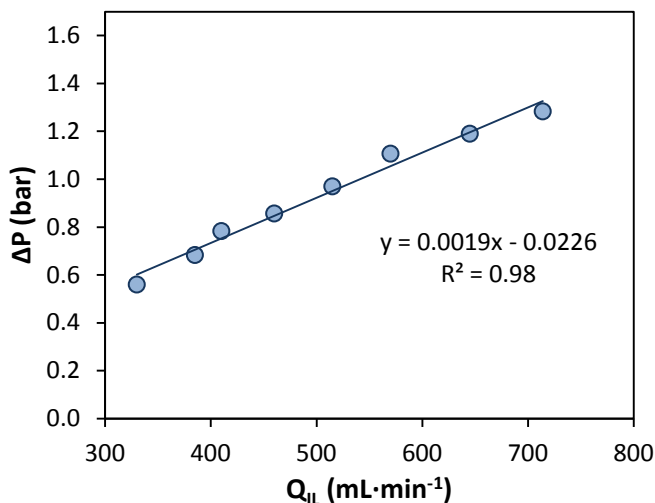


Figure 3.17. Pressure drop in the transverse flow module in the shell side.

Figure 3.17 shows the dependence of the pressure drop with the liquid flow rate in the shell side. It can be noted that in this case the pressure drop in the shell side is important due to the high viscosity of the ionic liquid, increasing from 0.68 bar to 1.28 bar following a linear trend when the liquid flow rate is increased from 300 to 700 mL·min⁻¹. On the other hand, it was demonstrated that the overall mass transfer resistance

decreases with increasing the liquid flow rate. Therefore a trade-off must be reached by selecting the operational flow rate that enhances the mass transfer rate not entailing excessive pressure drop. The values of the overall mass transfer coefficient have been calculated by fitting the experimental data to the mathematical model described in section 3.3 using the parameter estimation tool of the software Aspen Custom Modeler®. Table 3.5 reports the overall mass transfer coefficient as a function of the flow rate of ionic liquid flowing through the shell side.

Table 3.5. Experimental values of K_{overall} corresponding to different liquid flow rates.

$Q_{\text{IL}} \text{ (mL} \cdot \text{min}^{-1})$	$K_{\text{overall}} \cdot 10^5 \text{ (m} \cdot \text{s}^{-1})$
385	1.21
410	1.18
460	1.33
515	1.36
570	1.41
645	1.43
714	1.42

Figure 3.14 displays the Wilson-plot of K_{overall}^{-1} versus $u^{-\alpha}$ for the absorption of propylene in pure BMImBF₄ used as liquid absorbent. In this case the experimentally obtained value of the empirical parameter α for the hollow fiber membrane contactor Liqui-Cel® with the liquid absorbent flowing through the shell side was 0.32. The experiments were carried out with pure propylene, so that the gas phase resistance was neglected. Thus the value of the mass transfer resistance offered by the polypropylene fibers Celgard X50® ($d_{\text{out}}/k_{\text{mg}} \cdot d_{\text{lm}}$) has been obtained from the y-intercept ($1557.5 \text{ s} \cdot \text{m}^{-1}$). Equation 3.43 correlates the overall mass transfer resistance to the mean superficial velocity of the liquid phase.

$$\frac{1}{K_{\text{overall}}} = 7807u_e^{-0.32} + 1557.5 \quad (3.43)$$

Moreover, comparing the values of the individual mass transfer resistances it is observed that the contribution of the membrane resistance to the overall mass transfer resistance is always lower than 2.2 % as reported in table 3.6:

Table 3.6. Comparison of the individual mass transfer resistances.

Q_{IL} ($\text{mL} \cdot \text{min}^{-1}$)	R_{gas} ($\text{s} \cdot \text{m}^{-1}$)	$R_{\text{m}} \cdot 10^3$ ($\text{s} \cdot \text{m}^{-1}$)	$R_{\text{l}} \cdot 10^4$ ($\text{s} \cdot \text{m}^{-1}$)	$R_{\text{overall}} \cdot 10^4$ ($\text{s} \cdot \text{m}^{-1}$)
385	0	1.56	8.12	8.28
410	0	1.56	8.29	8.45
460	0	1.56	7.36	7.51
515	0	1.56	7.21	7.37
570	0	1.56	6.94	7.10
645	0	1.56	6.84	7.00
714	0	1.56	6.88	7.03

After having analyzed the resistance to the mass transfer process under the experimental conditions where the diffusional transport of the gas solute through the ionic liquid film becomes the slowest step, the analysis of the phenomena involved in the mass transfer rate through the liquid boundary layer becomes necessary. Many correlations have been published to estimate the mass transfer coefficient for the liquid phase flowing through the shell side in transverse flow membrane contactors (table 3.3). Unfortunately these correlations are usually developed for water or other conventional solvents and furthermore none is generally applicable to a wide range of systems because in contrast to the tube side, the module geometry, fiber arrangement and fluid flow pattern in the shell side are complex and poorly understood

yet. Therefore, in order to satisfactorily describe the mass transfer phenomena in the controlling step, an empirical correlation has been obtained by fitting the experimental data to the mathematical model described in section 3.3. The values of the Sherwood number obtained in this work were correlated to the Re and Sc numbers obtaining the empirical correlation shown in eq. 3.44:

$$Sh = 1.1 \cdot Re^{0.32} Sc^{0.33} \quad (3.44)$$

The value of the constant parameter “1.1” is within the range of the most common correlations reported in literature. Moreover, the Sherwood number dependence on the shell side Reynolds number was found to be very close to the values for gas-liquid systems previously obtained by Zheng et al. [9] ($Sh \propto Re^{0.42}$) and Fouad et al. [35] ($Sh \propto Re^{0.36}$). However these correlations have been usually developed for water or other conventional solvents and propose stronger dependence of the Sherwood number on the Reynolds number. The correlation obtained in this work is valid for the ionic liquid flowing through the shell side of the transverse flow membrane contactor Liqui-Cel® 2.5 x 8 Extra-Flow at low Reynolds numbers ($Re < 0.006$) and 293 K. The low values of the Reynolds number are mainly due to the high viscosity of the ionic liquid that, on the other hand is responsible for the high pressure drop in the module (figure 3.17). Figure 3.18 shows the reliability of the obtained correlation for the prediction of the experimental results with the ionic liquid flowing through the shell side of the 2.5 x 8 Extra Flow module.

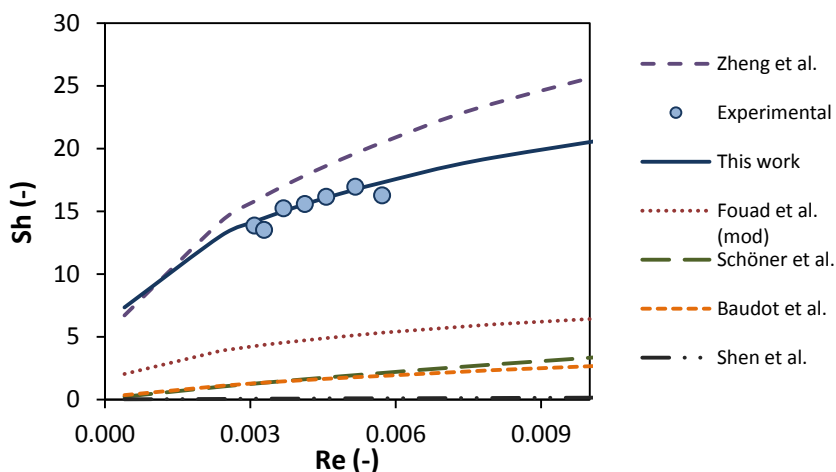


Figure 3.18. Comparison of predicted values of the shell side Sherwood numbers using different correlations and the experimental results of this work.

Although the Reynolds numbers are low, the experimental values of the Sherwood number on the shell side increased from 13.5 to 17.5 as the Reynolds number is gradually increased. The predicted values from the correlation of Zheng et al. [9] were slightly higher than the experimental results. On the other hand, the correlations of Fouad et al. [35], Schöner et al. [5], Baudot et al. [36] and Shen et al. [37] greatly underestimated the experimental results. On the contrary, the correlation proposed in this study fits the experimental results with a maximum error of 10 %.

After the mass transfer rate in the system has been evaluated, the separation performance of the system has been analyzed by carrying out experiments with 50/50 % v/v C_3H_8/C_3H_6 mixtures with different concentrations in the liquid absorbent in the range 0-0.25 M. Figure 3.19 shows the evolution of molar fluxes of propane and propylene in the membrane module. As expected, higher fluxes of propylene are obtained when increasing the silver concentration in the ionic liquid. This also involves an increase in the flux of propane due to the higher propane partial pressure in the gas phase which eventually leads to a higher propane driving force according to eq. 3.5.

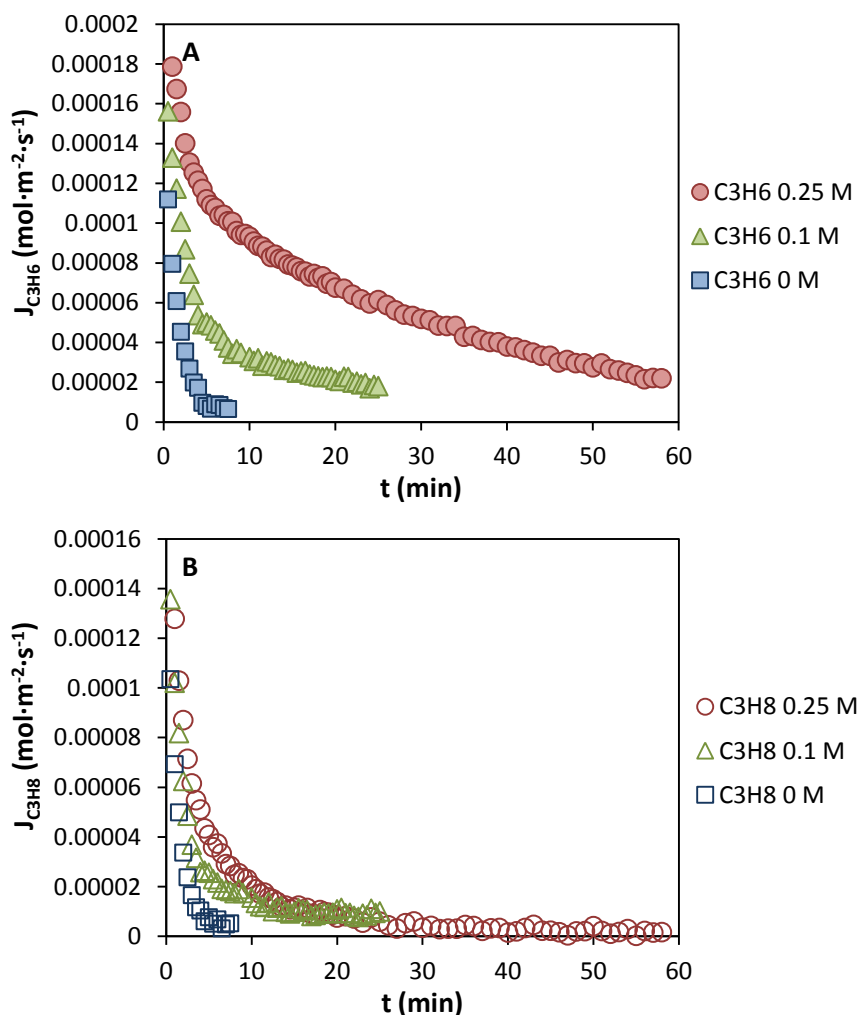


Figure 3.19. Evolution of the fluxes of A) propylene and B) propane in the membrane module versus time for constant inlet gas flow rate of $859 \text{ mL} \cdot \text{min}^{-1}$, 298 K and different silver concentrations.

Figure 3.20 depicts the experimentally measured change in the gas composition between the module inlet and outlet versus time working with constant inlet gas flow rate (50/50 % v/v $\text{C}_3\text{H}_6/\text{C}_3\text{H}_8$). Again an increase in the silver concentration in the reactive media results in a better separation performance, increasing the propylene molar fraction

at the module outlet from 0.54 to 0.71 when the silver concentration in the liquid phase is increased from 0 to 0.25 M. Although the transverse flow membrane contactor greatly improved the results previously obtained with the parallel flow membrane contactor, the system still presents severe limitations to mass transfer in the liquid side that limit the real application of this technology. Thus in order to overcome these limitations more research focused on finding new ionic liquids with low propane solubility and very low viscosity is needed.

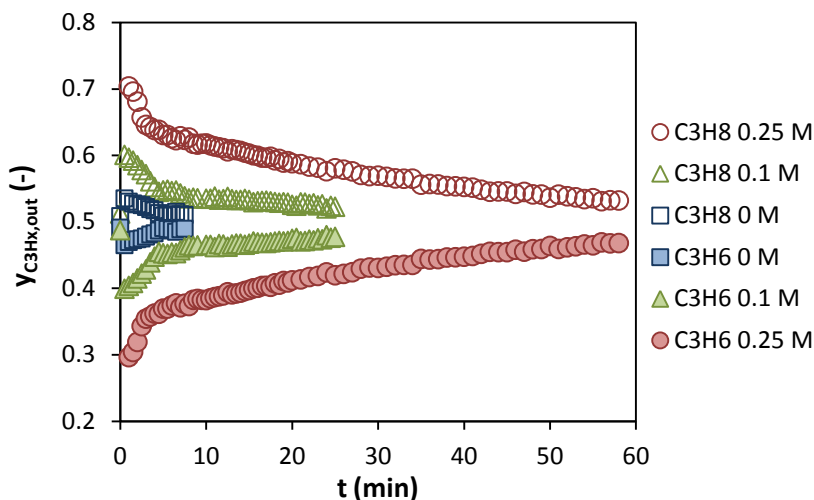


Figure 3.20. Evolution of the outlet gas compositions of A) propylene and B) propane in the membrane module versus time for constant inlet gas flow rate of $859 \text{ mL}\cdot\text{min}^{-1}$ at 298 K and different silver concentrations.

3.4.4. Mathematical model validation

Once the model was developed, a simulation analysis was performed in order to check the model sensitivity under different operational conditions such as different feed gas compositions in the range 30-70 % v/v $\text{C}_3\text{H}_6/\text{C}_3\text{H}_8$, different liquid flow rates between 300 and $900 \text{ mL}\cdot\text{min}^{-1}$ and different silver concentrations from 0 to 0.25 M. In order to solve

the mathematical model, the equations described in section 3.3 were implemented in Aspen Custom Modeler®. The parallel flow membrane contactor with tubular configuration has low interfacial area, which combined with the less favorable hydrodynamics for mass transfer in the shell side leads to a pseudo-steady state where the liquid is very far from saturation. Therefore the mathematical model was validated considering this pseudo-steady state. On the contrary the much higher gas fluxes obtained with the cross flow membrane contactor together with the higher membrane area force a fast liquid saturation leading to a dynamic state where the flux and the module outlet gas composition rapidly change with time and therefore a dynamic state must be considered. In this section the mathematical model was validated using the experimental data previously reported by Ortiz et al. [17] and in sections 3.4.2 and 3.4.3 of this chapter.

Figures 3.21-3.23 show the comparison between experimental and simulated data in terms of gas composition at the outlet of the parallel flow membrane contactor with tubular configuration (Microdyn MD020 TP 2N) with gas and liquid phases flowing in counter current mode, under different conditions. Based upon the comparison it can be confirmed that there is a good agreement between the experimental results and simulated data. Figure 3.21 depicts the effect of the silver salt concentration in the absorbing mixture, clearly showing that the separation efficiency improves with an increase in the concentration of silver. For a feed composition of 50/50 % v/v of C_3H_6/C_6H_8 in the parallel flow membrane contactor, the propylene flux is strongly enhanced from $1.59 \cdot 10^{-5}$ to $3.46 \cdot 10^{-5} \text{ mol} \cdot \text{m}^{-2} \cdot \text{s}^{-1}$ when the silver salt is added up to a concentration of 0.1 M in the ionic liquid. However when the silver ion concentration increases from 0.1 to 0.25 M the enhancement on the propylene flux is negligible. This phenomenon could be attributed to the strong dependency of the viscosity of the Ag^+ -BMImBF₄ reactive medium with the silver ions concentration, fact that induces gas diffusion rate limitations. Figure 3.22 depicts the comparison between experimental and simulated results at liquid flow rates (300-900 mL·min⁻¹) at a silver concentration of 0.25 M. It can be observed that increasing the liquid

flow rate results in better separation performance because the diffusional resistance of the liquid boundary layer is decreased. Figure 3.23 also shows the good agreement between the experimental data and model predictions for various feed gas compositions and different silver salt contents in the ionic liquid absorbing mixtures.

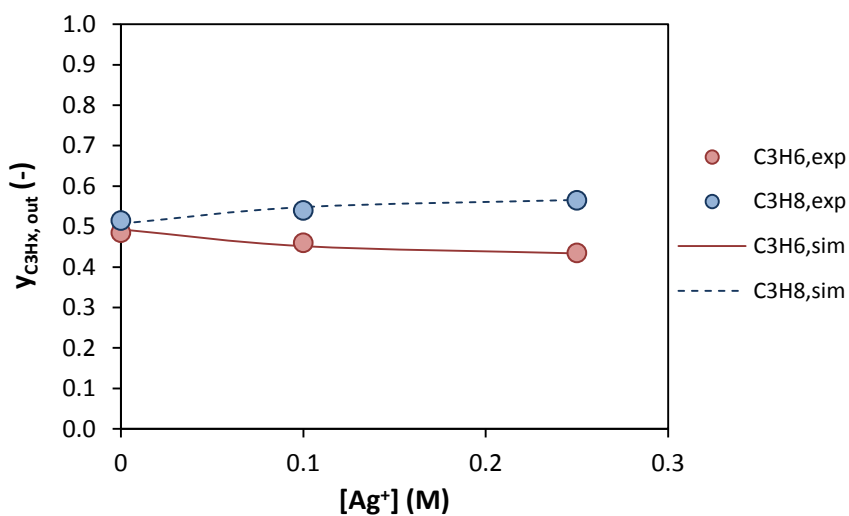


Figure 3.21. Comparison between experimental and simulated results at different silver concentrations (0-0.25 M), liquid flow rate of 300 mL·min⁻¹, gas flow rate of 16.66 mL·min⁻¹ and a feed gas composition of 50/50 % v/v C₃H₆/C₃H₈ at 1.2 bar.

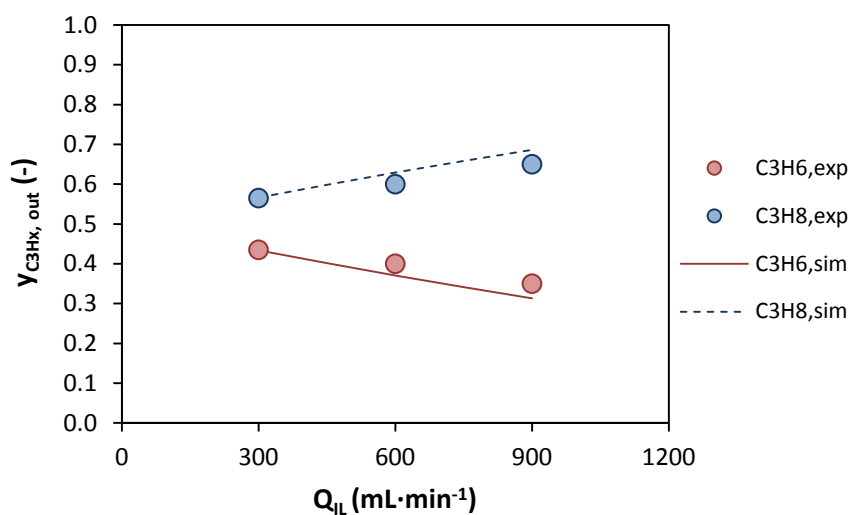
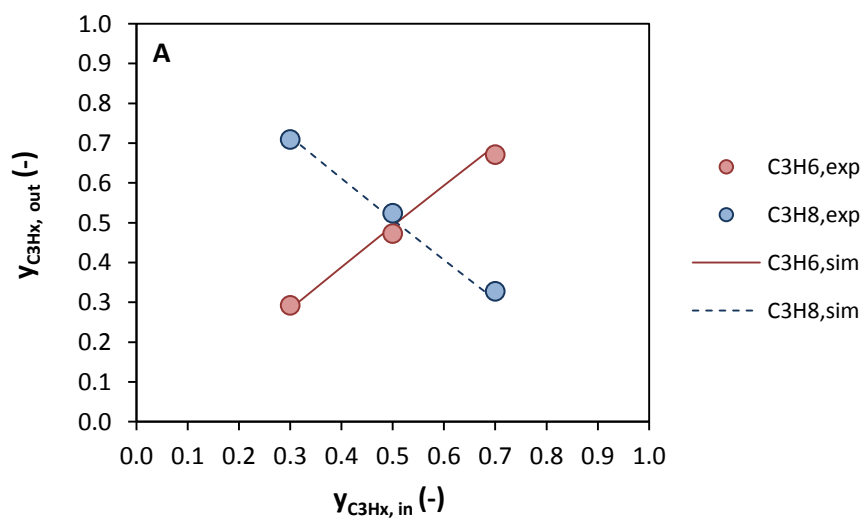


Figure 3.22. Comparison between experimental and simulated results at liquid flow rates (300-900 $\text{mL} \cdot \text{min}^{-1}$), silver concentration of 0.25 M, gas flow rate of 16.66 $\text{mL} \cdot \text{min}^{-1}$ and feed gas composition of 50/50 % v/v C_3H_6/C_3H_8 at 1.2 bar.



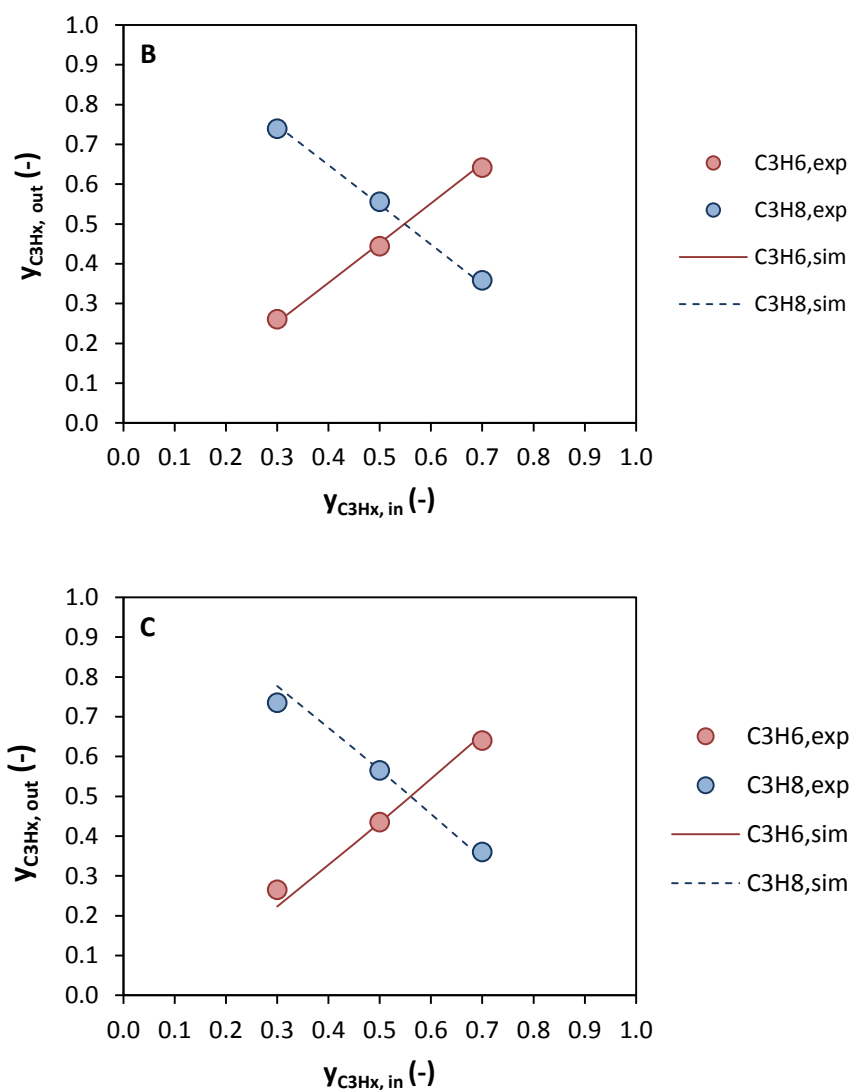


Figure 3.23. Comparison between experimental and simulated results at feed gas compositions (30-70 % v/v C₃H₆/C₃H₈), liquid flow rate of 300 mL·min⁻¹, gas flow rate of 16.66 mL·min⁻¹, 1.2 bar and silver salt concentrations of A) 0 M, B) 0.1 M and C) 0.25 M.

Regarding the model validation for the transverse flow membrane contactor figure 3.24 displays the change over time of the molar flux of propylene across the membrane for an inlet gas flow rate of 859 mL·min⁻¹ and a liquid flow rate of 714 mL·min⁻¹ at 293 K.

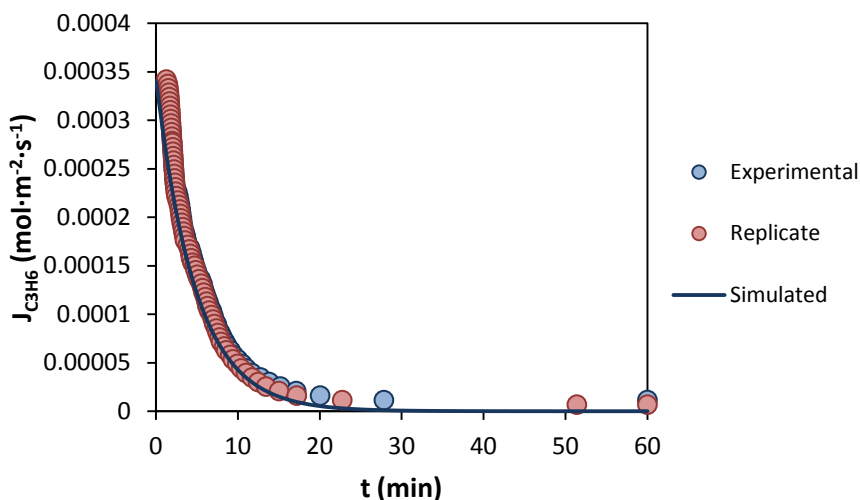


Figure 3.24. Comparison between experimental and simulated results of propylene flux across the membrane for an inlet gas flow rate of 859 mL·min⁻¹ of pure propylene and a liquid flow rate of 714 mL·min⁻¹ at 293 K.

A reasonable agreement is observed between experimental results and model simulated curves being the standard deviation (eq.3.2) in all cases less than 0.12. Thus, it is concluded that the developed model based on the resistances in series approach, predicts satisfactorily well the propane/propylene separation process by reactive absorption under the operational conditions studied in this thesis.

3.4.5. Comparison between different contactors

Finally a comparison of the performance of the contactors for the separation process has been done. In the comparison previous results

obtained in our research group using a conventional stirred tank reactor are included [17] (table 3.7). The comparison between the different contactors has been done in terms of mass transfer coefficients and interfacial area. The stirred tank reactor shows a very high overall mass transfer coefficient. However, the interfacial area is highly dependent on the stirring speed, and even in the best case the interfacial area is much lower than the one provided by the membrane contactors under study. Details concerning the interfacial area calculation in the stirred tank reactor can be found in a previously published work by our research group [17]. On the other hand, the tubular membrane contactor with parallel flow operated countercurrently, offers higher interfacial area than the stirred tank reactor but due to the poor fluid-dynamics of the ionic liquid circulating through the shell side, the overall mass transfer coefficient is much lower. In this sense, the obtained results show that the improved fluid-dynamics of the transverse flow membrane contactor can contribute to overcome these limitations leading to an overall mass transfer coefficient 17.6 times higher than that reported using a parallel-flow contactor when the silver concentration in the ionic liquid is 0 M. The values of $K_{overall}$ obtained with the transverse flow membrane contactor and a silver concentration of 0.25 M were obtained by simulation using the values of $K_{overall}$ determined from the experiments without silver and the enhancement factor estimated using the mathematical model described in section 3.3. These results show that the high specific area of the hollow fiber membrane contactor, together with the beneficial and improved fluid-dynamics of the transverse flow with the liquid circulating through the shell side, results in a higher mass transfer coefficient per specific area than the one obtained using conventional contactors. The new system, which uses a transverse flow membrane contactor to carry out the reactive absorption of propylene, succeeds also in intensifying the process by a factor of 17.4 in terms of mass transfer per specific area compared to the stirred tank reactor system ($K_{overall} * a(MC) / K_{overall} * a(CSTR)$) when a concentration of silver ions of 0.25 M in the IL is used.

Table 3.7. Comparison of the performances of different contactors.

	a ($\text{m}^2 \cdot \text{m}^{-3}$)	$K_{\text{overall}} \cdot 10^6$ ($\text{m} \cdot \text{s}^{-1}$)	$K_{\text{overall}} \cdot a \cdot 10^4$ (s^{-1})
Stirred tank reactor [$\text{Ag}^+ = 0.25 \text{ M}$] [17]	212	111	236
Microdyn MD020 TP 2N [$\text{Ag}^+ = 0 \text{ M}$] [17]	313	0.68	2.12
Microdyn MD020 TP 2N [$\text{Ag}^+ = 0.25 \text{ M}$]	313	3.4	10.7
Liqui-Cell® 2.5x8 EXTRA-FLOW [$\text{Ag}^+ = 0 \text{ M}$]	3500	12.1	423
Liqui-Cell® 2.5x8 EXTRA-FLOW [$\text{Ag}^+ = 0.25 \text{ M}$]*	3500	117	4109

*Results obtained by simulation

Since for the studied conditions the main resistance to mass transport is located in the liquid phase, the rheological properties of the liquid absorbent as well as the liquid flow rate have a great influence on the separation efficiency. Results show that the parallel flow membrane contactor presents severe limitations to mass transfer. As shown in figure 3.14 this phenomenon is greatly attenuated when using the transverse flow membrane contactor where the improved fluid-dynamics strongly reduce the diffusion rate limitations. However, the controlling step still remains in the liquid phase with a contribution above 97 %. This is mainly due to the high viscosity of BMImBF₄ (0.105 Pa·s at 293 K) which not only limits the diffusion rate of the components to be absorbed, but also limits the liquid velocity at which the process can be operated due to the high pressure drop. Therefore, new ionic liquids with low paraffin solubility and very low viscosity are needed to make the process commercially attractive. In order to solve these limitations the use of facilitated transport membranes will be explored in chapter 4.

3.5. Conclusions

The separation of gas olefins from paraffins streams using membrane contactors by reactive absorption with silver contained in ILs has been considered as an alternative and more efficient process to the conventional distillation separation. First of all a comparative analysis of the performance of 4 fibers of different nature, 2 polymeric (PVDF and PTFE) and 2 ceramic (with symmetric and asymmetric structures), and different properties has been carried out. It was found that PVDF membranes suffered from wetting phenomena by the liquid phase, which became more important over time. On the other hand, PTFE and ceramic membranes were proved to be suitable to carry out the separation process. However the use of highly hydrophobic polymeric membranes (such as PTFE) is still preferred over ceramic membranes due to economic considerations and the easier fabrication procedures.

Afterwards two different commercial membrane contactors: a parallel flow membrane contactor with tubular configuration and a hollow fiber transverse flow membrane contactor have been evaluated for the separation of propane/propylene gas mixtures. A mathematical model based on the resistances-in-series approach has been developed obtaining a good agreement between experimental and simulated results. Finally it was found that the improved fluid-dynamics of the transverse flow membrane contactor leads to an overall mass transfer coefficient 17.6 times higher than that reported using a parallel-flow membrane contactor. The results highlight that the process can be intensified by a factor of 17.4 in terms of mass transfer per specific area compared to a conventional stirred tank reactor system ($K_{overall} * a(MC) / K_{overall} * a(CSTR)$) when a concentration of silver ions of 0.25 M in the IL is used. However, the limiting step is still located in the liquid boundary layer, with a contribution higher than 97.8 % to the overall mass transfer resistance. Therefore, new ionic liquids with low paraffin solubility and very low viscosity are needed in order to make the process commercially attractive. In order to solve these limitations the use of facilitated transport membranes will be explored in chapter 4.

3.6. Nomenclature

A	effective membrane area (m^2)
C	concentration ($\text{mol}\cdot\text{m}^{-3}$)
D	diffusivity ($\text{m}^2\cdot\text{s}^{-1}$)
d_{out}	outer diameter of the fiber (m)
d_{in}	inner diameter of the fiber (m)
d_{cin}	inner diameter of the module (m)
d_{co}	outer diameter of the central delivery tube (m)
d_{h}	hydraulic diameter of the shell side (m)
d_{lm}	logarithmic mean diameter of the fiber (m)
d_{p}	pore diameter (m)
E_{A}	enhancement factor (-)
$E_{\text{A}\infty}$	infinite enhancement factor (-)
F	gas molar flow ($\text{mol}\cdot\text{s}^{-1}$)
H	Henry's constant ($\text{mol m}^{-3}\cdot\text{bar}^{-1}$)
Ha	Hatta number (-)
H_{di}	dimensionless Henry's constant (-)
ΔH_{sol}	standard solvation enthalpy ($\text{kJ}\cdot\text{mol}^{-1}$)
J	molar flux ($\text{mol}\cdot\text{m}^{-2}\cdot\text{s}^{-1}$)
K_{Eq}	equilibrium constant ($\text{m}^3\cdot\text{mol}^{-1}$)
$k_{1,1}$	kinetic constant of reaction 1,1 order ($\text{m}^3\cdot\text{mol}^{-1}\cdot\text{s}^{-1}$)
k_{g}	mass transfer coefficient in the gas phase ($\text{m}\cdot\text{s}^{-1}$)
k_{mg}	mass transfer coefficient in the membrane with the pores filled of gas ($\text{m}\cdot\text{s}^{-1}$)
k_{l}	mass transfer coefficient in the liquid phase ($\text{m}\cdot\text{s}^{-1}$)

K_{overall}	overall mass transfer coefficient ($\text{m}\cdot\text{s}^{-1}$)
N	number of fibers of the membrane module
L	effective fiber length (m)
P	pressure (bar)
Q	liquid flow rate ($\text{m}^3\cdot\text{s}^{-1}$)
R	universal gas constant ($\text{kJ}\cdot\text{mol}^{-1}\cdot\text{K}^{-1}$)
T	temperature (K)
u	mean superficial velocity of the liquid ($\text{m}\cdot\text{s}^{-1}$)
V	volume (m^3)
y	gas molar fraction (-)
z	axial distance (m)

Dimensionless numbers

Gz	Graetz number (-)
Sh	Sherwood number (-)
Sc	Schmidt number (-)
Re	Reynolds number (-)

Greek letters

δ	membrane thickness (m)
ε	porosity of the membrane (-)
θ	contact angle ($^{\circ}$)
μ	viscosity ($\text{Pa}\cdot\text{s}$)
ν	kinematic viscosity ($\text{m}^2\cdot\text{s}^{-1}$)
ρ	density ($\text{kg}\cdot\text{m}^{-3}$)

σ	surface tension ($\text{N}\cdot\text{m}^{-1}$)
τ	tortuosity (-)
\emptyset	form factor

Superscripts/subscripts

Ag^+	silver ion
C_3H_6	propylene
C_3H_8	propane
IL	ionic liquid

3.7. References

- [1] A. Gabelman, S.-T. Hwang. Hollow fiber membrane contactors. *J.Membr.Sci.*, 159 (1999) 61.
- [2] V.Y. Dindore. Gas purification using membranes gas absorption processes. PhD dissertation. University of Twente, (2003).
- [3] R. Klaassen, P.H.M. Feron, and A.E. Jansen. Membrane contactors in industrial applications. *Chem.Eng.Res.Design*, 83 (2005) 234.
- [4] H. Kreulen, C.A. Smolders, G.F. Versteeg, and W.P.M. Van Swaaij. Microporous hollow fibre membrane modules as gas-liquid contactors. Part 2. Mass transfer with chemical reaction. *J.Membr.Sci.*, 78 (1993) 217.
- [5] P. Schöner, P. Plucinski, W. Nitsch, and U. Daiminger. Mass transfer in the shell side of cross flow hollow fiber modules. *Chem. Eng. Sci.*, 53 (1998) 2319.
- [6] A. Sengupta, P.A. Peterson, B.D. Miller, J. Schneider, and C.W. Fulk Jr. Large-scale application of membrane contactors for gas transfer from or to ultrapure water. *Sep. Purif. Technol.*, 14 (1998) 189.
- [7] V.Y. Dindore, G.F. Versteeg. Gas-liquid mass transfer in a cross-flow hollow fiber module: Analytical model and experimental validation. *Int.J.Heat Mass Transfer*, 48 (2005) 3352.
- [8] V.Y. Dindore, D.W.F. Brilman, and G.F. Versteeg. Modelling of cross-flow membrane contactors: Physical mass transfer processes. *J.Membr.Sci.*, 251 (2005) 209.
- [9] J.-M. Zheng, Z.-. Dai, F.-. Wong, and Z.-. Xu. Shell side mass transfer in a transverse flow hollow fiber membrane contactor. *J.Membr.Sci.*, 261 (2005) 114.
- [10] S. Boributh, S. Assabumrungrat, N. Laosiripojana, and R. Jiraratananon. Effect of membrane module arrangement of gas-liquid membrane contacting process on CO₂ absorption performance: A modeling study. *J.Membr.Sci.*, 372 (2011) 75.

- [11] A.M. Barbe, P.A. Hogan, and R.A. Johnson. Surface morphology changes during initial usage of hydrophobic, microporous polypropylene membranes. *J.Membr.Sci.*, 172 (2000) 149.
- [12] J. Kamo, T. Hirai, and K. Kamada. Solvent-induced morphological change of microporous hollow fiber membranes. *J.Membr.Sci.*, 70 (1992) 217.
- [13] H.A. Rangwala. Absorption of carbon dioxide into aqueous solutions using hollow fiber membrane contactors. *J.Membr.Sci.*, 112 (1996) 229.
- [14] R. Wang, D.F. Li, C. Zhou, M. Liu, and D.T. Liang. Impact of DEA solutions with and without CO₂ loading on porous polypropylene membranes intended for use as contactors. *J.Membr.Sci.*, 229 (2004) 147.
- [15] K. Nymeijer, T. Visser, R. Assen, and M. Wessling. Super selective membranes in gas-liquid membrane contactors for olefin/paraffin separation. *J.Membr.Sci.*, 232 (2004) 107.
- [16] P. Luis, A. Garea, and A. Irabien. Zero solvent emission process for sulfur dioxide recovery using a membrane contactor and ionic liquids. *J.Membr.Sci.*, 330 (2009) 80.
- [17] A. Ortiz, D. Gorri, A. Irabien, and I. Ortiz. Separation of propylene/propane mixtures using Ag⁺-RTIL solutions. Evaluation and comparison of the performance of gas-liquid contactors. *J.Membr.Sci.*, 360 (2010) 130.
- [18] E. Drioli, A. Criscuoli, and E. Curcio, *Membrane Contactors: Fundamentals, Applications and Potentialities*, Amsterdam, Elsevier Science, 2006.
- [19] K. Li, *Ceramic membranes for separation and reaction*, Chichester, John Wiley & Sons Ltd., 2007.
- [20] B.F.K. Kingsbury, K. Li. A morphological study of ceramic hollow fibre membranes. *J.Membr.Sci.*, 328 (2009) 134.

- [21] B.F.K. Kingsbury, Z. Wu, and K. Li. A morphological study of ceramic hollow fibre membranes: A perspective on multifunctional catalytic membrane reactors. *Catal. Today*, 156 (2010) 306.
- [22] S. Koonaphapdeelert, K. Li. Preparation and characterization of hydrophobic ceramic hollow fibre membrane. *J.Membr.Sci.*, 291 (2007) 70.
- [23] S.R. Wickramasinghe, M.J. Semmens, and E.L. Cussler. Better hollow fiber contactors. *J.Membr.Sci.*, 62 (1991) 371.
- [24] D. DeMontigny, P. Tontiwachwuthikul, and A. Chakma. Comparing the absorption performance of packed columns and membrane contactors. *Ind. Eng. Chem. Res.*, 44 (2005) 5726.
- [25] R. Hiwale, S. Hwang, and R. Smith. Model building methodology for multiphase reaction systems-modeling of CO₂ absorption in monoethanolamine for laminar jet absorbers and packing beds. *Ind. Eng. Chem. Res.*, 51 (2012) 4328.
- [26] D. Yang, R.S. Barbero, D.J. Devlin, E.L. Cussler, C.W. Colling, and M.E. Carrera. Hollow fibers as structured packing for olefin/paraffin separations. *J.Membr.Sci.*, 279 (2006) 61.
- [27] K.K. Sirkar. Membranes, phase interfaces, and separations: Novel techniques and membranes-an overview. *Ind. Eng. Chem. Res.*, 47 (2008) 5250.
- [28] A.H.P. Skelland, *Diffusional Mass Transfer*, New York, Wiley, 1974.
- [29] R.H. Perry, D.W. Green, *Perry's Chemical Engineers' Handbook*, New York, McGraw-Hill, 2007.
- [30] M. Yang, E.L. Cussler. Designing hollow-fiber contactors. *AIChE J.*, 32 (1986) 1910.
- [31] R. Prasad, K.K. Sirkar. Dispersion-Free solvent extraction with microporous hollow-fiber modules. *AIChE J.*, 34 (1988) 177.
- [32] J. Wu, V. Chen. Shell-side mass transfer performance of randomly packed hollow fiber modules. *J.Membr.Sci.*, 172 (2000) 59.

- [33] M.J. Costello, A.G. Fane, P.A. Hogan, and R.W. Schofield. The effect of shell-side hydrodynamics on the performance of axial flow hollow fibre modules. *J.Membr.Sci.*, 80 (1993) 1.
- [34] K. Li, M.S.L. Tai, and W.K. Teo. Design of a CO₂ scrubber for self-contained breathing systems using a microporous membrane. *J.Membr.Sci.*, 86 (1994) 119.
- [35] E.A. Fouad, H.J. Bart. Separation of zinc by a non-dispersion solvent extraction process in a hollow fiber contactor. *Solvent Extr. Ion Exch.*, 25 (2007) 857.
- [36] A. Baudot, J. Flourey, and H.E. Smorenburg. Liquid-liquid extraction of aroma compounds with hollow fiber contactor. *AIChE J.*, 47 (2001) 1780.
- [37] S. Shen, S.E. Kentish, and G.W. Stevens. Shell-side mass-transfer performance in hollow-fiber membrane contactors. *Solvent Extr. Ion Exch.*, 28 (2010) 817.
- [38] K.C. Hansen, Z. Zhou, C.L. Yaws, and T.M. Aminabhavi. Determination of Henry's law constants of organics in dilute aqueous solutions. *J. Chem. Eng. Data*, 38 (1993) 546.
- [39] E.N. Fuller, P.D. Schettler, and J.C. Giddings. New method for prediction of binary gas-phase diffusion coefficients. *Ind. Eng. Chem.*, 58 (1966) 18-27.
- [40] C. Satterfield, *Mass transfer in heterogeneous catalysis*, Massachusetts, MIT Press: Cambridge, 1970.
- [41] E.L. Cussler, *Diffusion: Mass transfer in fluid systems*; 3rd edition, New York, Cambridge University Press, 2009.
- [42] C.R. Wilke, P. Chang. Correlation of diffusion coefficients in dilute solutions. *AIChE J.*, 1 (1955) 264-270.
- [43] D. Morgan, L. Ferguson, and P. Scovazzo. Diffusivities of gases in room-temperature ionic Liquids: Data and correlations obtained using a lag-time technique. *Ind. Eng. Chem. Res.*, 44 (2005) 4815.

- [44] A. Ortiz, A. Ruiz, D. Gorri, and I. Ortiz. Room temperature ionic liquid with silver salt as efficient reaction media for propylene/propane separation: Absorption equilibrium. *Sep. Purif. Technol.*, 63 (2008) 311.
- [45] W.J. DeCoursey. Absorption with chemical reaction: development of a new relation for the Danckwerts model. *Chem. Eng. Sci.*, 29 (1974) 1867-1872.
- [46] P.V. Danckwerts, *Gas-liquid reactions*, New York, McGraw-Hill, 1970.
- [47] S. Rajabzadeh, S. Yoshimoto, M. Teramoto, M. Al-Marzouqi, and H. Matsuyama. CO₂ absorption by using PVDF hollow fiber membrane contactors with various membrane structures. *Sep. Purif. Technol.*, 69 (2009) 210.
- [48] N. Ghasem, M. Al-Marzouqi, and L. Zhu. Preparation and properties of polyethersulfone hollow fiber membranes with o-xylene as an additive used in membrane contactors for CO₂ absorption. *Sep. Purif. Technol.*, 92 (2012) 1.
- [49] P. Chilukuri, K. Rademakers, K. Nymeijer, L. Van Der Ham, and H.D. Van Berg. Propylene/propane separation with a gas/liquid membrane contactor using a silver salt solution. *Ind. Eng. Chem. Res.*, 46 (2007) 8701.
- [50] I.M. Coelho, M.M. Cardoso, R.M.C. Viegas, and J.P.S.G. Crespo. Transport mechanisms and modelling in liquid membrane contactors. *Sep. Purif. Technol.*, 19 (2000) 183.
- [51] S. Atchariyawut, R. Jiraratananon, and R. Wang. Mass transfer study and modeling of gas-liquid membrane contacting process by multistage cascade model for CO₂ absorption. *Sep. Purif. Technol.*, 63 (2008) 15.



4

Facilitated transport membranes

Abstract

Novel facilitated transport membranes, including supported ionic liquid membranes (SILMs) and polymer/ionic liquid composite membranes, are proposed to carry out the separation of olefin/paraffin gas mixtures. First of all the performance of SILMs containing different silver salt concentrations were assessed. Afterwards, in order to improve the typical poor mechanical stability of SILMs, polymer/ionic liquid composite membranes were synthesised and their structural, thermal and mechanical properties were determined. The effect of membrane composition in the separation performance of both types of membranes was evaluated under different operational conditions and the stability of the membranes was also checked. The facilitated transport membranes herein prepared provided very promising results when tested with 50/50 % v/v C_3H_8/C_3H_6 mixtures, placing these membranes well above the Robeson upper bound for polymeric and inorganic membranes.

4.1. Introduction

Membrane technology holds a great potential for energy and capital saving in the separation process of olefins from paraffins. The criteria for selecting the most suitable membrane for a given application are complex; nonetheless, durability, mechanical and thermal stability at the operating conditions, productivity and separation efficiency and costs are important stipulations that must be considered [1]. Among these requirements selectivity and permeation rate are clearly the most basic, while the relative importance of the rest varies with the application. Therefore a wide variety of different membrane alternatives can be considered. The use of polymeric membranes for olefin/ paraffin separation has been studied rather extensively [2]. Among the wide variety of polymeric membranes studied in literature [3], polyimide membranes offer the highest flux and selectivity; however their performance has not met the requirements for commercial applications. In addition, it has been proved by many authors that polymeric membranes suffer severe plasticization effects, that lead to a dramatic decrease of the selectivity [4,5]. Inorganic membranes have been also explored because besides their higher tolerance to harsh environments, the gas separation performance of inorganic membranes can surpass the Robeson upper bound for conventional polymeric membranes [6]. However, the typical poor mechanical resistance of inorganic membranes, combined with their expensive and complex preparation methods have limited their use in large-scale applications. More recently the use of polymer composite membranes with enhanced separation properties is becoming increasingly important [7]. Thus, the use of polymer/ionic liquid composite membranes has been successfully applied to CO_2/H_2 [8] and CO_2/CH_4 [9-14] mixtures enhancing the separation performance of the polymeric membrane by itself. On the other hand many researchers have turned their attention to the use of facilitated transport membranes, both in liquid and solid state, in order to improve the olefin permeability without compromising the separation selectivity [15]. The separation performance is mostly associated to the ability of the olefins to reversibly react with silver cations (Ag^+), by π -

complexation mechanism. Consequently silver ions act as carriers for the transport of olefins, thus facilitating their selective permeation across the membrane. Kang et al. [16-19] have investigated extensively the separation performance of different types of facilitated transport membranes in the solid state for olefin/paraffin separation and reported high separation selectivities. However, the low olefin permeabilities obtained and the chemical instability of the carrier should be overcome before this technology can be implemented. Some authors [20,21] have studied the performance of supported liquid membranes (SLMs) using aqueous silver salt solutions for propylene/propane separation. Although good separation performances were reported, conventional SLMs suffer from critical drawbacks such as the evaporative loss of solvent and that the liquid can be expelled from the support due to the high trans-membrane pressure. Other authors [22-24] proposed the use of non-volatile solvents in order to avoid solvent losses by evaporation. Scovazzo et al. [25] determined the pure gas permeabilities and selectivities of N_2 , CH_4 and CO_2 and compared their results to those of polymeric membranes in the Robeson plot and concluded that supported ionic liquid membranes were competitive compared to other membrane materials. Neves et al. [26] studied the potential of using supported ionic liquid membranes for CO_2/N_2 and CO_2/CH_4 gas separation and the influence of the structure of the ionic liquid used in the performance of the separation process.

In this chapter, the performance of supported ionic liquid membranes and novel polymer-ionic liquid composite membranes to carry out the separation of propane/propylene mixtures is evaluated. Ionic liquids (ILs) were selected because in addition to their negligible vapour pressure that avoids solvent losses by evaporation, they offer more affinity for the olefinic compounds compared to saturated hydrocarbons and at the same time they provide stability to the dissolved metallic cation acting as a medium for facilitated transport with mobile carrier [27-29]. Based on previous results collected in the chapter 2 of this thesis, the pair ionic liquid-silver salt used in this case was 1-butyl 3-methylimidazolium tetrafluoroborate-silver tetrafluoroborate

(BMImBF₄-AgBF₄) since it provided the best results in terms of separation selectivity and propylene solubility. On the other hand, the polymer used in the fabrication of the polymer/ionic liquid composite membranes was poly(vinylidene fluoride-co-hexafluoropropylene) (PVDF-HFP) due to its well known thermal, chemical and mechanical properties. Furthermore, it is partially miscible with BMImBF₄ and compatible with hydrocarbons which avoid plasticization effects. Once the membrane has been fabricated the ionic liquid remains integrated within the polymer matrix, thereby increasing the stability of the membrane even at high transmembrane pressures. Several experiments were carried out in order to study the effect of different operating variables (transmembrane pressure, temperature, sweep gas flow rate membrane composition and silver concentration in the membrane) in the separation process. Moreover the stability of the membranes has been evaluated. Finally, the performance of both types of membranes has been compared with the most relevant data reported in literature.

4.2. Experimental methods

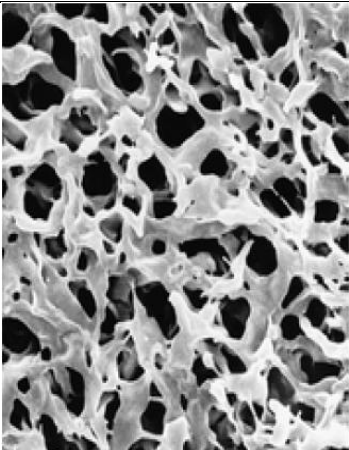
4.2.1. Materials

Propylene and propane gas were purchased from Praxair with a minimum purity of 99.5 %. The ionic liquid 1-butyl-3-methylimidazolium tetrafluoroborate (CAS number 174504-65-6) was supplied by Iolitec, with a minimum purity of 99 % and residual halide content less than 500 ppm. The silver salt used in this work is silver tetrafluoroborate (CAS number 14104-20-2) of 99 % purity purchased from Apollo Scientific Ltd. All chemicals were used as received. The polymeric support employed for the preparation of SILMs was a Durapore® plain membrane of PVDF supplied by Millipore. The polymer PVDF-HFP (CAS number 9011-17-0) was supplied by Sigma Aldrich. Tetrahydrofuran (THF) (CAS number 109-99-9) purchased from Panreac was used as a solvent to prepare the polymer/ionic liquid membranes.

4.2.2. Preparation of SILMs

First of all the reactive solution is prepared dissolving the silver tetrafluoroborate in the BMImBF₄ at room temperature and stirring with a magnet stirrer. Then the polymeric membrane used as support was placed in a flask, which was closed with a septum, and then vacuum was applied for 30 minutes in order to remove the air inside the pores. The microporous membrane used as polymeric support was a hydrophilic PVDF polymeric membrane supplied by Millipore. The main characteristics of the membrane are shown in table 4.1. Then 2 mL of the reactive solution were injected through the septum with a syringe and the reactive liquid fills the void pores. The system remains under vacuum 90 more minutes to let the reactive solution to impregnate completely the porous support. Finally the excess of liquid is removed from the polymeric surface using a tissue. The supported ionic liquid membrane thickness has been considered to be equal to the thickness of the polymeric support (125 μm).

Table 4.1. Characteristics of the PVDF microporous membrane.

	Material	PVDF
	Wettability	Hydrophilic
	Refractive index	1.42
	Water flow rate ($\text{mL}\cdot\text{min}^{-1}\cdot\text{cm}^{-2}$)	2.5
	Bubble point at 23°C (bar)	≥ 4.8
	Maximum operating T (K)	358
	Pore size (μm)	0.1
	Porosity (%)	70
	Thickness (μm)	125
	Membrane diameter (mm)	90

4.2.3. Preparation of polymer/ionic liquid composite membranes

The PVDF-HFP/BMImBF₄/Ag⁺ composite membranes were prepared by the solvent casting technique. First of all the polymer is dissolved in 10 mL of THF at 313 K for 8 hours in a closed vial to avoid evaporation of the solvent. Once the polymer has been dissolved, it is mixed with the ionic liquid and the silver salt and stirred for 5 minutes. Finally the membrane precursor mixture is placed in a Petri dish and the solvent is evaporated at 293 K and 300 mbar under dark conditions for 24 h. For better understanding of the results presented in this chapter, it would be appropriate to clarify that the silver content of the membranes is expressed as a percentage of the silver salt weight compared with the weight of the membranes without silver AgBF₄/(PVDF-HFP + BMImBF₄). The thickness of the membranes prepared in this work depends on the membrane composition, but in all cases they presented an average thickness around 120 ± 20 µm. Permeabilities have been calculated taking into account the real thickness of each membrane which was measured using a digital micrometer Mitutoyo Digimatic Series 369 (accuracy ± 0.001 mm).

4.2.4. Characterization of polymer/ionic liquid composite membranes

Membranes thermal and mechanical stability was determined together with structural properties by thermogravimetric analysis (TGA), tensile tests, polarized light microscopy (PLM) and FTIR techniques. First of all membrane structure was analyzed by PLM using a SZH Olympus lens equipped with a camera CCD Color Video Camera SSC-C350P/C370P Sony that was used to characterize the morphology and phase behavior of the ionic liquid/polymer composite membranes. The thermal stability of the membranes has been studied by thermogravimetric analysis (TGA) using a thermobalance TG-DTA 60H Shimadzu. The mechanical strength of the membranes was assessed by tensile tests using a

Zwick/Roell Z100 machine according to the standard method UNE-EN ISO 527-3:1996 and AC:2002. In PVDF-HFP/BMI mBF_4 composite membranes, possible interactions between the cation of the ionic liquid and the polymer backbone can occur. In this work, these possible interactions were investigated by FTIR spectroscopy using a spectrometer Nicolet Nexus.

4.2.5. Permeation cell

A schematic diagram of the permeation cell is shown in figure 4.1.

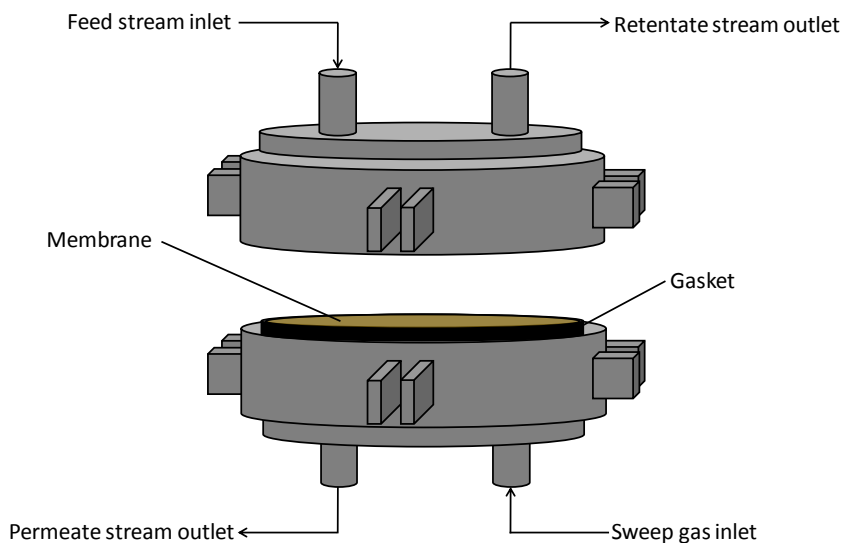


Figure 4.1. Schematic diagram of the permeation cell.

The upper and lower compartments, with an inner and outer diameter of 90 and 102 mm respectively were made of stainless steel (AISI 316L). The supported ionic liquid membrane is placed in the lower chamber, over a disc made of porous stainless steel which provides mechanical strength to the membrane. A gasket of synthetic rubber allows to close hermetically both chambers avoiding the leakage of the gas. In the

upper chamber there are two ports which correspond to the feed gas inlet and the retentate gas outlet. Similarly, in the lower chamber there are also two connections corresponding to the sweep gas inlet and the permeate stream outlet.

4.2.6. Methods

Once the membrane has been prepared it is placed into the permeation cell (membrane effective area = 39.6 cm²) inside a water bath in order to control the temperature. In the start-up of the gas permeation experiments the presence of possible defects in the membrane was checked. Vacuum was applied to the permeate side; if the membrane does not present any defect the pressure fell below 1 mbar, however, if there were any defect (any unfilled pore in the SILMs or a small hole in the polymer/ionic liquid composite membranes) the gas would pass from the feed side to the permeate side and the vacuum of 1 mbar would not be achieved anymore.

The flow rate of each gas is adjusted by a mass flow controller (Brooks Instrument SLA 5850) and before starting the experiment the composition of the feed stream is analyzed by gas chromatography. The feed stream flows through the upper chamber, while the nitrogen used as sweep gas flows through the permeate side. The pressure of both streams, measured by a pressure transducer (Aplisens PCE-28 with an accuracy of ± 0.001 bar), is controlled using two micrometric valves. The flow rate of the permeate stream is measured using a mass flowmeter (Brooks Instrument SLA 5850) and at the cell outlet the composition of both, the feed stream and the permeate stream are analyzed by gas chromatography. The analysis was performed in a gas chromatograph HP 6890 equipped with a thermal conductivity detector (TCD) and a column HP Al/S (30 m length, nominal diameter of 0.53 mm). A schematic diagram of the experimental set-up is shown in figure 4.2.

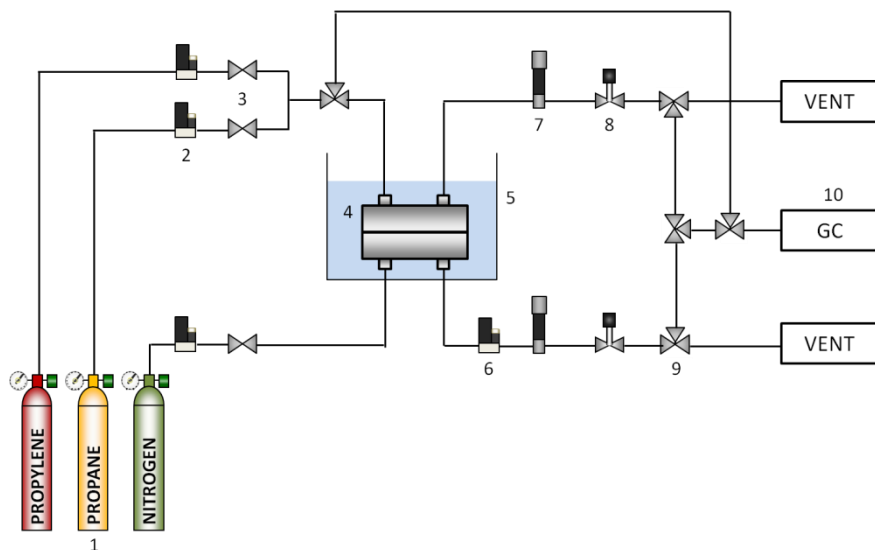


Figure 4.2. Diagram of the experimental setup.

1-Gas bottles, 2-Mass flow controllers, 3-Two way valves, 4-Permeation cell, 5-Water bath 6-Mass flowmeter, 7-Pressure transducer, 8-Micrometric valve, 9-Three way valves, 10-Gas chromatograph.

In order to check the experimental reliability each experiment was performed twice and the standard deviation between experimental results and the replicates (eq. 4.1) was calculated. The obtained values were lower than 0.04 for the SILMs and 0.05 for the PVDF-HFP/BMIImBF₄ composite membranes concluding that there was a good experimental reliability.

$$\sigma = \sqrt{\frac{\sum_{i=1}^n \left(\frac{J_{C_3H_x} - J'_{C_3H_x}}{J_{C_3H_x}} \right)^2}{n-1}} \quad (4.1)$$

The experimental flux of each gas was calculated by performing a mass balance to the permeation cell.

$$F_{in} \cdot y_{i,in} - F_{out} \cdot y_{i,out} = J_i \cdot A \quad (4.2)$$

where F_{in} and F_{out} ($\text{mol} \cdot \text{s}^{-1}$) are the total molar flow rate at the inlet and the outlet of the cell respectively, y_i (-) is the molar fraction of the gas, J_i ($\text{mol} \cdot \text{m}^{-2} \cdot \text{s}^{-1}$) is the flux of the specie i across the membrane and A (m^2) is the membrane effective area.

Then the experimental permeabilities of each gas were calculated according to eq. 4.3:

$$J_i = P_i \frac{\Delta p_i}{\delta} \quad (4.3)$$

where P_i ($\text{mol} \cdot \text{m}^{-1} \cdot \text{bar}^{-1} \cdot \text{s}^{-1}$) is the permeability of each gas, Δp_i (bar) is the difference in the partial pressure of the gas between both sides of the membrane and δ (m) is the thickness of the membrane.

4.3. Results and discussion

4.3.1. Supported ionic liquid membranes (SILMs)

The separation of propane/propylene gas mixtures through supported ionic liquid membranes is a combination of three processes: absorption, diffusion and desorption which take place in the feed side, in the liquid membrane and in the permeate side respectively. The transport of both species across the membrane is a process driven by the partial pressure difference between both sides of the membrane. Therefore, the higher the transmembrane pressure, the higher driving force for the separation is obtained. In supported ionic liquid membranes in absence of a carrier, the transport of the gaseous species (propane and propylene) is due to Fickian diffusion. However, when a carrier (Ag^+) is added to the membrane system, propylene permeation is the contribution of two mechanisms: Fickian diffusion and facilitated transport with mobile carrier. Based upon facilitated transport mechanism, higher carrier concentration in the membrane will enhance the transport of propylene

along the membrane thickness, and as a result the membrane would have a better separation performance. In this section gas mixture permeation experiments were carried out in order to measure gas permeabilities and determine the selectivities of the separation of C_3H_6/C_3H_8 mixtures. First of all, the effect of the silver content in the membrane as well as the influence of the operational conditions such as the transmembrane pressure (0.2-1.65 bar) and sweep gas flow rate ($0-15\text{ mL}\cdot\text{min}^{-1}$) on the gas permeation fluxes and separation selectivity was studied. Moreover, in order to increase the knowledge on the separation fundamentals, the results of the permeability of the components of gas mixtures were compared to the experiments performed with pure gases.

Stability of SILMs

The durability of the supported ionic liquid membrane was studied by performing medium-term gas permeation experiments working with 50/50 % v/v C_3H_8/C_3H_6 gas mixtures. The liquid membrane showed good stability over the experimental period operating with a transmembrane pressure of 0.2 bar. Figure 4.3 shows the evolution of the permeation fluxes of propane and propylene across the supported ionic liquid membrane with time. It can be observed that during the first hours the flux of both gases decreases. The $BMImBF_4$ is hygroscopic, and during the start-up procedure the membrane takes some water from atmosphere. During the first hours this water is removed from the membrane by evaporation and drops dragging. Thus, the viscosity of the liquid membrane increases and therefore the diffusivity of both species across the liquid membrane decreases, which finally leads to lower gas permeabilities.

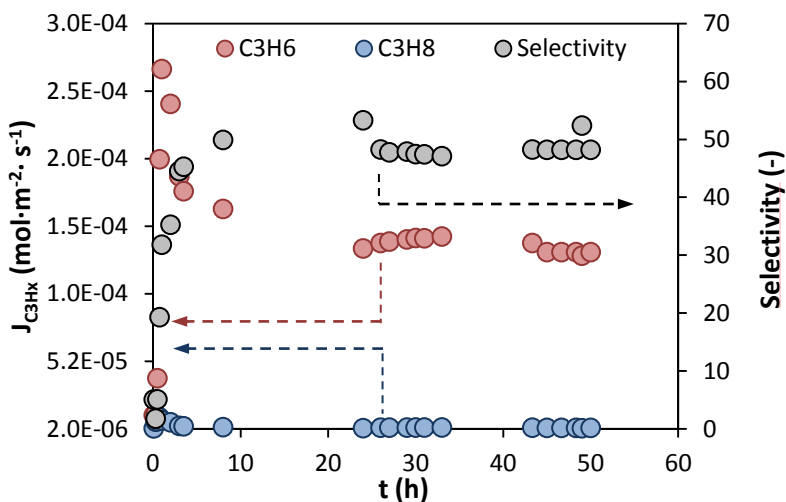


Figure 4.3. Change of the fluxes of C_3H_8 and C_3H_6 across the supported ionic liquid membranes with time at 293 K, transmembrane pressure of 0.2 bar, flow rate of the sweep gas $2 \text{ mL}\cdot\text{min}^{-1}$ composed by BMImBF₄ and $[Ag^+] = 2 \text{ M}$.

One of the critical issues related to supported liquid membranes is the carrier poisoning with time. In the case of silver-based facilitated transport membranes one of the major issues is the reduction of silver cations to metallic silver, which is not active in the separation process, according to reaction 4.a.



As the cationic silver degradation is catalyzed by light, the carrier poisoning effects can be minimized as long as the liquid membrane remains under dark conditions. In this case the selectivity remained constant during the experiment revealing that no carrier degradation is taking place. The macroscopic studies confirmed that after the experiment the ionic liquid solution remains inside the pores of the membrane. Moreover the color of the membrane did not change indicating that the reduction of part of the silver ions to metallic silver was not taking place. All the experiments reported in this section were

obtained after all the water present in the liquid membrane was removed, and therefore the pseudo-steady state was achieved.

For both components, a comparison of pure gas and mixed gas permeabilities under the following operation conditions: pressure of the feed gas of 1.2 bar, pressure of the permeate stream of 1 bar and temperature of 293 K was carried out. The results collected in table 4.2 show that the permeabilities obtained from the runs with mixed gas feeds differ from the values obtained working with pure gas phases; actually propane permeability is 6.1 % lower in the mixed gas whereas propylene permeability is increased by 15 %. Those results are in agreement with the differences in gas solubilities previously determined in the absence of the complexing agent that showed a considerably lower equilibrium solubility of propane and at the same time a slightly higher solubility of propylene compared to the values obtained with pure gases [29]. A similar behavior was evidenced by the results obtained by Neves et al. [26] from gas permeation studies working with CO₂/CH₄ and CO₂/N₂ mixtures and supported ionic liquid membranes.

Table 4.2. Pure and mixed gas permeabilities for 50/50 % v/v C₃H₈ and C₃H₆ gas mixtures at 293 K in the SILM without silver.

Permeability (mol·bar ⁻¹ ·m ⁻¹ ·s ⁻¹)					
C ₃ H ₈			C ₃ H ₆		
PURE	MIX	$\left(\frac{PURE - MIX}{PURE}\right) \cdot 100$	PURE	MIX	$\left(\frac{PURE - MIX}{PURE}\right) \cdot 100$
1.66·10 ⁻⁹	1.56·10 ⁻⁹	6.1	4.41·10 ⁻⁹	5.07·10 ⁻⁹	-15.0

Effect of the sweep gas flow rate

The effect of the sweep gas flow rate in the fluxes of propane and propylene across the membrane was studied in the range from 2 to 15 mL·min⁻¹. Non linear profiles of the flux of propylene across the membrane with the flow rate of the sweep gas were observed as is depicted in figure 4.4.

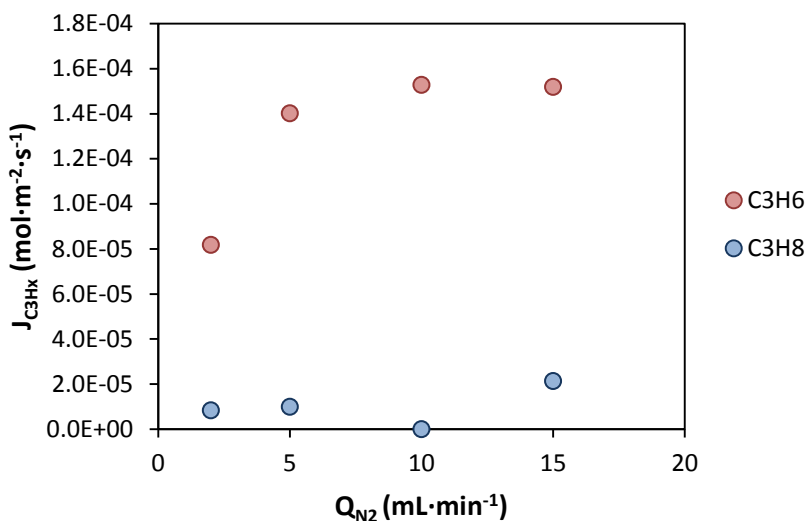


Figure 4.4. Effect of the sweep gas flow rate in the flux of C_3H_8 and C_3H_6 at 293 K, at pressures of the feed and permeate streams of 1.2 and 1.0 bar respectively and $[Ag^+] = 1$ M.

The flux of propane is almost unaffected by changes in the sweep gas flow rate. However, the flux of propylene increases as the sweep gas flow rate was increased, at a higher rate at low flow rates and achieving asymptotically a maximum value at flow rates of the sweep gas over 10 mL·min⁻¹. This is because higher flow rates of the sweep gas remove more efficiently the gas molecules which arrive to the permeate side, allowing to operate with higher driving forces. For this reason a trade-off solution must be found in order to maximize the flux of propylene across the membrane without diluting in excess the permeate stream.

Effect of the transmembrane pressure

The effect of the transmembrane pressure was studied in the range from 0.2 to 1.65 bar. Figure 4.5 shows that higher transmembrane pressures result in higher fluxes of both gases due to the higher driving force (eq. 4.3). At the same time it is worth noticing that increasing the transmembrane pressure in the range 0.2-1.65 bar the selectivity is not affected. Therefore, it would be interesting to work at the highest

possible transmembrane pressure, in order to maximize the flux of propylene, without compromising the stability of the supported ionic liquid membrane. In order to check the maximum transmembrane pressure at which the supported ionic liquid membranes under study could operate, the stability against pressure was assessed. For this purpose as the pressure in the permeate side remained constant at 1 bar, the pressure in the feed stream was increased gradually at intervals of 0.25 bar. It was observed that the liquid membranes remained stable until a threshold differential pressure between both sides of the membrane of 2.75 bar was achieved. Above this pressure it was observed that the separation capability of the membrane gradually decreased because part of the ionic liquid that was immobilized inside the polymeric support was being expelled from the membrane pores.

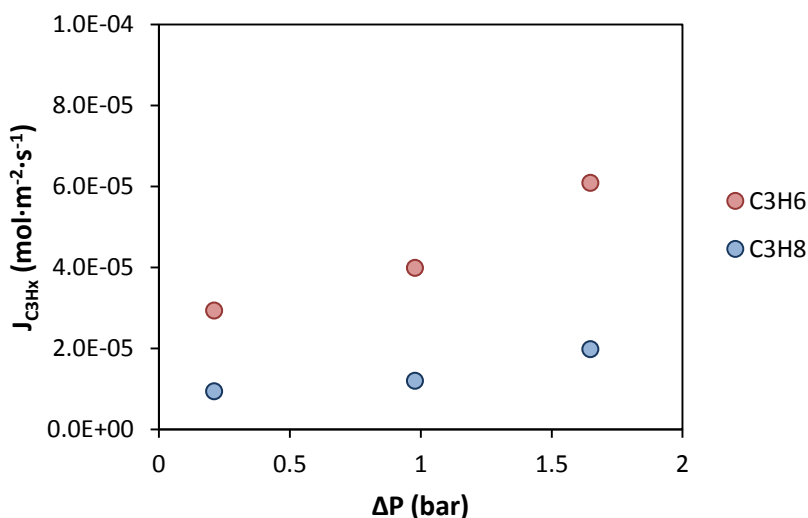


Figure 4.5. Effect of the transmembrane pressure in the flux of C_3H_8 and C_3H_6 at 293 K, and a $[Ag^+] = 0.1$ M and a flow rate of the sweep gas of $2 \text{ mL}\cdot\text{min}^{-1}$.

Effect of silver ions concentration

Many authors have reported previously the enhancement in the permeation flux of olefins across a supported liquid membrane under the presence of silver cations. This is because the silver ions act as carriers facilitating the transport of the olefins from the feed stream to the permeate side [23,30]. Several experiments were carried out at different silver concentrations and results are shown in figure 4.6:

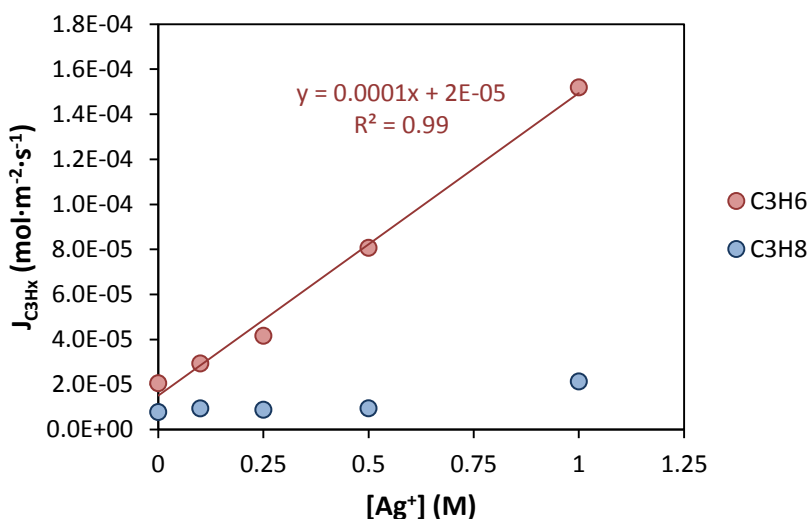


Figure 4.6. Effect of the silver concentration in the flux of C₃H₈ and C₃H₆ at 293 K, a pressure of the feed and permeate streams of 1.2 and 1.0 bar respectively and a flow rate of the sweep gas which allows to operate with the maximum driving force.

Figure 4.6 shows that although the flux of propane is not influenced by the addition of silver to the supported liquid membrane ($\approx 9.4 \cdot 10^{-6} \text{ mol} \cdot \text{m}^{-2} \cdot \text{s}^{-1}$), the flux of propylene is gradually increased from $2 \cdot 10^{-5}$ to $1.5 \cdot 10^{-4} \text{ mol} \cdot \text{m}^{-2} \cdot \text{s}^{-1}$ following a linear trend when the silver concentration in the membrane was increased from 0 to 1 moles per liter. The mixed gas permeabilities were calculated from the experimental results according to eq. 4.3. The selectivity for a given gas

pair ($\alpha_{i/j}$) is calculated as the ratio of the permeabilities of the gases of interest (eq. 4.4):

$$\alpha_{i/j} = \frac{P_i}{P_j} \quad (4.4)$$

where $\alpha_{i/j}$ is the selectivity and P_i and P_j are the experimental permeabilities of the species i and j respectively.

Table 4.3. Influence of silver concentration on the permeabilities and selectivities at 293 K, pressure of the feed and permeate streams of 1.2 and 1.0 bar respectively and a flow rate of the sweep gas that allows operation with the maximum driving force.

[Ag ⁺] (M)	P C ₃ H ₈ (mol·bar ⁻¹ ·m ⁻¹ ·s ⁻¹)	P C ₃ H ₆ (mol·bar ⁻¹ ·m ⁻¹ ·s ⁻¹)	$\alpha_{i/j}$ (-)
0	1.56·10 ⁻⁹	5.07·10 ⁻⁹	3.25
0.1	1.91·10 ⁻⁹	7.52·10 ⁻⁹	3.93
0.25	1.82·10 ⁻⁹	1.11·10 ⁻⁸	9.26
0.5	1.88·10 ⁻⁹	2.09·10 ⁻⁸	11.2
1	2.03·10 ⁻⁹	3.96·10 ⁻⁸	19.5
2	1.06·10 ⁻⁹	5.51·10 ⁻⁸	52.9

The achieved selectivity in the separation process using pure BMImBF₄, with no addition of silver ions, in the supported liquid membrane is 3.25. However this selectivity is increased to almost 53 when the silver concentration is increased up to 2 mol·L⁻¹. The permeability of a gas is a contribution of both, the solubility and the diffusivity through the membrane (eq. 4.5).

$$P_i = S_i \cdot D_i \quad (4.5)$$

where P_i is the permeability of each gas and S_i and D_i are the solubility coefficient and diffusivity of the specie “ i ” in the supported ionic liquid membrane.

The solubility coefficients were obtained from the solubility isotherms of propane and propylene in the BMImBF₄-Ag⁺ medium, thus after having calculated the experimental permeabilities in this work it is possible to calculate the experimental diffusivities of propane and propylene in the ionic liquid membrane at different concentrations of silver ions (table 4.4).

Table 4.4. Experimental solubility coefficients and diffusivities for C₃H₈ and C₃H₆ at 293 K and different silver concentrations.

[Ag ⁺] (M)	S C ₃ H ₈ (mol·m ⁻³ ·bar ⁻¹)	D C ₃ H ₈ (m ² ·s ⁻¹)	S C ₃ H ₆ (mol·m ⁻³ ·bar ⁻¹)	D C ₃ H ₆ (m ² ·s ⁻¹)
0	33.7	4.62·10 ⁻¹¹	85.3	5.94·10 ⁻¹¹
0.1	33.7	5.67·10 ⁻¹¹	200	3.76·10 ⁻¹¹
0.25	33.7	5.39·10 ⁻¹¹	372	2.98·10 ⁻¹¹
0.5	33.7	5.58·10 ⁻¹¹	659	3.17·10 ⁻¹¹
1	33.7	6.03·10 ⁻¹¹	1233	3.22·10 ⁻¹¹

The diffusivities of gases in the Ag⁺-BMImBF₄ liquid membrane were also predicted using the correlation proposed by Morgan for imidazolium-based ionic liquids in terms of the gas molar volume and the ionic liquid viscosity [31] (eq. 4.6).

$$D_{12} = 2.66 \cdot 10^{-3} \frac{1}{\mu_2^{0.66 \pm 0.03} V_1^{1.04 \pm 0.08}} \quad (4.6)$$

where D_{12} is the diffusivity of the gas in the ionic liquid in cm²·s⁻¹, μ_2 is the ionic liquid viscosity in cP and V_1 is the molar volume of the gas in cm³·mol⁻¹.

It is also known that the rheological properties of the ionic liquid may change with the concentration of silver salts. This influence previously reported by Ortiz et al. [28] must be considered in the estimation of the

diffusivity of both gases using equation 4.6. Figure 4.7 shows a comparison between the experimentally determined diffusivities and the diffusivities obtained using eq. 4.6. It can be seen that the diffusivities of propane and propylene irrespective of the concentration of silver ions in the membrane are well predicted by Morgan's equation. Moreover, figure 4.7 shows that the diffusivity of propylene in the liquid membrane slightly decreases when adding silver cations. This is in good agreement with previous results published by Teramoto et al. [32] who reported a decrease in the observed diffusivity of ethylene in water from $1.45 \cdot 10^{-9}$ to $9.83 \cdot 10^{-10} \text{ m}^2 \cdot \text{s}^{-1}$ when the concentration of silver nitrate was increased from 0 to 4 mol L^{-1} . This can be attributed to the formation of the olefin-silver complex with a bigger molar volume and therefore lower diffusivity. Then the observed diffusivity results from the contributions of the diffusivity of free propylene in the liquid membrane and the diffusion of the different organometallic complexes formed.

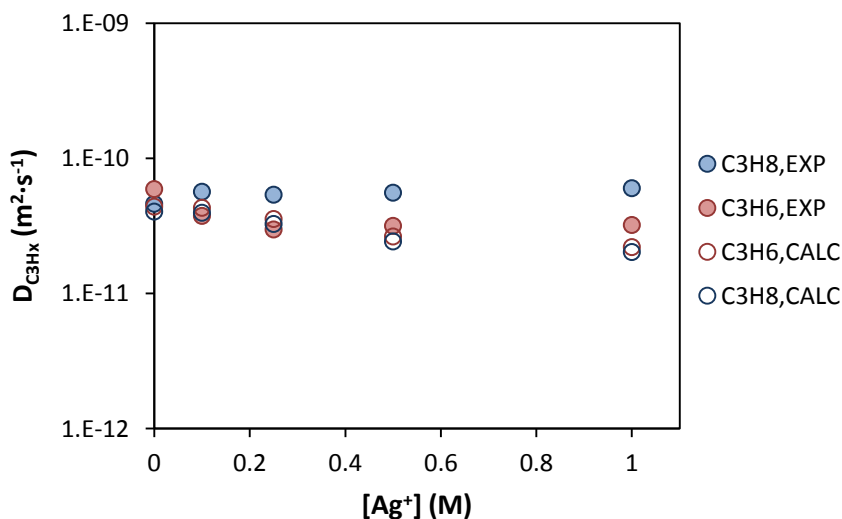


Figure 4.7. Comparison between experimental diffusivities of C_3H_8 and C_3H_6 and calculated using Morgan's equation.

Figure 4.8 shows the influence of the silver concentration in the membrane on the composition of the permeate stream calculated on

N_2 -free basis. This is because due to the high difference in the normal boiling points between nitrogen (≈ 77 K) and propane (≈ 231 K) and propylene (≈ 226 K), after obtaining a permeate stream mixture of nitrogen, propane and propylene it would be easy to remove the nitrogen from the mixture by just compressing and partially condensing this stream. Then on one hand pure nitrogen ready to be reused as sweep gas would be obtained, and on the other hand a final stream with high purity in propylene could be stored for example as liquefied gas. As depicted in figure 4.8, the propylene percentage in the permeate stream greatly increases when increasing the silver concentration in the liquid membrane. At silver concentrations in the membrane above 1 M, the propylene purity in the permeate stream is high enough to be used in most applications of propylene with the exception of the fabrication of polyolefins.

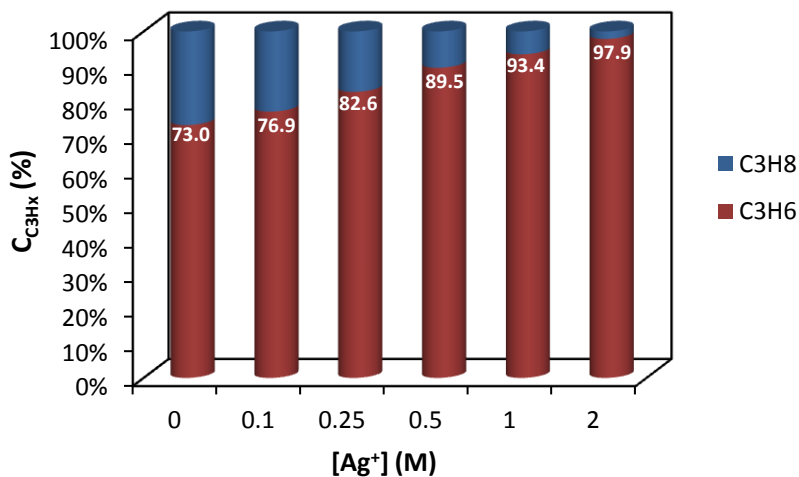


Figure 4.8. Composition of the permeate stream (on N_2 -free basis) at different silver concentrations in the membrane at 293 K, pressure of the feed and permeate streams of 1.2 and 1.0 bar respectively and flow rate of the sweep gas that allows to operate with the maximum driving force.

4.3.2. Polymer/ionic liquid composite membranes

Membrane characterization

In this work PLM was used to characterize the morphology and phase behavior of the ionic liquid/polymer composite membranes. Figure 4.9 shows the PLM images of pure PVDF-HFP, BMImBF₄ and different polymer/ionic liquid composite membranes. The images of pure PVDF-HFP and pure BMImBF₄ are smooth and clear. The PLM image of the membrane composed by 80 % PVDF-HFP/20 % BMImBF₄ is both clear and homogeneous, that indicates the miscibility of the components highlighting that the ionic liquid is embedded inside the polymer matrix. Nevertheless, as the percentage of ionic liquid increases, phase separation phenomena can be observed, leading to the formation of microcapsules of ionic liquid that become more obvious when increasing the ionic liquid percentage in the membrane.

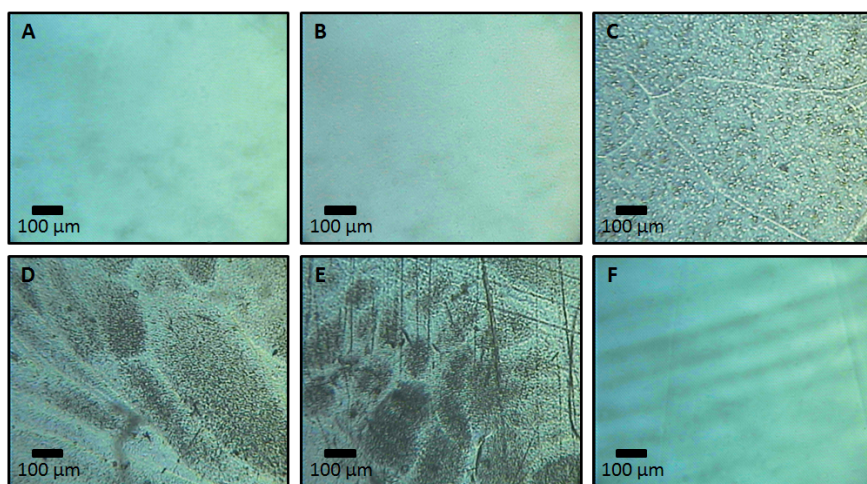


Figure 4.9. Polarized light microscopy images of the pure components and blend membranes. A) Pure PVDF-HFP, B) 80 % PVDF-HFP/20 % BMImBF₄, C) 65 % PVDF-HFP/35 % BMImBF₄, D) 50 % PVDF-HFP/50 % BMImBF₄, E) 35 % PVDF-HFP/65 % BMImBF₄, F) Pure BMImBF₄.

The thermal stability of the membranes has been studied by thermogravimetric analysis (TGA). Figure 4.10 shows the thermogravimetric curves of pure PVDF-HFP, pure BMImBF₄ and for PVDF-HFP/BMImBF₄ composite membranes containing different amounts of ionic liquid. Pure PVDF-HFP decomposes at ≈ 707 K and pure BMImBF₄ decomposes at 661 K (figure 4.10) in a single step. However, the polymer/ionic liquid composite membranes began to degrade at temperatures around 615 K that is below the degradation temperature of the pure components. These results are in agreement with those previously reported by Shalu et al. [33] who found that the PVDF-HFP/IL membranes exhibited a multistep decomposition mechanism.

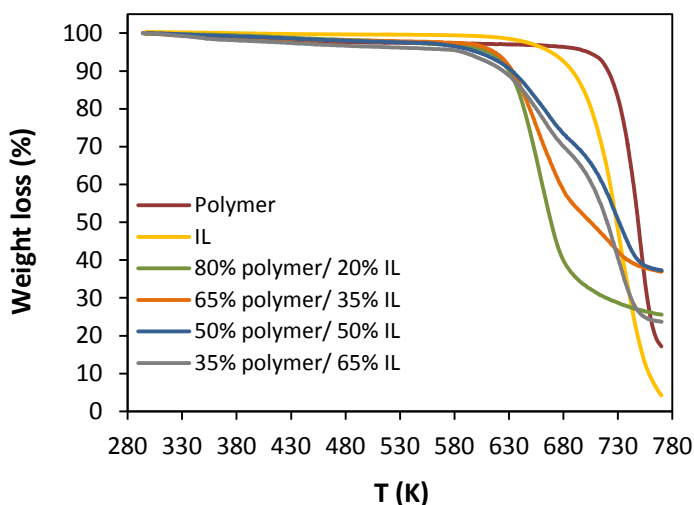


Figure 4.10. Thermogravimetric analysis of the PVDF-HFP/BMImBF₄ composite membranes.

The mechanical strength of the membranes was assessed by tensile tests. Figure 4.11 depicts the tensile curves obtained for the 5 different membrane compositions used in this work, 100 % polymer, 80 % polymer/20 % IL, 65 % polymer/35 % IL, 50 % polymer/50 % IL and 35 % polymer/65 % IL. In general it is observed that the mechanical properties such as the yield stress (σ_y), rupture stress (σ_M) as well as the

rupture strain (ϵ_M) decrease as the IL content in the membrane is increased. Similar behavior has been previously reported by Jansen et al. [10] for PVDF-HFP/[EMIm][TFSI] mixtures and by Chen et al. [8] for PVDF/[EMIm][B(CN)₄] mixtures. On the other hand, the yield strain slightly increases as the IL content in the membrane is increased until a critical IL content is achieved (65 %) when the elastic deformation of the membrane greatly decreases (table 4.5). Nevertheless, although the addition of the ionic liquid inside the polymer matrix compromises the mechanical resistance of the film, the mechanical properties of the membrane with 80 % polymer/20 % IL are good enough to prevent rupture of the membrane under the operating conditions employed in this work.

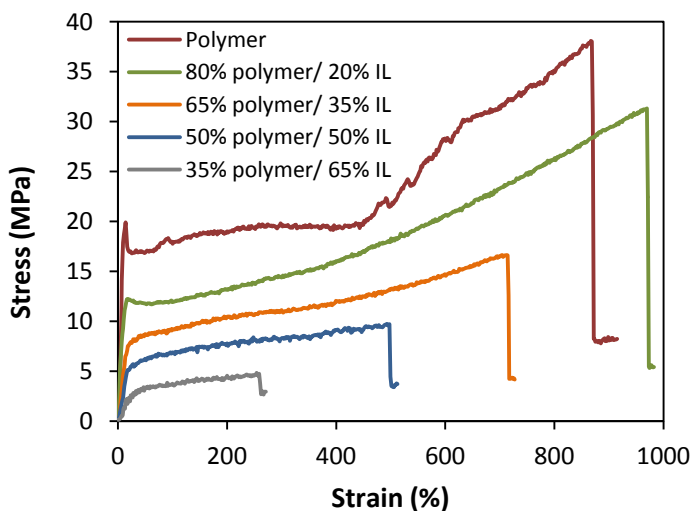


Figure 4.11. Tensile tests of the PVDF-HFP/BMImBF₄ composite membranes.

Table 4.5. Mechanical parameters of the PVDF-HFP/BMImBF₄ composite membranes.

% polymer	% IL	σ_y (MPa)	σ_M (MPa)	ϵ in σ_y (%)	ϵ in σ_M (%)	Young Modulus (MPa)
100	0	20.5	47.2	13.7	868	1.5
80	20	11.9	29.8	18.7	984	0.64
65	35	7.80	17.4	19.5	693	0.40
50	50	5.61	10.0	22.4	493	0.25
35	65	0.75	4.62	6.02	195	0.12

In PVDF-HFP/BMImBF₄ composite membranes, possible interactions between the cation of the ionic liquid and the polymer backbone can occur. In this work, these possible interactions were investigated by FTIR spectroscopy using a spectrometer Nicolet Nexus. The FTIR spectra of pure PVDF-HFP, pure BMImBF₄ and PVDF-HFP/BMImBF₄ membranes with different compositions in the region 500-4000 cm⁻¹ are shown in figure 4.12. Two regions, region-I and region-II in the spectra of figure 5 are of particular interest for the present discussion. The peaks in region I are due to the C-H stretching vibrations of butyl chain of IL (also those of polymer backbone stretching) and imidazolium cation ring of BMImBF₄ respectively. Although an overview of the peaks located in zones 1 and 2 of region I do not show significant changes, Shalu et al. [33] carried out a deconvolution explaining that there exist some peaks shifting. This indicates that a certain interaction between the imidazolium ring of the ionic liquid and the polymer chains is taking place. Therefore they concluded that at low amounts of BMImBF₄ doped into the PVDF-HFP membrane, most of the IL complexes with the polymer and less uncomplexed IL is entrapped in the matrix. This uncomplexed IL increases as the total IL content in the membrane is increased which is in good agreement with the results obtained by PLM in this work. The expanded spectra of region II correspond with the vibrational bands of the crystalline phase (zone 4) of the PVDF-HFP while the bands located around 850 cm⁻¹ are related to the amorphous phase of the polymer

(zone 3). Upon incorporation of BMImBF₄ to the PVDF-HFP the peak located at 750 cm⁻¹ shifts to 755 cm⁻¹ when the IL content is increased. Moreover the bands at 850 cm⁻¹ become more prominent indicating that the addition of BMImBF₄ to the membrane increases the polymer amorphicity.

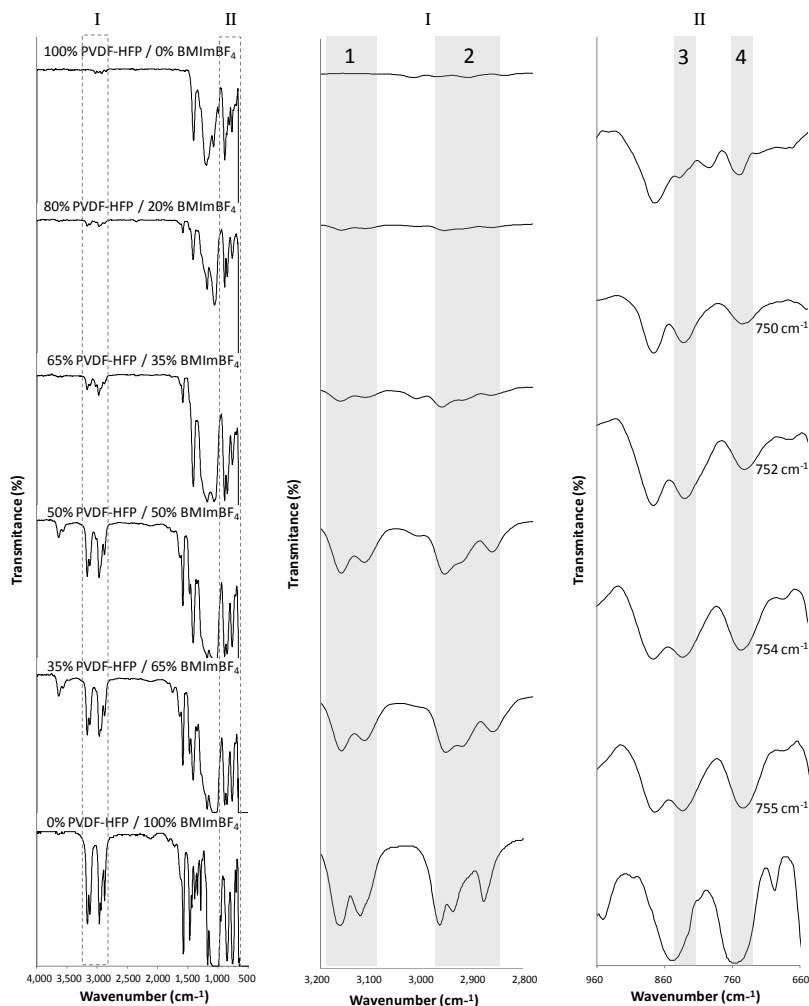


Figure 4.12. FTIR spectra of pure PVDF-HFP, pure BMImBF₄ and PVDF-HFP/BMImBF₄ composite membranes with different compositions.

Gas permeation

Mixed gas permeation experiments were carried out in order to measure gas permeabilities and determine the C_3H_6/C_3H_8 separation selectivity. The influence of the membrane composition as well as the different operational conditions such as the sweep gas flow rate (0-20 mL·min⁻¹), gas partial pressure (0.5-3 bar) and temperature (293-323 K) on the separation of propane/propylene gas mixtures was studied.

Effect of the membrane composition

To investigate the effect of membrane composition the permeation of 50/50 % v/v C_3H_8/C_3H_6 mixtures across composite membranes without silver salt at 293 K was analyzed in first place. Membranes with compositions ranging from 0 % PVDF-HFP/100 % BMImBF₄ (supported liquid membrane) to 100 % PVDF-HFP/0 % BMImBF₄ (conventional polymeric membrane) were analyzed. As depicted in figures 4.13 A and 4.13 B, in absence of silver salt in the membrane the permeability of both gases across the membrane decreases as the polymer content of the membrane increases. Moreover, the permeability curve presents a breakthrough around 70 % of polymer content which is around the composition range where 2 phase formation occurs as evidenced by PLM. However, when the silver salt is added to the membrane the permeation flux of propylene greatly increases regardless of the polymer content of the membrane. This occurs until a limit value is achieved above 80 % of polymer when the permeation flux of propylene is compromised. This phenomenon may be due to the decrease of the liquid concentration in the membrane below a threshold value that restricts the mobility of the carrier, therefore decreasing the flux of the transported gas across the membrane. Moreover, from figure 4.13 B it can be noted that the addition of silver salt to the membrane leads to a slight increase in the flux of propane. This fact will be discussed later.

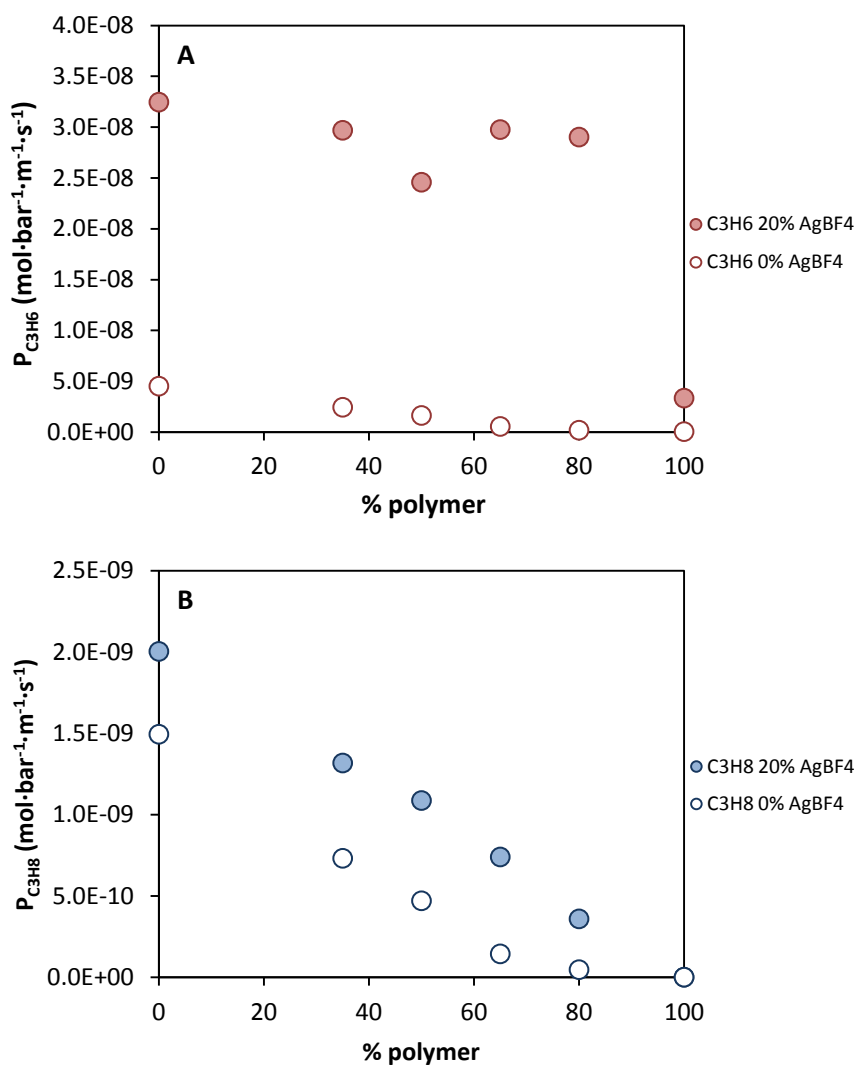


Figure 4.13. Effect of the membrane composition on the permeability of propylene A) and propane B) at 293 K.

Stability of PVDF-HFP/BMImBF₄-Ag⁺ membranes

As the main issue of the facilitated transport membranes is the carrier stability with time, long-term experiments were performed for 10 days, with a feed stream composed by 50/50 % v/v C₃H₆/C₃H₈ at 1 bar and 293 K. The evolution of propylene and propane fluxes with time is plotted in figure 4.14, where it can be observed that during the first hours the flux of both gases decreases. As explained before, the BMImBF₄ is hygroscopic and therefore during the start-up procedure the membrane takes some water from atmosphere. During the first 80 hours this water, together with some traces of THF that may remain in the membrane are removed from the membrane by evaporation and dragging. As a consequence the polymer chains mobility decreases and at the same time the BMImBF₄ viscosity increases leading to lower fluxes of both gases until a steady state is achieved when no further water or THF remain in the membrane. The PVDF-HFP/BMImBF₄/Ag⁺ showed excellent stability as evidenced by the steady C₃H₆ and C₃H₈ partial fluxes of $1.2 \cdot 10^{-4}$ and $2.2 \cdot 10^{-7}$ mol·m⁻²·s⁻¹ respectively. Therefore an exceptionally high C₃H₆/C₃H₈ separation selectivity value of 545 was obtained and kept constant during long-term stability tests of 10 days. After the experiments it was checked that the IL remained entrapped inside the polymer matrix and no carrier degradation had occurred. In this sense several authors have reported that the use of some polymers or ionic liquids can minimize the reduction of the silver cations [34,35]. Thus the combined effect of the presence of the ionic liquid and the polymer contributes to stabilize the silver cations under the operational conditions used in this work over a period of 10 days. It is also worth noting that experiments were carried out in the absence of any reducing gas so that longer times together with the use of real streams that contain traces of reducing components such as H₂ or H₂S should be performed in further stability analysis. All the experiments reported in this work were obtained after 100 hour operating time to assure that pseudo-steady state had been achieved.

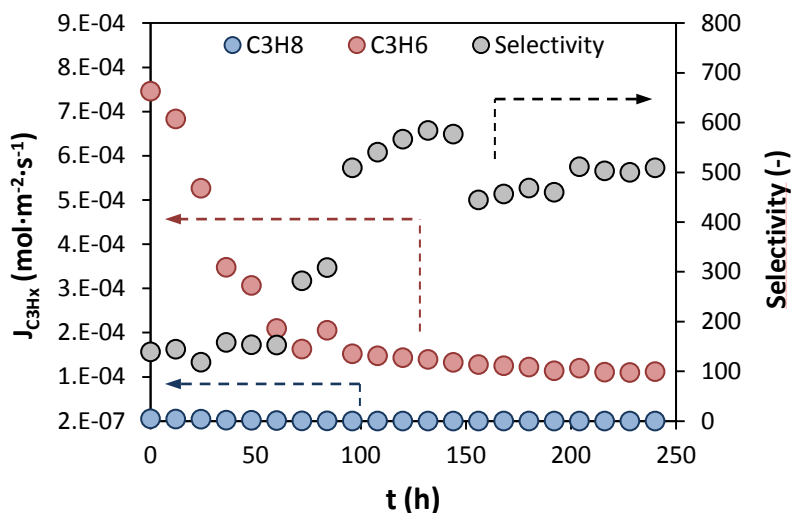


Figure 4.14. Long-term stability experiments of with the 80 % PVDF-HFP/20 % BMImBF₄/60 % AgBF₄ membrane at 293 K.

Effect of the sweep gas flow rate

The effect of the sweep gas flow rate in the fluxes of propane and propylene across the membrane was studied. Figure 4.15 shows that although the flux of propane remained unaffected, the flux of propylene across the membrane increased asymptotically achieving a maximum value with a non linear profile when increasing the sweep gas flow rate. The effect of the sweep gas flow rate in membrane separation processes has been extensively studied in literature, concluding that such improvement resulted from the rise of the driving force by lowering the C_3H_6 partial pressure in the permeate side due to both, sweeping and dilution of the C_3H_6 molecules which are present in the permeate side. Nonetheless, it should be necessary to carry out the separation of C_3H_6 from the N_2 stream in an additional step, being the operating costs mostly associated to the amount of gas to be treated. Therefore for practical operation of the membrane unit, a trade-off must be found in order to maximize the flux of propylene across the membrane without excessive dilution of the permeate stream. All the experiments in this

work were performed using a flow rate of the sweep gas that allows the operation under the maximum driving force.

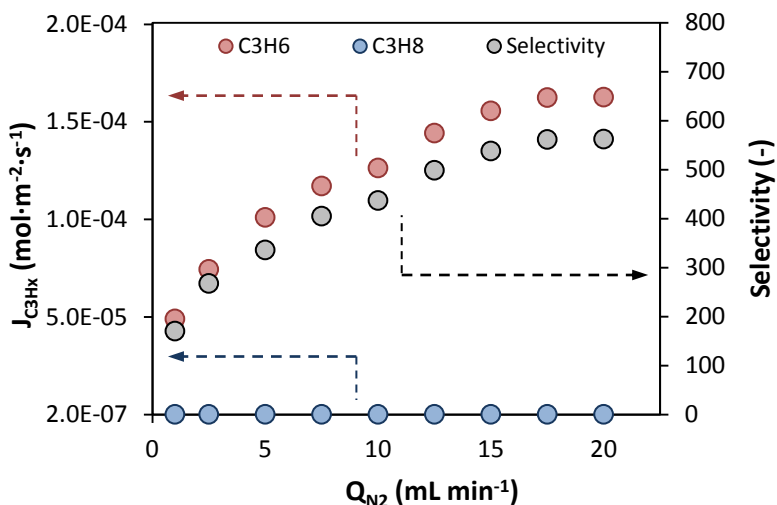


Figure 4.15. Effect of the sweep gas flow rate in the fluxes of C_3H_6 and C_3H_8 at 293 K in 80 % PVDF-HFP/20 % BMimBF₄/60 % AgBF₄ membrane.

Effect of temperature and silver concentration

Figures 4.16 A and 4.16 B plot the permeability of propylene and propane respectively for different silver contents in the membrane at temperatures between 293 and 323 K. Mixed C_3H_6 and C_3H_8 gas permeabilities were measured following the procedure described in the experimental section. Gas transport measurements indicate that an increase in the silver concentration in the membrane leads, as previously expected, to higher propylene permeabilities because more carrier molecules are available for the transport of propylene (figure 4.16 A). On the other hand, although propane should not be affected by the presence of silver ions in the membrane, the permeability of propane slightly increases when silver is added to the membrane. This phenomenon could be explained because the addition of silver salt

greatly increases the flux of propylene, which indeed could sweep some propane molecules dissolved in the membrane.

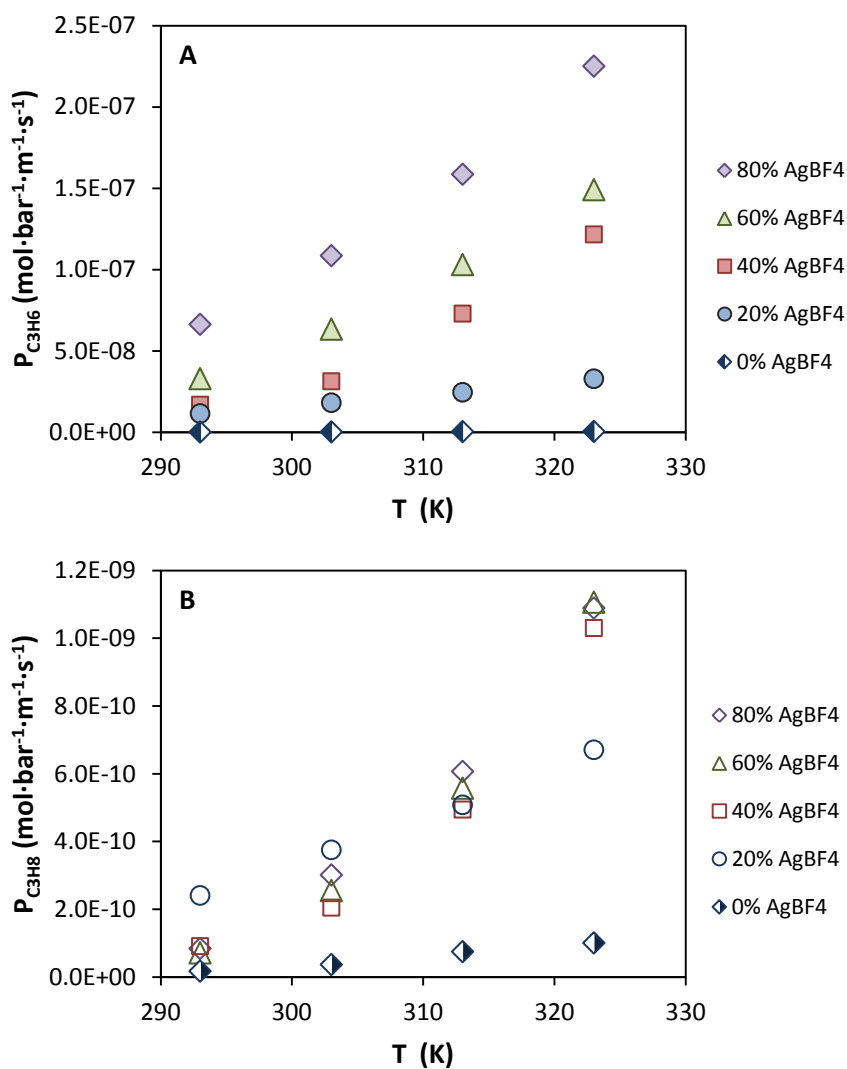


Figure 4.16. Effect of temperature and silver concentration in 80 % PVDF-HFP/ 20 % BMimBF₄ membrane on the propylene A) and propane B) permeabilities.

Regarding the effect of temperature the results show that higher operating temperatures increase gas permeability. This can be explained because at higher temperatures two simultaneous effects take place; the polymer chain mobility increases and the viscosity of the ionic liquid drastically decreases. These two phenomena lead to higher diffusion coefficients for both C_3H_8 and C_3H_6 . However, C_3H_8 is affected to a larger extent over C_3H_6 that already had a very fast permeation due to facilitated transport. As a consequence, the higher temperature decreases the permeation advantage of C_3H_6 over C_3H_8 resulting in lower separation selectivities. The temperature dependence of the permeabilities of both gases can be described by an Arrhenius-type equation [36].

Following the same procedure described in section 4.3.1 for SILMs, figure 4.17 shows the influence of silver concentration in the membrane on the composition of the permeate stream.

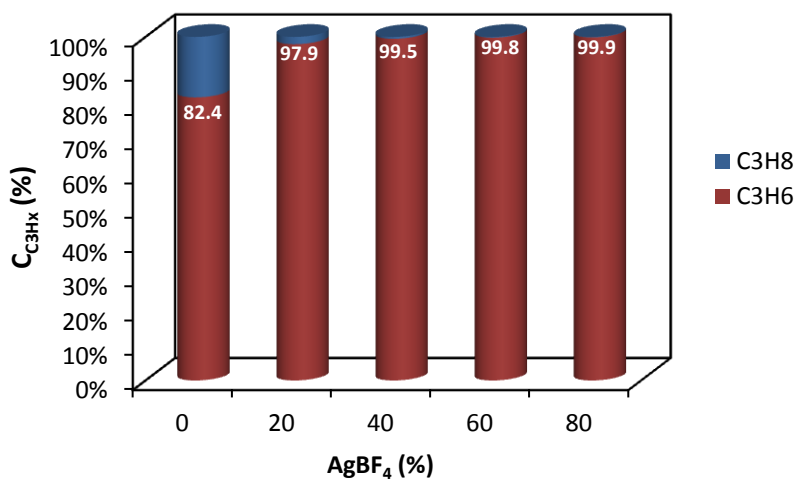


Figure 4.17. Composition of the permeate stream at different silver loadings in the membrane at 293 K, pressure of the feed and permeate streams of 1.0 and a flow rate of the sweep gas that allows to operate under the maximum driving force.

Again it can be noted that the propylene composition in the permeate stream greatly increases when increasing the amount of silver in the membrane. At silver loadings in the membrane above 40 %, the propylene purity in the permeate stream is high enough to be used in any application of propylene including the production of polyolefins which commonly requires propylene purities above 99.5 %.

Effect of pressure

The effect of feed pressure on C_3H_6 and C_3H_8 permeability and flux was investigated in the pressure range of 0.5-3 bar. Figure 4.18 illustrates the effect of pressure on permeation fluxes of both gases at 293 K for PVDF-HFP/BMIImBF₄ with and without silver salt.

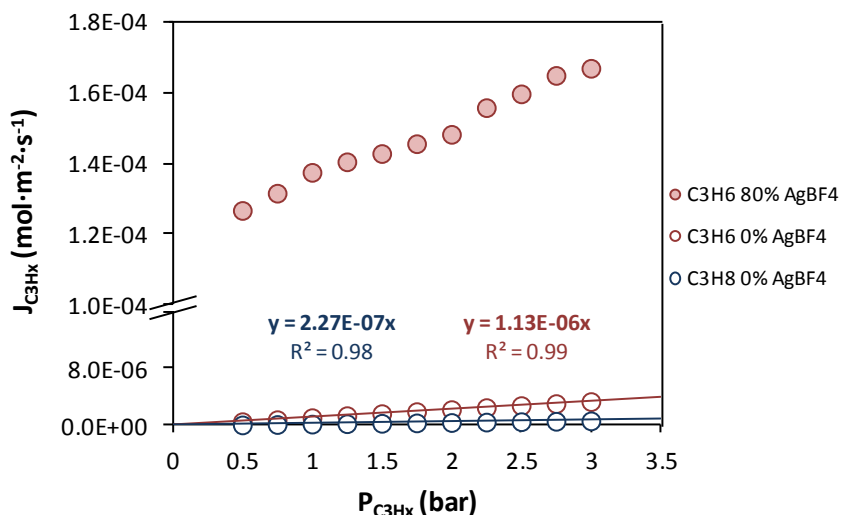


Figure 4.18. Effect of the pressure on the fluxes of C_3H_8 and C_3H_6 in 80 % PVDF-HFP/ 20 % BMIImBF₄ membranes and different AgBF₄ loadings.

It can be seen that the flux of both gases for the composite membrane without silver salt increases following a linear trend from $1.1 \cdot 10^{-7}$ to $6.8 \cdot 10^{-7}$ mol·m⁻²·s⁻¹ for propane and from $5.6 \cdot 10^{-7}$ to $3.4 \cdot 10^{-6}$ mol·m⁻²·s⁻¹

for propylene. On the other hand, as expected the membrane with 80 % AgBF_4 exhibits much higher fluxes of propylene because facilitated transport mechanism takes place. Nevertheless, when the feed pressure is increased only a slightly increment on the flux of propylene has been observed. This indicates that most of the carrier molecules are saturated even at low propylene partial pressures. Therefore it is suggested that the total observed flux of propylene is the sum of two contributions: the first one that depends on the concentration driving force within the membrane, as predicted from Fick's law and the second one that is the facilitated transport contribution by both mechanisms, with fixed carrier and mobile carrier (eqs. 4.7 and 4.8) which is in good agreement with the results obtained by Rabago et al. [37] Figure 4.19 shows a schematic diagram of the transport mechanisms of propane and propylene across the polymer/ionic liquid composite membranes studied in this section.

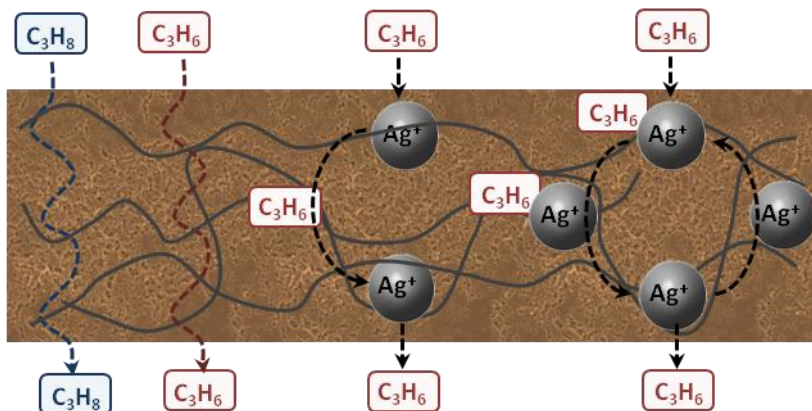


Figure 4.19. Transport mechanisms of propane and propylene in a polymer/ionic liquid composite membrane.

$$J_{\text{C}_3\text{H}_8} = J_{\text{D,C}_3\text{H}_8} = \frac{P_{\text{C}_3\text{H}_8}}{\delta} \Delta p_{\text{C}_3\text{H}_8} \quad (4.7)$$

$$J_{\text{C}_3\text{H}_6} = J_{\text{D,C}_3\text{H}_6} + J_{\text{FT,C}_3\text{H}_6} = \frac{P_{\text{C}_3\text{H}_6}}{\delta} \Delta p_{\text{C}_3\text{H}_6} + J_{\text{FT,C}_3\text{H}_6} \quad (4.8)$$

Therefore, the polymer/ionic liquid facilitated transport membranes studied in this work would be suitable for operation even with feed streams with low olefin content, allowing to obtain high olefin fluxes combined with good separation selectivities.

4.3.3. Comparison with other membranes

The gas separation properties of PVDF-HFP/BMImBF₄-Ag⁺ composite membranes for C₃H₆/C₃H₈ separation has been compared with other existing membranes on a Robeson plot including the most relevant data published in literature updated to 2013 (figure 4.20). On this chart, the selectivity for a gas pair is plotted against permeability expressed in barrers ($1 \text{ barrer} = \frac{\text{cm}^3(\text{STP}) \cdot \text{cm}}{\text{s} \cdot \text{cm}^2 \cdot \text{cm Hg}}$) of the more permeable gas on a log-log scale. The empirical “upper bound” in this plot, that shows the well-known flux/selectivity tradeoff for a given type of membrane, approximates the best selectivity/permeability combination for a certain separation. The results collect most of the different types of membranes studied for this application, including conventional polymeric membranes, inorganic membranes such as carbon molecular sieve and zeolite-based membranes as well as facilitated transport membranes in both the liquid and solid state. In order to facilitate the data comparison with some of the most common membranes the “upper bound” for conventional polymeric [38] and inorganic membranes [39] have been represented. The values obtained in this work represented in the Robeson plot were obtained after more than 100 hours operating time to assure that the pseudo-steady state has been reached.

From figure 4.20 it can be seen that for the BMImBF₄-Ag⁺ SILMs studied in this work the separation selectivity strongly depends on the carrier concentration in the membrane. However these membranes resulted highly permeable towards propylene even at silver concentrations. This was previously expected due to the high propylene solubility together with the fast diffusion rate of species in the liquid state compared to

that observed in solid membranes. From the experimental results it can be noted that the SILMs prepared in this work with carrier concentrations higher than 0.25 M are located well above the upper bound previously reported for organic and inorganic membranes. Regarding the experimental results for the PVDF-HFP/BMImBF₄-Ag⁺ composite membranes herein reported correspond to the values obtained with 80 % PVDF-HFP/20 % BMImBF₄ membranes with AgBF₄ contents varying from 0 to 80 % w/w. Although commonly dense solid membranes present relative low permeabilities, as it can be observed in figure 4.20, the facilitated transport membranes herein presented provided high permeabilities for propylene and with reasonable separation selectivities. This is due to the presence of the ionic liquid phase integrated within the polymer matrix that provides a medium for facilitated transport in liquid state, similar to that present in conventional liquid membranes. At the same time, the membranes showed very low propane permeability which finally leads to high separation selectivities. Again it was observed a big influence of the silver concentration on the propylene permeability as well as on the separation selectivity. On the other hand as the temperature increases the permeability of propylene greatly increases at the expense of decreasing the efficiency of the separation. Based upon the experimental results it can be concluded that with the exception of the results obtained with the membranes without carrier, all the data obtained with PVDF-HFP/BMImBF₄-Ag⁺ composite membranes greatly surpass the upper bounds for the most common membranes reported in literature placing these membranes in the commercially attractive zone in the Robeson plot.

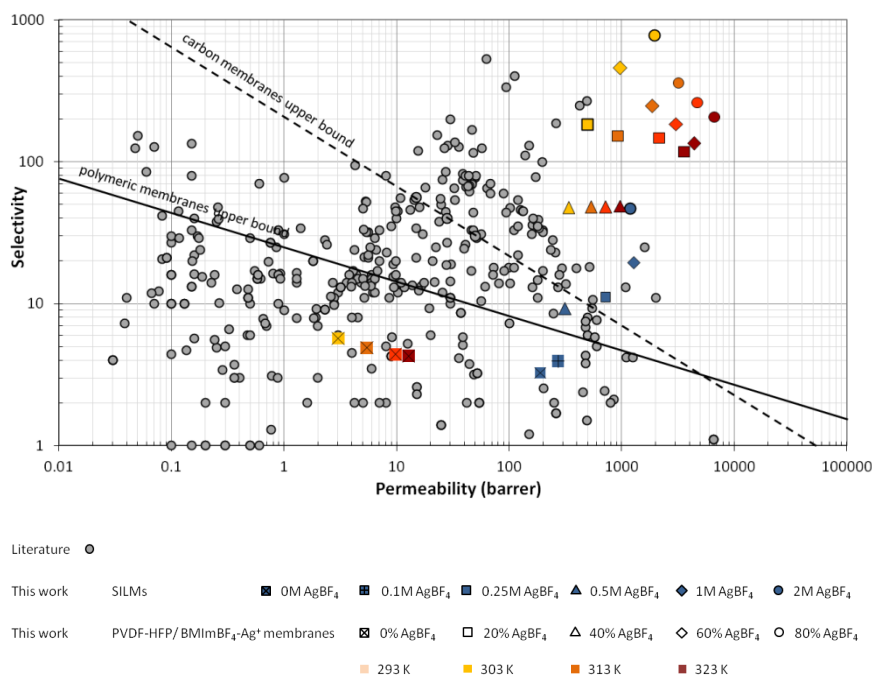


Figure 4.20. Robeson plot for C_3H_6/C_3H_8 separation.

4.3.4. Comparison with distillation

As described in chapter 1 of this thesis, the cracking of different feedstocks remains one of the most important and widely employed processes for light olefins production. It typically consists of four distinct steps: cracking stage and quenching, compression and acid gas removal (H_2S , CO_2 , etc.), subcooling and product separation and refrigeration. The feedstocks are fed to a bank of parallel pyrolysis furnaces where they are cracked at temperatures above 873 K. At the exit of the cracking furnace, the outputs are immediately cooled to about 623 K in a transfer-line exchanger to stop reactions and recover the waste heat for steam generation. The cracked gases are cooled to about 313 K in a water quench tower to condense the heavy products like fuel oil and most of the dilution steam. The cooled gases are then compressed in

different compression stages scrubbed with caustic gas to remove H_2S and CO_2 . Afterwards the gases are cooled to about 288 K and dehydrated with molecular sieves. The dried gases are chilled to low temperatures in a series of heat exchangers before they enter the separation section. Then a train of distillation units separates the gases according to the different number of carbon atoms. In the demethanizer methane is obtained overhead and the C_2+ fraction goes into the deethanizer. There C_2 fraction is recovered on the top of the distillation column and the bottoms consisting of a fraction heavier than C_3 is introduced into the depropanizer where C_3 components are separated from the heavier components (C_4+). The deethanizer and depropanizer overheads are hydrogenated in a catalytic reactor to convert acetylene into ethylene and propyne into propylene respectively, increasing the process yield to olefins. Figure 4.21 illustrates a schematic flow diagram for a typical light olefins production process.

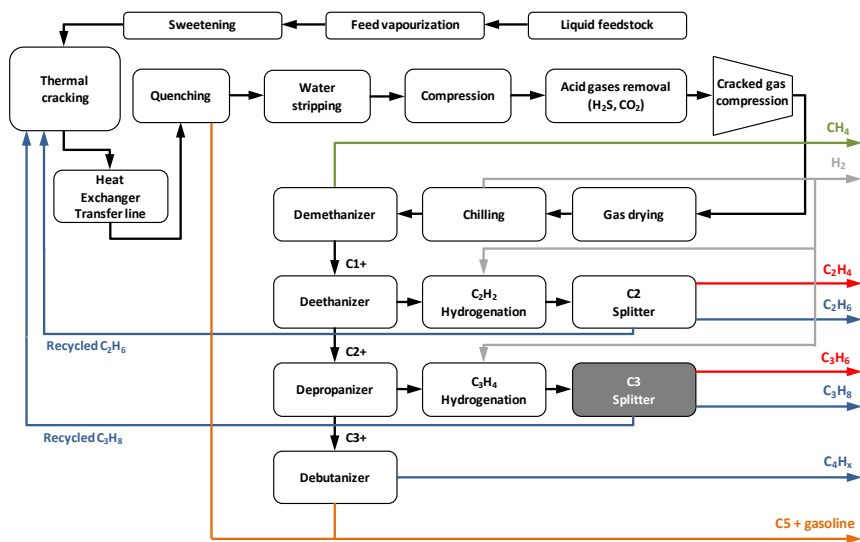


Figure 4.21. Flow diagram of a typical ethylene production process (adapted from [40]).

In this complex system the wide number of optimization opportunities include design changes, product purity enhancement, energy reduction,

production capacity increase, by-products minimizing, revamp economics, and reduction of greenhouse gases. However, due to the low relative volatilities between olefins and their corresponding paraffins about 70 % of the total required energy is consumed in the purification/separation subsystem. Therefore, any reduction in energy consumed mainly in the compression and refrigeration load will result in a significant decrease of the operating cost of the entire plant. As stated in literature [41], ethane/ethylene, and propane/propylene separations are potential steps for an energy saving of 33 % through hybrid technologies involving both membranes and distillation processes. Different technologies were investigated to intensify the traditional distillation processes. Ghosh et al. [42] evaluated the potential of a hybrid adsorption–distillation system for propane/propylene separation. According to their findings, although there is a reduction in energy requirements there is a need of an innovative adsorption–desorption process or new adsorbents with higher selectivity. Schmal et al. [43] compared the use of a heat integrated distillation column (HIDiC) with a vapor recompression (VR) distillation column. They found HIDiC to be 14 % more economical than VR in operating cost. Finally, membranes combined with distillation columns were demonstrated in the literature as a technological option to optimize the performance of hydrocarbon separation and purification [44–48]. In this section membrane separations, which are generally less energy-intensive than distillation processes, have been considered as promising alternatives to enhance the purity of ethylene and propylene as well as to reduce the capital and operating costs of the existing separation processes. For the discussion the comparison between the propane/propylene splitter and the PVDF-HFP/BMIImBF₄-Ag⁺ membranes described in section 4.3.2 of this chapter will be considered.

Figure 4.22 shows the operational conditions of a conventional propane/propylene splitter. The unit allows the treatment of 285 kmol·h⁻¹ of a liquid stream at nearly 325 K with a propylene content around 59 % v/v. The productivity of the plant is fixed, to meet the demand of propylene, in 160 kmol·h⁻¹ for a medium-size plant. High

reflux ratios (≈ 14) are required to achieve the required purity of the propylene stream above 99 % in order to meet the commercial requirements of propylene, that correspond to a propylene recovery of 96 %.

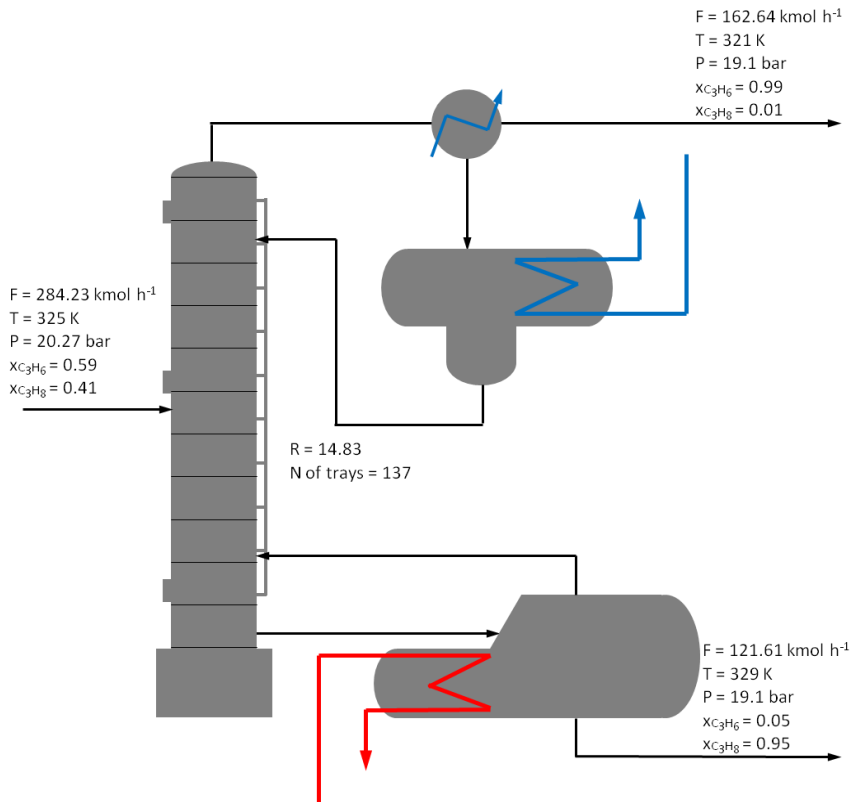


Figure 4.22. Operational conditions of a propane/propylene splitter.

The objective is to compare the distillation unit for propane/propylene separation above described with a membrane system which allows to replace the distillation column obtaining the same streams as the conventional process. The membranes considered for the separation are the composite membranes studied in this chapter with 80 % PVDF-HFP/20 % BMImBF₄-80 % AgBF₄ as they showed the best separation performance combined with a good stability. At 323 K and 1 bar these membranes exhibited a flux of propylene of $7.76 \cdot 10^{-3} \text{ kmol} \cdot \text{m}^{-2} \cdot \text{h}^{-1}$ and a separation selectivity of 206. Therefore, the required

membrane area to meet the propylene production requirements of $162.64 \text{ kmol} \cdot \text{h}^{-1}$ is 57800 m^2 .

Taking into account the processability of the composite membranes, the most convenient module configuration to consider is the spiral wound configuration (figure 4.23).

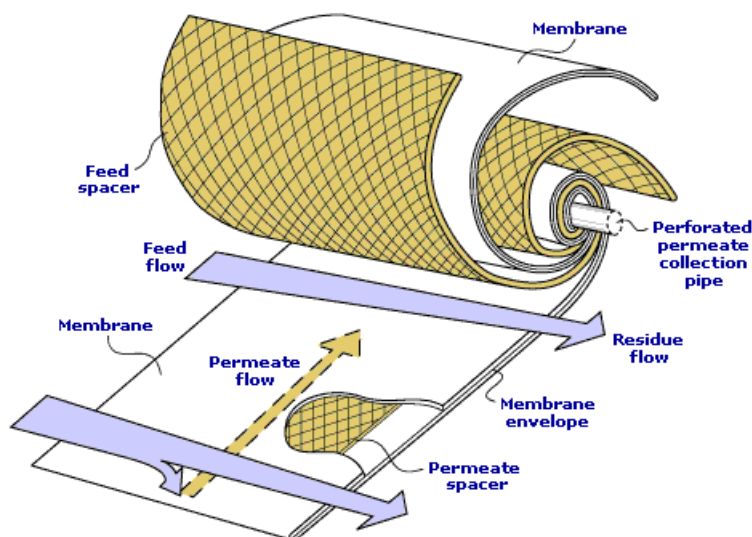


Figure 4.23. Structure of a spiral-wound module [49].

Although the major application of spiral-wound modules is in desalination of sea and brackish water by reverse osmosis, they are also extensively used in gas separation. The spiral-wound configuration usually provides a membrane area per unit volume in the range $800\text{--}1000 \text{ m}^2 \cdot \text{m}^{-3}$. Large-scale production is quite cost effective and module costs per membrane area are quite low. However, the spiral-wound module is quite sensitive to fouling, and the feed channels can easily be blocked, so the presence of particles and other impurities should be carefully controlled from the feed stream by a proper pretreatment procedure [50]. Therefore the required volume of equipment considering the fabrication of the composite membranes herein prepared in spiral-wound configuration is 57.8 m^3 . This represents an

important reduction in volume of the equipment compared to the conventional distillation unit of 6 m diameter and up to 100 m tall. In addition the reduction in the heating, cooling and compressing requirements that often results in huge equipments should be also considered. Moreover, the major part of the energy consumption associated to the conventional splitter could be saved, since no liquid pumping, compressing, heating or cooling facilities are required. Thus the PVDF-HFP/BMIImBF₄-Ag⁺ facilitated transport membranes studied in this work, represent a progress towards the development of new technologies to carry out the separation of gaseous olefin/paraffin mixtures more efficiently, reducing the equipment size, the required capital investment and the associated operating costs.

4.4. Conclusions

The use novel facilitated transport membranes for the separation of propane/propylene mixtures like supported ionic liquid membranes (SILMs) and polymer/ionic liquid composite membranes has been evaluated. It was observed that for the SILMs the flux of propane across the membrane does not depend on the carrier concentration; however the flux of propylene increases following a linear trend with the concentration of Ag^+ . Increasing the flow rate of the sweep gas, the fluxes of both gases are increased because the molecules of gas that arrive at the permeate side were removed more efficiently. Also higher transmembrane pressures result in higher fluxes because the driving force is higher, whereas the stability of the SILM could be compromised. In order to improve the stability of SILMs new PVDF-HFP/BMImBF₄-Ag⁺ facilitated transport membranes were synthesized and characterized by polarized light microscopy, thermogravimetric analysis, tensile tests and FTIR spectroscopy. The membranes containing 80 % PVDF-HFP/20 % BMImBF₄ exhibited the best trade-off between separation performance and mechanical resistance. Results showed that again for the PVDF-HFP/BMImBF₄-Ag⁺ facilitated transport membranes an increase in the silver concentration has a positive effect in the propylene permeabilities but at the same time the permeability of propane slightly increases due to sweeping effects. Regarding the effect of temperature, the flux of both gases greatly increases with temperature following an Arrhenius-type dependence in the range 293-323 K while the separation selectivity decreases. The facilitated transport membranes studied in this work exhibited an excellent stability along time and provided very promising results placing these membranes well above the Robeson upper bound. Finally the performance of these composite facilitated transport membranes was compared to a conventional distillation unit. Based upon the obtained results the PVDF-HFP/BMImBF₄-Ag⁺ facilitated transport membranes studied in this work, represent a progress toward the development of new technologies to carry out the separation of gaseous olefin/paraffin mixtures more efficiently, reducing the required capital investment and the associated operating costs.

4.5. Nomenclature

A	effective membrane area (m^2)
D	diffusivity ($\text{m}^2 \cdot \text{s}^{-1}$)
F	gas molar flow ($\text{mol} \cdot \text{s}^{-1}$)
J	molar flux ($\text{mol} \cdot \text{m}^{-2} \cdot \text{s}^{-1}$)
P	permeability ($\text{mol} \cdot \text{bar}^{-1} \cdot \text{m}^{-1} \cdot \text{s}^{-1}$)
p	pressure (bar)
S	solubility coefficient ($\text{mol} \cdot \text{m}^{-3} \cdot \text{bar}^{-1}$)
V	molar volume (m^3)
y	gas molar fraction (-)

Greek letters

δ	membrane thickness (m)
μ	viscosity (Pa s)
σ	standard deviation (-)

Superscripts/subscripts

C_3H_6	propylene
C_3H_8	propane

4.6. References

- [1] W.J. Koros, R. Mahajan. Pushing the limits on possibilities for large scale gas separation: Which strategies? *J.Membr.Sci.*, 175 (2000) 181.
- [2] R. Faiz, K. Li. Polymeric membranes for light olefin/paraffin separation. *Desalination*, 287 (2012) 82.
- [3] M.L. Chng, Y. Xiao, T.-. Chung, M. Toriida, and S. Tamai. Enhanced propylene/propane separation by carbonaceous membrane derived from poly (aryl ether ketone)/2,6-bis(4-azidobenzylidene)-4-methyl-cyclohexanone interpenetrating network. *Carbon*, 47 (2009) 1857.
- [4] K. Tanaka, A. Taguchi, J. Hao, H. Kita, and K. Okamoto. Permeation and separation properties of polyimide membranes to olefins and paraffins. *J.Membr.Sci.*, 121 (1996) 197.
- [5] C. Staudt-Bickel, W.J. Koros. Olefin/paraffin gas separations with 6FDA-based polyimide membranes. *J.Membr.Sci.*, 170 (2000) 205.
- [6] S.M. Saufi, A.F. Ismail. Fabrication of carbon membranes for gas separation - A review. *Carbon*, 42 (2004) 241.
- [7] T. Ueki, M. Watanabe. Macromolecules in ionic liquids: Progress, challenges, and opportunities. *Macromolecules*, 41 (2008) 3739.
- [8] H.Z. Chen, P. Li, and T.-S. Chung. PVDF/ionic liquid polymer blends with superior separation performance for removing CO₂ from hydrogen and flue gas. *Int. J. Hydrogen Energy*, 37 (2012) 11796.
- [9] Y. Gu, T.P. Lodge. Synthesis and gas separation performance of triblock copolymer ion gels with a polymerized ionic liquid mid-block. *Macromolecules*, 44 (2011) 1732.
- [10] J.C. Jansen, K. Friess, G. Clarizia, J. Schauer, and P. Izák. High ionic liquid content polymeric gel membranes: Preparation and performance. *Macromolecules*, 44 (2011) 39.
- [11] P. Bernardo, J.C. Jansen, F. Bazzarelli, F. Tasselli, A. Fuoco, K. Friess, et al. Gas transport properties of Pebax®/room temperature ionic liquid gel membranes. *Sep. Purif. Technol.*, 97 (2012) 73.

- [12] K. Friess, J.C. Jansen, F. Bazzarelli, P. Izák, V. Jarmarová, M. Kačírková, et al. High ionic liquid content polymeric gel membranes: Correlation of membrane structure with gas and vapour transport properties. *J.Membr.Sci.*, 415-416 (2012) 801.
- [13] Y. Gu, E.L. Cussler, and T.P. Lodge. ABA-triblock copolymer ion gels for CO₂ separation applications. *J.Membr.Sci.*, 423-424 (2012) 20.
- [14] L.C. Tomé, D. Mecerreyes, C.S.R. Freire, L.P.N. Rebelo, and I.M. Marrucho. Pyrrolidinium-based polymeric ionic liquid materials: New perspectives for CO₂ separation membranes. *J.Membr.Sci.*, 428 (2013) 260.
- [15] R. Faiz, K. Li. Olefin/paraffin separation using membrane based facilitated transport/chemical absorption techniques. *Chem. Eng. Sci.*, 73 (2012) 261.
- [16] J.H. Kim, B.R. Min, C.K. Kim, J. Won, and Y.S. Kang. New insights into the coordination mode of silver ions dissolved in poly(2-ethyl-2-oxazoline) and its relation to facilitated olefin transport. *Macromolecules*, 35 (2002) 5250.
- [17] J.H. Kim, B.R. Min, J. Won, S.H. Joo, H.S. Kim, and Y.S. Kang. Role of polymer matrix in polymer/silver complexes for structure, interactions, and facilitated olefin transport. *Macromolecules*, 36 (2003) 6183.
- [18] J.H. Kim, B.R. Min, J. Won, and Y.S. Kang. Revelation of facilitated olefin transport through silver-polymer complex membranes using anion complexation. *Macromolecules*, 36 (2003) 4577.
- [19] S.W. Kang, D.H. Lee, J.H. Park, K. Char, J.H. Kim, J. Won, et al. Effect of the polarity of silver nanoparticles induced by ionic liquids on facilitated transport for the separation of propylene/propane mixtures. *J.Membr.Sci.*, 322 (2008) 281.
- [20] M. Teramoto, H. Matsuyama, T. Yamashiro, and Y. Katayama. Separation of ethylene from ethane by supported liquid membranes containing silver nitrate as carrier. *J.Chem.Eng.Japan*, 19 (1986) 419.

- [21] M.T. Ravanchi, T. Kaghazchi, and A. Kargari. Separation of propylene-propane mixture using immobilized liquid membrane via facilitated transport mechanism. *Sep.Sci.Technol.*, 44 (2009) 1198.
- [22] A.S. Kovvali, H. Chen, and K.K. Sirkar. Glycerol-based immobilized liquid membranes for olefin-paraffin separation. *Ind. Eng. Chem. Res.*, 41 (2002) 347.
- [23] S. Duan, A. Ito, and A. Ohkawa. Separation of propylene/propane mixture by a supported liquid membrane containing triethylene glycol and a silver salt. *J.Membr.Sci.*, 215 (2003) 53.
- [24] F. Pitsch, F.F. Krull, F. Agel, P. Schulz, P. Wasserscheid, T. Melin, et al. An adaptive self-healing ionic liquid nanocomposite membrane for olefin-paraffin separations. *Adv. Mater.*, 24 (2012) 4306.
- [25] P. Scovazzo, J. Kieft, D.A. Finan, C. Koval, D. DuBois, and R. Noble. Gas separations using non-hexafluorophosphate $[PF_6]^-$ anion supported ionic liquid membranes. *J.Membr.Sci.*, 238 (2004) 57.
- [26] L.A. Neves, J.G. Crespo, and I.M. Coelho. Gas permeation studies in supported ionic liquid membranes. *J.Membr.Sci.*, 357 (2010) 160.
- [27] A. Ortiz, A. Ruiz, D. Gorri, and I. Ortiz. Room temperature ionic liquid with silver salt as efficient reaction media for propylene/propane separation: Absorption equilibrium. *Sep. Purif. Technol.*, 63 (2008) 311.
- [28] A. Ortiz, L.M. Galán, D. Gorri, A.B. De Haan, and I. Ortiz. Kinetics of reactive absorption of propylene in RTIL- Ag^+ media. *Sep. Purif. Technol.*, 73 (2010) 106.
- [29] A. Ortiz, L.M. Galán Sanchez, D. Gorri, A.B. De Haan, and I. Ortiz. Reactive ionic liquid media for the separation of propylene/propane gaseous mixtures. *Ind. Eng. Chem. Res.*, 49 (2010) 7227.
- [30] M. Teramoto, H. Matsuyama, T. Yamashiro, and S. Okamoto. Separation of ethylene from ethane by a flowing liquid membrane using silver nitrate as a carrier. *J.Membr.Sci.*, 45 (1989) 115.

- [31] D. Morgan, L. Ferguson, and P. Scovazzo. Diffusivities of gases in room-temperature ionic Liquids: Data and correlations obtained using a lag-time technique. *Ind. Eng. Chem. Res.*, 44 (2005) 4815.
- [32] M. Teramoto, N. Takeuchi, T. Maki, and H. Matsuyama. Ethylene/ethane separation by facilitated transport membrane accompanied by permeation of aqueous silver nitrate solution. *Sep. Purif. Technol.*, 28 (2002) 117.
- [33] Shalu, S.K. Chaurasia, R.K. Singh, and S. Chandra. Thermal stability, complexing behavior, and ionic transport of polymeric gel membranes based on polymer PVdF-HFP and ionic liquid, [BMIM][BF₄]. *J Phys. Chem. B*, 117 (2013) 897.
- [34] W.K. Sang, H.K. Jong, K. Char, and S.K. Yong. Long-term separation performance of phthalate polymer/silver salt complex membranes for olefin/paraffin separation. *Macromolecular Research*, 13 (2005) 162.
- [35] S.W. Kang, K. Char, J.H. Kim, and Y.S. Kang. Ionic liquid as a solvent and the long-term separation performance in a polymer/silver salt complex membrane. *Macromol. Res.*, 15 (2007) 167.
- [36] T.-S. Chung, C. Cao, and R. Wang. Pressure and Temperature Dependence of the Gas-Transport Properties of Dense Poly[2,6-toluene-2,2-bis(3,4-dicarboxylphenyl)hexafluoropropane diimide] Membranes. *J.Polym.Sci.Part B*, 42 (2004) 354.
- [37] R. Rabago, D.L. Bryant, C.A. Koval, and R.D. Noble. Evidence for Parallel Pathways in the Facilitated Transport of Alkenes through Ag⁺-Exchanged Nafion Films. *Ind. Eng. Chem. Res.*, 35 (1996) 1090.
- [38] R.L. Burns, W.J. Koros. Defining the challenges for C₃H₆/C₃H₈ separation using polymeric membranes. *J.Membr.Sci.*, 211 (2003) 299.
- [39] Y. Pan, T. Li, G. Lestari, and Z. Lai. Effective separation of propylene/propane binary mixtures by ZIF-8 membranes. *J.Membr.Sci.*, 390-391 (2012) 93.

- [40] M. Benali, B. Aydin. Ethane/ethylene and propane/propylene separation in hybrid membrane distillation systems: Optimization and economic analysis. *Sep. Purif. Technol.*, 73 (2010) 377.
- [41] G.E. Keller, R.R. Beebe, R.J. Fruehan, N.N. Li, E.L. Menger, G.P. Pez, et al, *Separation Technologies for the Industries of the Future*, Washington DC, National Academies Press, 1998.
- [42] T.K. Ghosh, H. Lin, and A.L. Hines. Hybrid adsorption-distillation process for separating propane and propylene. *Ind. Eng. Chem. Res.*, 32 (1993) 2390.
- [43] J.P. Schmal, H.J. Van der Kooi, A. de Rijke, Ž. Olujic, and P.J. Jansens. Internal versus external heat integration: Operational and economic analysis. *Chem.Eng.Res.Design*, 84 (2006) 374.
- [44] S. Moganti, R.D. Noble, and C.A. Koval. Analysis of a membrane/distillation column hybrid process. *J.Membr.Sci.*, 93 (1994) 31.
- [45] T. Pettersen, A. Argo, R.D. Noble, and C.A. Koval. Design of combined membrane and distillation processes. *Separ. Technol.*, 6 (1996) 175.
- [46] I.K. Kookos. Optimal design of membrane/distillation column hybrid processes. *Ind. Eng. Chem. Res.*, 42 (2003) 1731.
- [47] D.E. Suk, T. Matsuura. Membrane-based hybrid processes: A review. *Sep.Sci.Technol.*, 41 (2006) 595.
- [48] J.A. Caballero, I.E. Grossmann, M. Keyvani, and E.S. Lenz. Design of hybrid distillation-vapor membrane separation systems. *Ind. Eng. Chem. Res.*, 48 (2009) 9151.
- [49] Membrane Technology & Research, www.mtrinc.com, 30-4-2013.
- [50] H. Strathmann, *Membranes and Membrane Separation Processes*, 3. Membrane Preparation and Membrane Module Constructions, Ullman's Encyclopedia of Industrial Chemistry, Wiley-VCH, 2012.



5

Conclusions and challenges for future research

Abstract

The aim of this thesis has been the development of a novel olefin/paraffin separation process through the integration of the reaction between olefins and silver ions, ionic liquids and membrane technology. After the detailed description of the objectives of this work, this chapter summarizes the main results that have been achieved, draws the conclusions derived from the analysis of the results and highlights future challenges and perspectives in the separation of olefins from paraffins in order to boost the practical application of the novel separation process.

5.1. Conclusions

This thesis focuses on the development of an alternative separation process of olefin/paraffin gas mixtures through the integration of ionic liquids and membrane technology. The work covers the selection of the most suitable ionic liquid-silver salt system to carry out the separation process as well as the evaluation of the separation performance of different membrane technologies including membrane contactors, supported ionic liquid membranes (SILMs) and polymer/ionic liquid composite membranes.

The first step was the selection of the most favorable Ag^+ -RTIL reaction medium for the separation of propane/propylene mixtures. Equilibrium data of the absorption of propane and propylene in 7 ILs with different structures were obtained and the characteristic parameters of the physical and chemical solubility were determined. Afterwards, a screening of ILs using the COSMO-RS methodology was applied to select the most effective ionic liquid-silver salt system to carry out the separation of olefin/paraffin gas mixtures. Based upon the obtained results it can be concluded that the most suitable system to carry out the separation of propane/propylene gas mixtures by reactive absorption should be based on an ionic liquid with the BF_4^- anion and an imidazolium-based cation with the lowest number and shortest alkyl groups as possible and silver tetrafluoroborate (AgBF_4) as silver salt.

Having defined the ionic liquid-silver salt system, the implementation of the separation process in gas-liquid membrane contactors was addressed. First of all a comparative analysis of the performance of different fibers including both, polymeric (PVDF, PTFE) and ceramic (with symmetric and asymmetric structures) has been carried out. It was found that PVDF membranes suffered from wetting, which became more important over time. On the other hand, PTFE and ceramic membranes were proved to be suitable to accomplish the separation process. However the use of highly hydrophobic polymeric membranes

(such as PTFE or polyolefin) is still preferred over ceramic membranes due to economic considerations and the easier fabrication procedures.

Afterwards, two different membrane contactors, a parallel flow membrane contactor with tubular configuration and a hollow fiber transverse flow membrane contactor have been evaluated. A mathematical model based on the resistances-in-series approach has been developed obtaining a good agreement between experimental and simulated results. It was found that the improved fluid-dynamics of the transverse flow membrane contactor leads to an overall mass transfer coefficient 17.6 times higher than that reported using a parallel-flow contactor. At the same time it was achieved a process intensification by a factor of 17.4 in terms of mass transfer per specific area compared to a conventional stirred tank reactor system ($K_{\text{overall}}^*a(\text{MC})/K_{\text{overall}}^*a(\text{CSTR})$) when a concentration of silver ions of 0.25 M in the IL is used. However, the rate limiting step was still located in the liquid boundary layer, with a contribution higher than 97.8 % to the overall mass transfer resistance. In order to overcome the observed mass transfer limitations the use of novel facilitated transport membranes was proposed.

First, the use of supported ionic liquid membranes (SILMs) and was considered. It was observed that the flux of propane across the membrane does not depend on the carrier concentration; however the flux of propylene increases following a linear trend with the concentration of Ag^+ . Increasing the flow rate of the sweep gas, leads to an increment of the fluxes of both gases because the molecules of gas that arrive at the permeate side are removed more effectively. Also higher transmembrane pressures result in higher fluxes because the driving force is higher, whereas the stability of the SILM could be compromised. In order to improve the stability of SILMs, new composite (PVDF-HFP/BMIImBF₄-Ag⁺) facilitated transport membranes were synthesized and characterized by polarized light microscopy, thermogravimetric analysis, tensile tests and FTIR spectroscopy. The membranes containing 80 % PVDF-HFP/20 % BMIImBF₄ presented the best trade-off between separation performance and mechanical

resistance. Results showed that again for the PVDF-HFP/BMImBF₄-Ag⁺ facilitated transport membranes an increase in the silver concentration has a positive effect in the propylene permeabilities but at the same time the permeability of propane slightly increases due to sweeping effects. Regarding the effect of temperature, the flux of both gases greatly increases with temperature following an Arrhenius-type dependence in the range 293-323 K while the separation selectivity decreases. The facilitated transport membranes studied in this work exhibited an excellent stability along time and provided very promising results placing these membranes well above the Robeson upper bound. Finally, the performance of these composite facilitated transport membranes was compared to a conventional distillation unit. Based upon the obtained results the PVDF-HFP/BMImBF₄-Ag⁺ facilitated transport membranes studied in this work, represent a big progress in the development of new technologies to carry out the separation of gaseous olefin/paraffin mixtures more efficiently, reducing the required capital investment as well as the operating costs associated to the conventional distillation process.

5.2. Challenges for future research

This thesis intends to open up the possibility of new pathways to the development of an alternative separation process of olefin/paraffin gas mixtures. Despite the achievements that have been described through the chapters of this thesis, there are still new challenges ahead and disadvantages that must be overcome before the separation of gaseous olefins from their corresponding paraffins assisted by membranes becomes a reality.

Room temperature ionic liquids (RTILs) containing a silver salt have been proved to be suitable solvents for the separation of olefin/paraffin gas mixtures. Nevertheless, more solubility data and a better understanding of the molecular interactions that take place in such a complex system are needed. In addition, as the main disadvantage of ionic liquids is their

relatively high viscosity, new ionic liquids with very low viscosity and higher inherent selectivity towards the olefin are still needed. In this sense the development of novel ionic liquids that incorporate the silver ions as integral components of the ionic liquid at the molecular level can suppose a possible solution.

Regarding the polymer/ionic liquid composite membranes it is necessary to increase the fundamental knowledge of the transport mechanisms that are taking place. Furthermore, it might be also interesting to test the performance of these membranes with real streams in order to check the membrane and the possible carrier poisoning effect in the long-term under harsh conditions. Furthermore, in order to bring the polymer/ionic liquid composite membrane technology to its real implementation it is essential to adapt and scale-up the current manufacturing process to produce spiral wound membrane modules, that will allow to obtain devices with high specific area.



5

Conclusiones y retos para investigaciones futuras

Abstract

El objetivo del trabajo descrito en esta tesis es el desarrollo de un nuevo proceso de separación de mezclas olefina/parafina a través de la integración de la reacción selectiva entre las olefinas y los iones plata, líquidos iónicos y tecnologías de membrana. Después de haber descrito en detalle los principales aspectos de este trabajo, este capítulo resume los principales resultados obtenidos, destaca las conclusiones que se derivan del análisis de los resultados y expone los retos y perspectivas para futuras investigaciones en la separación de mezclas olefina/parafina con el fin de desarrollar un nuevo proceso de separación.

5.1. Conclusiones

Esta tesis se centra en el desarrollo de un nuevo proceso de separación alternativo de mezclas de olefina/parafina mediante la integración de líquidos iónicos y tecnologías de membrana. El trabajo abarca la selección de la combinación líquido iónico-sal de plata más adecuada para llevar a cabo el proceso de separación así como el estudio de la eficacia de separación de diferentes tecnologías de membrana, incluyendo contactores de membrana, membranas de líquido iónico soportadas (SILMs) y membranas compuestas polímero/líquido iónico.

El primer paso fue la selección del medio de reacción Ag^+ -RTIL más adecuado para llevar a cabo la separación de mezclas propano/propileno. Se obtuvieron datos de equilibrio de absorción ambos gases en 7 iónicos con diferentes estructuras y se calcularon los parámetros característicos de solubilidad tanto física como química. Posteriormente se realizó un barrido de líquidos iónicos empleando la metodología COSMO-RS para seleccionar el sistema de líquido iónico-sal de plata más eficaz para llevar a cabo el proceso de separación. De acuerdo con los resultados obtenidos, se puede concluir que el sistema más adecuado para llevar a cabo la separación de mezclas gaseosas propano/propileno mediante absorción reactiva debe basarse en un líquido iónico con el anión BF_4^- y un catión con base imidazolio con el menor número de grupos alquilo tan cortos como sea posible y tetrafluoroborato de plata (AgBF_4) como sal de plata.

Definido el sistema líquido iónico-sal de plata para llevar a cabo el proceso de separación, se abordó la implementación del proceso en contactores de membrana gas-líquido. En primer lugar se realizó un análisis comparativo de la utilización de diferentes tipos de fibras poliméricas (PVDF y PTFE) y cerámicas (con estructura simétrica y asimétrica). Se observó que las membranas de PVDF presentaron fenómenos de mojado, que se hicieron más importantes con el paso del tiempo. Por otro lado, las membranas de PTFE y cerámicas resultaron ser apropiadas para llevar a cabo el proceso de separación. Sin embargo,

para esta aplicación resulta más adecuado el uso de membranas poliméricas altamente hidrófobas (PTFE o poliolefina) en lugar de membranas cerámicas debido a consideraciones económicas y a que habitualmente sus procedimientos de fabricación son más sencillos.

Posteriormente se analizaron dos contactores de membrana diferentes, un contactor de membranas de flujo paralelo con configuración tubular y un contactor de fibras huecas de flujo transversal. Además se desarrolló un modelo matemático basado en la aproximación de resistencias en serie que permite describir de forma satisfactoria los resultados experimentales obtenidos. Se observó que la mejora de la fluidodinámica del contactor de membranas de flujo transversal se traduce en un coeficiente de transferencia de materia global 17.6 veces más alto que el obtenido previamente empleando un contactor de flujo paralelo. Al mismo tiempo se logra un intensificación del proceso de separación por un factor de 17.4 en términos de transferencia de materia por área específica en comparación con un sistema de reactor de tanque agitado convencional ($K_{overall} \cdot a(MC) / K_{overall} \cdot a(CSTR)$) cuando la concentración de iones de plata en el IL es 0,25 M. Sin embargo, la etapa limitante se encuentra localizada todavía en la capa límite de la fase líquida, con una contribución superior al 97,8 % a la resistencia global de transferencia de materia. Con el fin de superar las limitaciones de transferencia de masa observadas se propuso el uso de nuevas membranas de transporte facilitado.

En primer lugar se consideró el uso de membranas de líquido iónico soportadas (SILMs). Se observó que el flujo de propano a través de la membrana no depende de la concentración de portadores, sin embargo el flujo de propileno aumenta siguiendo una tendencia lineal con la concentración de Ag^+ . El aumento del caudal del gas de arrastre conlleva un incremento de los flujos de ambos gases debido a que las moléculas de gas que llegan al lado del permeado son arrastradas de manera más eficiente. Del mismo modo, presiones transmembrana más elevadas resultan en flujos de ambos gases más altos debido a que la fuerza impulsora es mayor, sin embargo a elevadas diferencias de presión la

estabilidad de la SILM podría verse comprometida. Con el fin de mejorar la estabilidad de las SILMs, nuevas membranas compuestas (PVDF-HFP/BMIImBF₄-Ag⁺) de transporte facilitado fueron sintetizadas y caracterizadas mediante microscopía de luz polarizada, análisis termogravimétrico, ensayos de tracción y espectroscopia de FTIR. Se comprobó que las membranas compuestas por 80 % PVDF-HFP/20 % BMIImBF₄ presentaron el mejor compromiso entre eficacia de separación y resistencia mecánica. Los resultados mostraron que de nuevo para las membranas de PVDF-HFP/BMIImBF₄-Ag⁺ de transporte facilitado un aumento en la concentración de plata tiene un efecto positivo en la permeabilidad de propileno, pero al mismo tiempo la permeabilidad del propano aumenta ligeramente debido a efectos de arrastre. En cuanto al efecto de la temperatura, el flujo de ambos gases aumenta de forma notable con la temperatura mostrando una dependencia de tipo Arrhenius en el rango de 293-323 K mientras que la selectividad de la separación disminuye. Las membranas de transporte facilitado estudiadas en este trabajo mostraron una excelente estabilidad a lo largo del tiempo a la vez que proporcionaron resultados muy prometedores situándolas muy por encima del límite superior en el gráfico de Robeson. Por último, se comparó el rendimiento de estas membranas de transporte facilitado compuestas con una unidad de destilación convencional. En base a los resultados obtenidos, se puede concluir que las membranas de transporte facilitado PVDF-HFP/BMIImBF₄-Ag⁺ estudiadas en este trabajo, representan un considerable progreso hacia el desarrollo de nuevas tecnologías para llevar a cabo la separación de mezclas gaseosas olefina/parafina de manera más eficiente, reduciendo los costes de inversión de capital y los costes de operación asociados con el proceso de destilación convencional.

5.2. Retos para investigaciones futuras

Esta tesis pretende abrir nuevas vías para el desarrollo de un proceso de separación alternativo de mezclas de olefina/parafina. A pesar de los logros descritos en los capítulos de esta tesis, todavía hay nuevos retos por delante y desventajas que deben ser superados antes de la separación de olefinas gaseosas de sus correspondientes parafinas asistida por membranas sea una realidad.

Los líquidos iónicos a temperatura ambiente (RTILs) que contienen una sal de plata han demostrado ser disolventes adecuados para la separación de mezclas gaseosas olefina/parafina. Sin embargo, se necesitan más datos de solubilidad y una mejor comprensión de las interacciones moleculares que tienen lugar en un sistema tan complejo. Además, dado que la principal desventaja de los líquidos iónicos es su relativamente alta viscosidad, es necesaria la obtención de nuevos líquidos iónicos con muy baja viscosidad y mayor selectividad hacia la olefina. En este sentido, el desarrollo de nuevos líquidos iónicos que incorporen los iones plata como componentes integrales a nivel molecular puede suponer una posible solución.

Respecto a las membranas compuestas de polímero/líquido iónico, es necesario avanzar en el conocimiento fundamental de los mecanismos de transporte que tienen lugar durante el proceso de separación. Por otra parte, también sería interesante evaluar el rendimiento de estas membranas con corrientes reales con el fin de comprobar la estabilidad de la membrana y el posible efecto de envenenamiento del portador a largo plazo. Del mismo modo, con la finalidad de acercar la tecnología de membranas compuestas polímero/líquido iónico a su aplicación real resulta fundamental adaptar y escalar el proceso de fabricación actual de las membranas para producir módulos de membrana con configuración en espiral, que proporcionen equipos con elevada área específica.

List of scientific contributions

Publications in international journals

1. Effect of liquid flow on the separation of propylene/propane mixtures with a gas/liquid membrane contactor using Ag^+ -RTIL solutions. **M. Fallanza**, A. Ortiz, D. Gorri, I. Ortiz. *Desalination and Water Treatment* 27 (2011) pp. 123-129. (Chapter 3 of this thesis).
2. Improving the mass transfer rate in G-L membrane contactors with ionic liquids as absorption medium. Recovery of propylene. **M. Fallanza**, A. Ortiz, D. Gorri, I. Ortiz. *Journal of Membrane Science* 385-386 (2011), pp. 217-225. (Chapter 3 of this thesis).
3. Experimental study of the separation of propane/propylene mixtures by supported ionic liquid membranes containing Ag^+ -RTILs as carrier. **M. Fallanza**, A. Ortiz, D. Gorri, I. Ortiz. *Separation & Purification Technology* 97 (2012), pp. 83-89. (Chapter 4 of this thesis).
4. Using membrane reactive absorption modelling to predict optimum process conditions in the separation of propane-propylene mixtures. **M. Fallanza**, A. Ortiz, D. Gorri, I. Ortiz. *Industrial & Engineering Chemistry Research* (2013). DOI: 10.1021/ie302614r. (Chapter 3 of this thesis).
5. Screening of RTILs for propane/propylene separation using COSMO-RS methodology. **M. Fallanza**, A. Ortiz, D. Gorri, I. Ortiz. *Chemical Engineering Journal* 220 (2013), pp. 284-293. (Chapter 2 of this thesis).
6. Long term stability of PTFE and PVDF membrane contactors in the application of propylene/propane separation using AgNO_3 solution. Rami Faiz, Marcos Fallanza, Somnuk Boributh, Ratana Jiratananon, Inmaculada Ortiz, K. Li. *Chemical Engineering Science* 94 (2013), pp. 108-119. (Chapter 3 of this thesis).
7. Olefin/paraffin separation using ceramic hollow fiber membrane contactors. Rami Faiz, **Marcos Fallanza**, Inmaculada Ortiz, K. Li. *Industrial & Engineering Chemistry Research* (2013). DOI: 10.1021/ie400870n (Chapter 3 of this thesis).

8. Propylene and propane solubility in imidazolium, pyridinium and tetralkylammonium based ionic liquids containing a silver salt. **M. Fallanza**, A. Ortiz, D. Gorri, I. Ortiz. Submitted to Journal of Chemical and Engineering Data. (Chapter 2 of this thesis).
9. Polymer-ionic liquid composite membranes for propane/propylene separation by facilitated transport. **M. Fallanza**, A. Ortiz, D. Gorri, I. Ortiz. Journal of Membrane Science, DOI:10.1016/j.memsci.2013.05.015. (Chapter 4 of this thesis).

Contributions to international conferences

1. Propylene/propane separation using RTIL containing silver salt in gas-liquid membrane contactors. A. Ortiz, **M. Fallanza**, D. Gorri, I. Ortiz. Conference on Molten Salts and Ionic Liquids 2010 (EUCHEM2010). Bamberg (Germany). March 2010. Oral presentation.
2. Intensification of separation processes of propylene/propane mixtures with a gas-liquid membrane contactor using Ag^+ -RTIL solution. A. Ortiz, **M. Fallanza**, D. Gorri, I. Ortiz. VII Ibero-American Conference on Membrane Science and Technology (CITEM2010). Sintra (Portugal). April 2010. Oral presentation.
3. Separation of gaseous olefin/paraffin mixtures by reactive absorption in a membrane contactor. A. Ortiz, **M. Fallanza**, D. Gorri, I. Ortiz. EUROPEAN MEMBRANE SOCIETY – XXVII SUMMER SCHOOL. Bucharest (Romania). June 2010. Poster.
4. Comparison of gas/liquid stirred tank and membrane contactors for the separation processes of propylene/propane mixtures using Ag^+ -RTIL solution. A. Ortiz, **M. Fallanza**, D. Gorri, I. Ortiz. 19th International Congress of Chemical and Process Engineering (CHISA2010). Prague (Czech Republic). September 2010. Oral presentation.
5. On the use of membrane contactors for the separation of gaseous mixtures of olefins and paraffins. A. Ortiz, **M. Fallanza**, D. Gorri, I. Ortiz. 5th Conference on the Membrane Science and Technology (PERMEA2010). Tatranské Matliare (Slovakia). September 2010. Oral presentation.
6. Separation of gaseous olefin/paraffin mixtures by reactive absorption in a membrane contactor. A. Ortiz, **M. Fallanza**, D. Gorri, I. Ortiz. XIX

- INTERNATIONAL Conference on Chemical Reactors (CHEMREACTOR-19). Vienna (Austria). September 2010. Oral presentation.
7. Solvent potential Improvements of the reactive ionic liquids for the olefin/paraffin gas mixture separation. **M. Fallanza**, A. Ortiz, D. Gorri, I. Ortiz. 2nd Iberian Meeting on Ionic Liquids (2IMIL). Santiago de Compostela and La Coruña (Spain). July 2011. Oral presentation.
 8. The use of membrane contactors for the separation of paraffin/olefin mixtures by absorption into RTILs reactive media. **M. Fallanza**, A. Ortiz, D. Gorri, I. Ortiz. International Congress on Membranes and Membrane Processes (ICOM2011). Amsterdam (The Netherlands). July 2011. Oral presentation.
 9. Advanced processes for the separation of olefin/paraffin mixtures. Integrated use of Ag^+ - RTIL reactive media and membrane contactors. **M. Fallanza**, A. Ortiz, D. Gorri, I. Ortiz. 8th European Congress of Chemical Engineering (ECCE-8). Berlin (Germany). September 2011. Poster.
 10. New challenges on the use of Ag^+ -RTIL reactive media for the separation of olefin/paraffin gas mixtures. **M. Fallanza**, A. Ortiz, D. Gorri, I. Ortiz. 1st International Conference on Ionic Liquids in Separation and Purification Technology (ILSEPT2011). Sitges (Spain). September 2011. Poster.
 11. On the use of supported ionic liquid membranes containing silver ions for the separation of propylene/propane gas mixtures. A. Ortiz, **M. Fallanza**, D. Gorri, I. Ortiz. 1st International Conference on Ionic Liquids in Separation and Purification Technology (ILSEPT2011). Sitges (Spain). September 2011. Oral presentation.
 12. Innovative process design using membrane contactors for the separation of olefin/paraffin mixtures. **M. Fallanza**, A. Ortiz, D. Gorri, I. Ortiz. 12th Mediterranean Congress of Chemical Engineering. Barcelona (Spain). November 2011. Oral presentation.
 13. New challenges in the separation of olefin/paraffin mixtures. Integrated use of RTIL and membrane contactors. **M. Fallanza**, A. Ortiz, D. Gorri, I. Ortiz. International congress on Green process Engineering (GPE3). Kuala Lumpur (Malaysia). December 2011. Oral presentation.
 14. New research and developments in olefin/paraffin separation by absorption into RTILs reactive media in a membrane contactor. **M. Fallanza**, A. Ortiz, D. Gorri, I. Ortiz. VIII Congreso Ibero-Americano en

- Ciencia y Tecnología de Membranas (CITEM 2012), Salta (Argentina). April 2012. Oral presentation.
15. Propylene/propane separation by facilitated transport mechanism in mobile and fixed site carrier membranes. A. Ortiz, **M. Fallanza**, D. Gorri, I. Ortiz. VIII Congreso Ibero-Americano en Ciencia y Tecnología de Membranas (CITEM 2012), Salta (Argentina). April 2012. Oral presentation.
 16. Innovative separation of propylene/propane gas mixtures. On the use of membrane contactor and pressure swing technique. **M. Fallanza**, A. Ortiz, D. Gorri, I. Ortiz. International Congress of Chemical Engineering (ANQUE), Sevilla (Spain). June 2012. Oral presentation.
 17. Olefin/paraffin separation using ceramic hollow fiber membrane contactors. R. Faiz, **M. Fallanza**, I. Ortiz, K. Li. (EUROMEMBRANE 2012). London (UK). September 2012. Poster.
 18. Comparison of reactive membranes containing ILs in the separation of gaseous olefin-paraffin mixtures. **M. Fallanza**, A. Ortiz, D. Gorri, I. Ortiz. (EUROMEMBRANE 2012). London (UK). September 2012. Oral presentation.
 19. Novel membrane reactor for the separation of olefin/paraffin gas mixtures. **M. Fallanza**, A. Ortiz, D. Gorri, I. Ortiz. 22nd International Symposium on Chemical Reaction Engineering (ISCRE22). Maastricht (The Netherlands) September 2012. Poster.
 20. Ag⁺-BmimBF₄ based polymer composite as facilitated transport membranes for propane/propylene separation. **M. Fallanza**, A. Ortiz, D. Gorri, I. Ortiz. 5th Congress on Ionic Liquids (COIL5). Algarve (Portugal). April 2013. Poster.
 21. Polymer-Ionic Liquid composite as facilitated transport membranes for propane/propylene separation. **M. Fallanza**, A. Ortiz, D. Gorri, I. Ortiz. 9th European Congress of Chemical Engineering (ECCE9). The Hague (The Netherlands). April 2013. Poster.
 22. The role of ionic liquid based selective membrane on the separation of olefin-paraffin mixtures. **M. Fallanza**, A. Ortiz, D. Gorri, I. Ortiz. 9th World Congress of Chemical Engineering (WCCE9). Seoul (Korea). August 2013. Oral presentation.

About the author

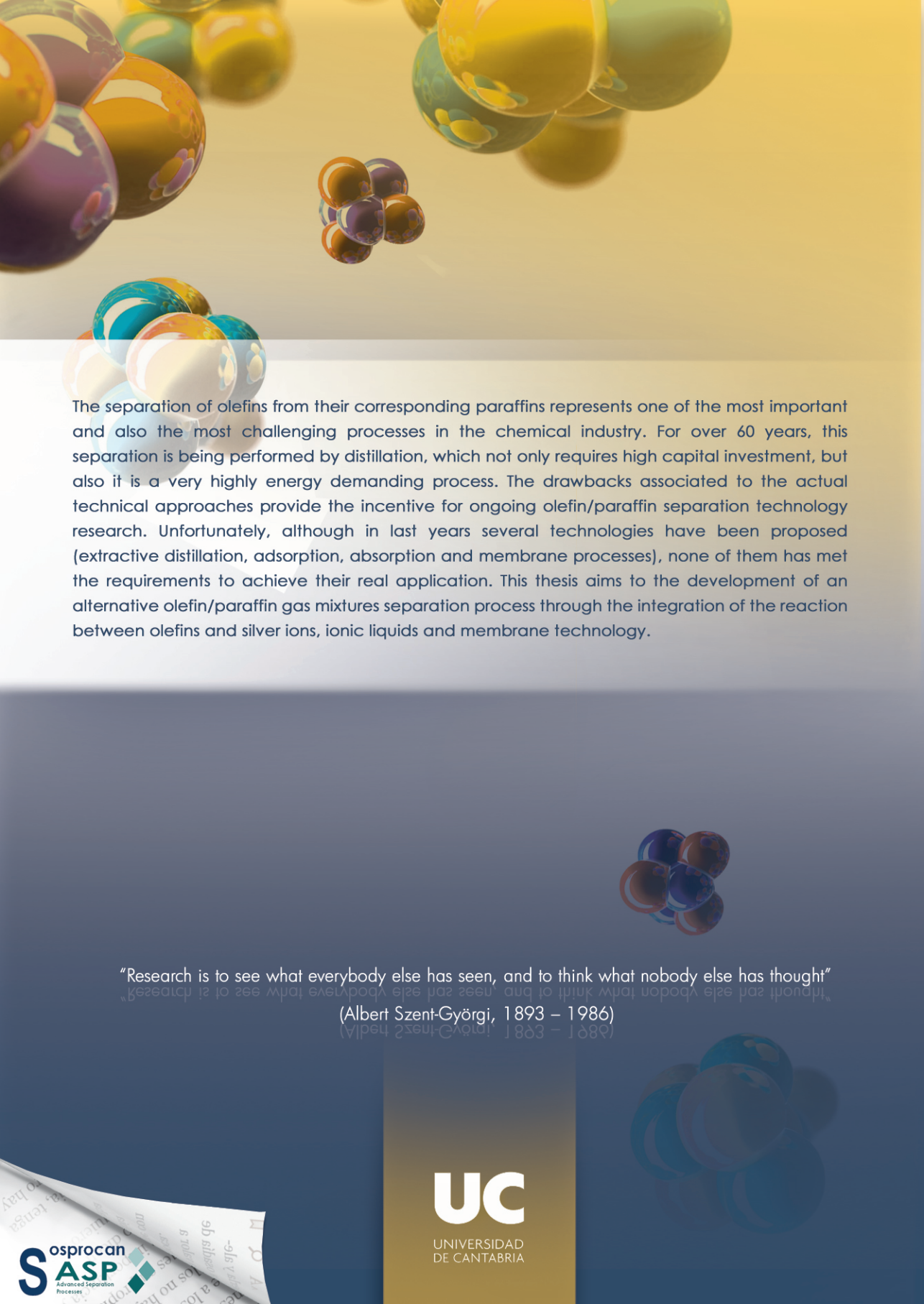
Marcos Fallanza Torices was born on 4th July 1986 in Torrelavega, a small city located in the region of Cantabria (Spain). In 2009 he obtained a Bachelor Degree in Chemical Engineering at Universidad de Cantabria. After the graduation, he joined the Advanced Separation Processes research group where he performed R&D activities within the project “Research and development of reactive separations. Contribution to sustainable development”, and started his PhD work in the field of advanced separation processes for olefin/paraffin gas mixtures supported by a FPI grant sponsored by the Spanish Ministry of Economy and Competitiveness. In 2010 He obtained a Bachelor Degree in Industrial Engineering specialty in Industrial Chemistry at Universidad de Cantabria and he succeeded in the Master in Chemical Engineering “Sustainable Production and Consumption”. In 2011 he completed a short research stage in the Departamento de Química Física Aplicada at Universidad Autónoma de Madrid (Spain) under the supervision of Dr. José Francisco Palomar. One year later, in 2012, he completed another research stage in the Department of Chemical Engineering and Chemical Technology at Imperial College London (UK) under the supervision of Prof. Kang Li. Currently, he is the author of 9 scientific articles in indexed journals, as well as 22 contributions in international conferences.



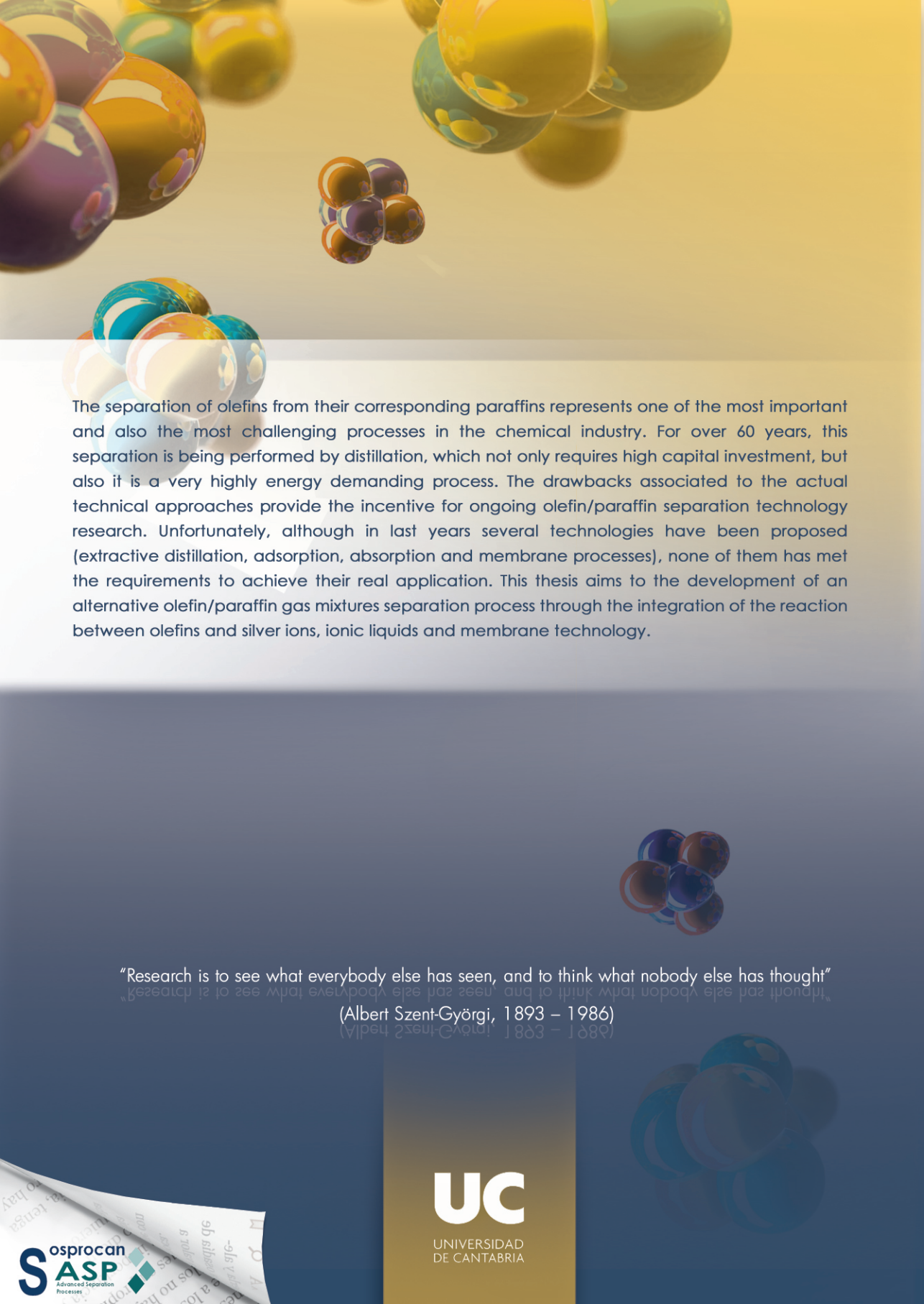
Sobre el autor

Marcos Fallanza Torices nació el 4 de julio de 1986 en Torrelavega, una pequeña ciudad de la comunidad autónoma de Cantabria (España). En 2009 obtuvo su licenciatura en Ingeniería Química en la Universidad de Cantabria. Después de la graduación, se unió al grupo de investigación Procesos avanzados de Separación donde realizó actividades de I+D dentro del proyecto "Investigación y desarrollo de separaciones reactivas. Contribución al desarrollo sostenible" donde comenzó sus estudios de doctorado en el campo de los procesos avanzados de separación de mezclas de olefina/parafina apoyado por una beca FPI concedida por el Ministerio de Economía y Competitividad. En 2010 obtuvo el título en Ingeniería Industrial especialidad Química Industrial de la Universidad de Cantabria así como el Máster en Ingeniería Química "Producción y Consumo Sostenible". En 2011 completó una estancia breve de investigación en el Departamento de Química Física Aplicada de la Universidad Autónoma de Madrid (España) bajo la supervisión del Dr. José Francisco Palomar. Un año más tarde, en 2012, completó otra estancia en el Department of Chemical Engineering and Chemical Technology del Imperial College de Londres bajo la supervisión del profesor Kang Li. Actualmente, es autor de 9 artículos científicos así como de 22 contribuciones en congresos internacionales.





The separation of olefins from their corresponding paraffins represents one of the most important and also the most challenging processes in the chemical industry. For over 60 years, this separation is being performed by distillation, which not only requires high capital investment, but also it is a very highly energy demanding process. The drawbacks associated to the actual technical approaches provide the incentive for ongoing olefin/paraffin separation technology research. Unfortunately, although in last years several technologies have been proposed (extractive distillation, adsorption, absorption and membrane processes), none of them has met the requirements to achieve their real application. This thesis aims to the development of an alternative olefin/paraffin gas mixtures separation process through the integration of the reaction between olefins and silver ions, ionic liquids and membrane technology.



"Research is to see what everybody else has seen, and to think what nobody else has thought"

(Albert Szent-Györgi, 1893 – 1986)